



Ultrasonic Transducer Design: Feasibility as parametric echosounder in shallow water

Patricia Ordóñez Cebrián

Institut per a la Gestió Integrada de Zones Costaneres

UNIVERSITAT POLITÈCNICA DE VALÈNCIA

Gandia, June 2017

Tesis Doctoral dirigida por:

Dr. Víctor Espinosa Roselló

Dr. Miguel Jover Cerdá

Dra. Isabel Pérez Arjona

Index

Resumen	9
Resum	13
1.Introduction	19
1.1. Motivation and objectives.....	19
2. Ultrasound theory.....	25
2.1. Acoustic waves	25
2.2. Linear acoustic wave equation in fluids	31
2.3. Non-linear regime: parametric sound generation	32
2.3.1. Historical Background	32
2.3.2. Parametric array: operating regimes	34
2.3.3. Nonlinear acoustic models.....	39
2.3.3.1. Westervelt equation	39

2.3.3.2. Burgers equation.....	39
2.3.3.3. KZK equation	40
2.4. Propagation medium.....	40
2.4.1. Acoustic medium properties	40
3. Ultrasound generation: Ultrasonic Piezoelectric Transducer	47
3.1. Historical background.....	47
3.2. Ultrasound generation: Piezoelectricity.....	49
3.2.1. Piezoelectric constitutive relations	52
3.2.1.1. Piezoelectric ceramic case	54
3.3. Ultrasonic transducer as a transmitter.....	57
3.3.1. characterization OF Electroacoustic parameters.....	64
3.4. Transducer elements	73
3.5. Scientific echosounder.....	79
3.6. Active Sonar equation.....	83
4. Numerical Simulation Methods.....	85
4.1. Transducer design and wave propagation.....	85
4.1.1. Brief historical background	86
4.1.2. Main concepts and Procedure	88
4.1.3. Mathematical description.....	89
4.1.4. Considerations	91
4.1.4.1. Limitations in the spatial discretization	92
4.1.4.2. Model convergence.....	92

4.1.4.3. Model simplification.....	93
4.1.4.4. Artificial boundary condition.....	94
4.1.5. Finite element software.....	94
4.2. K-SPACE PSEUDO SPECTRAL METHOD	96
5.Ultrasonic Transducer Design	101
5.1. Introduction	101
5.2. Active materials characterization.....	104
5.2.1. Parameters under test.....	105
5.2.2. Materials and methods.....	107
5.2.2.1. Acoustic impedance.....	110
5.2.2.2. Piezoelectric properties adjustment	114
5.2.2.3. Resonance frequency study as function of diameter/thickness ratio...	126
5.2.3. Active materials characterization results	127
5.2.3.1. Acoustic impedance.....	127
5.2.3.2. Piezoelectric coefficients adjustment.....	129
5.2.3.3. Resonance frequency study as function of diameter/thickness ratio...	134
5.3. Passive materials characterization	136
5.3.1. Parameters under test.....	136
5.3.2. Materials and Methods	138
5.3.2.1. Acoustic impedance.....	139
5.3.2.2. Transversal sound speed and attenuation coefficient experimental adjustment.....	142

5.3.3. Passive materials characterization results	144
5.3.3.1. Acoustic impedance	144
5.3.3.2. Transversal sound speed and attenuation coefficient adjustment	146
5.4. Prototype Modelling and Implementation	148
5.5. Transducer Characterization	154
5.5.1. Materials and methods	154
5.5.1.1. Electrical admittance measurement.	154
5.5.1.2. Sensitivity and directivity measurements	155
5.5.2. Results	161
5.6. Fem modelling validation and design options	164
5.6.1. Fem modelling validation	164
5.6.1.1. Prototype 1: Pic255.....	165
5.6.1.2. Prototype 2: Pz37.....	168
5.6.2. Design improvement.....	170
5.7. Conclusions	173
6.Parametric echosounding in shallow water.....	175
6.1. Parametric array: Preliminary study	176
6.2. Materials and methods	180
6.2.1. Transducer under study.....	180
6.2.2. Experimental set-up.....	183
6.2.3. Methodology	183
6.2.3.1. Amplitude in function of voltage measurement.....	183

6.2.3.2. Directivity measurement.....	185
6.2.3.3. Amplitude in function of distance measurement	186
6.2.4. Measurement parameters	187
6.2.4.1. Parametric frequencies selection.....	187
6.2.4.2. Amplitude signal.....	189
6.2.4.3. Signal length	189
6.3. Results	190
6.3.1. Parametric amplitude in function of voltage.....	191
6.3.2. Directivity measurements results.....	193
6.3.3. Amplitude as function of distance results.....	199
6.3.4. Experimental measurements Vs Numerical simulation	201
6.4. Transducer viability	205
6.5. Conclusions	214
Conclusions.....	217
Acknowledgements	221
Referencias	225
Table Index.....	237
Figure index.....	241

Resumen

Las técnicas acústicas se han convertido en las últimas décadas en las herramientas más apropiadas para la estimación de biomasa en el sector pesquero. Esto es debido a que las ondas acústicas son las únicas que pueden utilizarse para teledetección en el medio acuático, por su baja atenuación, comparadas con las ondas electromagnéticas, que son las usadas habitualmente en comunicaciones a larga distancia en la atmósfera. Las ecosondas ultrasónicas permiten muestrear la columna de agua y cubrir grandes extensiones de océano mediante campañas de muestreo realizadas por buques oceanográficos, ofreciendo información de las poblaciones de peces de interés comercial.

Por otro lado, como consecuencia de la sobreexplotación de los recursos pesqueros y para cubrir la demanda creciente para su consumo, se ha desarrollado como alternativa a la captura, la producción piscícola. Aunque hay diversas especies que se crían en cautividad, en España podemos destacar tres en particular, por el alto impacto económico y grado de implantación: Dorada (*Sparus aurata*), lubina (*Dicentrarchus labrax*) y atún rojo (*Thunnus thynnus*). La aplicación de las técnicas desarrolladas en el campo de la acústica de pesquerías para el control y estimación de la biomasa en jaulas flotantes, es una

demanda del sector acuicultor. Sin embargo, diferentes problemas relacionados con la geometría de la aplicación y las altas densidades de peces con las que se trabaja en acuicultura intensiva, han dificultado la aplicación directa de las mismas.

Los avances en el estudio de la biomasa o en la clasificación de especies han ido en paralelo con el desarrollo de los sistemas sonar y ecosondas usados para este tipo de aplicaciones, y particularmente con la evolución de los transductores ultrasónicos empleados. La frecuencia de trabajo, la potencia de emisión, el ancho de banda, así como la directividad son factores clave en los métodos acústicos aplicados a la pesca.

Además, otras vertientes de investigación están adquiriendo mayor relevancia en este sector, como por ejemplo, el estudio de la generación no lineal paramétrica de sonido. Esta generación o efecto paramétrico, producido en el medio, se ha enfocado hasta ahora especialmente en batimetrías o en la clasificación del subsuelo oceánico, por ofrecer frecuencias de trabajo mucho más bajas con la misma directividad que el haz generado a alta frecuencia. Actualmente, se estudia su viabilidad para ser aplicado a pesquerías o a acuicultura, debido a la posibilidad de trabajar a varias frecuencias con un mismo transductor, presentado éstas las mismas características de radiación, lo que no es posible en el régimen lineal.

Esta tesis presenta el diseño de un transductor de ultrasonidos para la estimación de biomasa con unas características específicas. Demostrando, además, la capacidad de éste para poder trabajar en régimen no lineal con aperturas adecuadas para su uso en aguas poco profundas o en jaulas de acuicultura.

En el capítulo 2 se presenta información general sobre las ondas de ultrasonidos y el medio por donde se propagan, así como una introducción a la generación no-lineal. Conceptos generales sobre la generación de los ultrasonidos y el diseño se presentan en el capítulo 3.

En el capítulo 4, se muestran los modelos numéricos utilizados para afianzar los resultados experimentales presentados durante la tesis.

El capítulo 5 recoge el diseño del transductor, que englobará todos los procesos, desde la caracterización de los materiales, hasta el montaje, puesta en marcha y simulación de los prototipos creados.

Para finalizar el capítulo 6 presenta el comportamiento de los prototipos en régimen no lineal y su viabilidad para estimar biomasa de diferentes especies en aguas poco profundas

Resum

Les tècniques acústiques s'han convertit en les últimes dècades en les ferramentes més apropiades per a l'estimació de biomassa en el sector pesquer. Això és degut a que les ones acústiques són les úniques que poden utilitzar-se per teledetecció en el medi aquàtic, per la seva baixa atenuació, comparades amb les ones electromagnètiques, que són les usades habitualment en comunicacions a llarga distància en l'atmosfera. Les ecosondes ultrasòniques permeten mostrejar la columna d'aigua i cobrir grans extensions d'oceà mitjançant campanyes de mostreig realitzades per vaixells oceanogràfics, oferint informació de les poblacions de peixos d'interès comercial.

Per altre costat, com a conseqüència de la sobreexplotació dels recursos pesquers i per cobrir la demanda creixent per al seu consum, s'ha desenvolupat com a alternativa a la captura, la producció piscícola. Encara que hi ha diverses espècies que es crien en captivitat, a Espanya podem destacar tres en particular, per l'alt impacte econòmic i grau d'implantació: Daurada (*Sparus aurata*), llobarro (*Dicentrarchus labrax*) i tonyina vermella (*Thunnus thynnus*). L'aplicació de les tècniques desenvolupades en el camp de l'acústica de pesqueres pel control i estimació de la biomassa en gàbies flotants, és una

demanda del sector aquíiculator. No obstant això, diferents problemes relacionats amb la geometria de l'aplicació i les altes densitats de peixos amb les que es treballa en aquíicultura intensiva, han dificultat l'aplicació directa de les mateixes.

Els avanços en l'estudi de la biomassa o en la classificació d'espècies han anat en paral·lel amb el desenvolupament dels sistemes sonar i ecosondes usats per a aquest tipus d'aplicacions, i particularment amb l'evolució dels transductors ultrasònics empleats. La freqüència de treball, la potència d'emissió, l'ample de banda, així com la directivitat són factors clau en els mètodes acústics aplicats a la pesca.

A més, altres vessants d'investigació estan adquirint major rellevància en aquest sector, com per exemple, l'estudi de la generació no lineal paramètrica de so. Aquesta generació o efecte paramètric, produït en el medi, s'ha enfocat fins ara especialment en batimetries o en la classificació del subsòl oceànic, per oferir freqüències de treball molt més baixes amb la mateixa directivitat que el feix generat a alta freqüència. Actualment, s'estudia la seva viabilitat per a ser aplicat a pesqueries o a aquíicultura, a causa de la possibilitat de treballar a diverses freqüències amb un mateix transductor, presentat aquestes les mateixes característiques de radiació, el que no és possible en el règim lineal.

Esta tesi presenta el disseny d'un transductor d'ultrasons per a l'estimació de biomassa amb unes característiques específiques. Demostrant, a més, la capacitat d'aquest per poder treballar en règim no lineal amb obertures adequades per al seu ús en aigües poc profundes o en gàbies d'aquíicultura.

En el capítol 2 es presenta informació general sobre els ultrasons i el mitjà pel qual es propaguen, així com una introducció a la generació no-lineal. Conceptes generals sobre la generació dels ultrasons i el disseny es presenten en el capítol 3.

En el capítol 4, es mostren també els models numèrics utilitzats per a refermar els resultats experimentals presentats durant la tesi.

El capítol 5 recull el disseny del transductor, que englobarà tots els processos, des de la caracterització dels materials fins al muntatge, posada en marxa i simulació dels prototips creats.

Finalment, el capítol 6 presenta el comportament dels prototips en règim no lineal i la seua viabilitat per a estimar biomassa de diferents espècies en aigües poc profundes.

Abstract

In recent decades, acoustic techniques have become the most appropriate tools for biomass estimation in the fishing industry. This is because acoustic waves are the only waves that can be used for remote sensing in the aquatic environment due to their low attenuation compared to electromagnetic waves, which are usually used in long-distance communications in the atmosphere. Ultrasonic echo sounders allow sampling of water columns and cover large areas of ocean by means of sampling campaigns conducted by oceanographic vessels, providing information on fish stocks of commercial interest.

Furthermore, as a result of the overexploitation of fishery resources and to cover increasing demand, fish production has been developed as an alternative to capture. Although several species are bred in captivity, in Spain we can highlight three in particular, due to the high economic impact and degree of implantation: Gilt-head bream (*Sparus aurata*), sea bass (*Dicentrarchus labrax*) and Bluefin tuna (*Thunnus thynnus*). There is demand in the aquaculture industry for techniques developed in the field of fishery acoustics to control and estimate biomass. However, various problems related to the geometry of the application and high fish densities in intensive aquaculture have made these techniques difficult to apply directly.

The study of biomass and species classification has progressed in parallel with the development of sonar and echo sounder systems used for this type of applications, and particularly with the evolution of ultrasonic transducers. Operation frequency, transmission power, bandwidth and directivity are key factors in the acoustic methods applied to fishing.

In addition, other aspects of research are becoming more relevant in this sector, such as the study of nonlinear parametric sound generation. This generation or parametric effect, produced in the medium, has focused so far especially on bathymetry or classification of the oceanic subsoil, by offering much lower operation frequencies with the same directivity as the beam generated at high frequency. Nowadays, their feasibility is studied for application to fisheries or aquaculture, due to the possibility of working at several frequencies with the same transducer, given the same radiation characteristics, which is not possible in the linear regime.

This thesis presents the design of an ultrasound transducer for biomass estimation with specific characteristics and demonstrates its capacity to work in a non-linear regime with optimum apertures for use in shallow water or in aquaculture cages.

Chapter 2 presents general information on ultrasound waves, the medium through which they are propagated and an introduction to non-linear generation. General concepts in ultrasound generation and design are presented in Chapter 3.

Chapter 4 shows the numerical models used to reinforce the experimental results presented during this thesis.

Chapter 5 covers the design of the transducer, encompassing all the processes, from characterization of the materials, to assembly, operation and simulation of designed prototypes. To conclude, Chapter 6 presents the behavior of prototypes in a nonlinear regime and their feasibility for estimating biomass of different species in shallow water.

1

Introduction

1.1. MOTIVATION AND OBJECTIVES

This thesis deals with the application of parametric echosounding for fisheries acoustics in very shallow waters. It considers the development of an acoustic transducer prototype, designing all its constituent parts, and its feasibility for operation in a non-linear regime. This work seeks to provide technological tools for sustainable fishing (in the case of wild species capture), or proper monitoring of marine aquaculture exploitations (fish farms, etc.).

According to experts from the Food and Agriculture Organization (FAO), a global extraction of more than 100 million tonnes per year can generate irreversible ecological alterations in marine resources. The growth in human population and changes in dietary habits led to the need to exceed 167 million tonnes of catches by 2014 (FAO Statistics 2014).

Due to the growing demand for fishery resources, marine aquaculture has considerably increased production in recent years. In Spain, for example, this growth is mainly due to the cultivation of sea bream (*Sparatus aurata*) and sea bass (*Dicentrarchus labrax*) (APROMAR 2009) and a catch-based aquaculture industry of Bluefin tuna (*Thunnus thynnus*).

Application of underwater acoustics techniques offer the chance to study both fish size and the amount of total biomass contained in a given volume of the medium. These two estimations are of vital importance both in fisheries (helping to make selective catches), and in marine farms, optimizing productivity and reducing environmental impacts in both cases. Information provided by sonar and echo sounder (the most commonly used instruments in aquaculture studies) is an important factor in the efficiency of modern fishery operations.

Thus from the outset in the application of acoustic techniques for fish biomass estimation, a considerable number of scientists have been conducting research on acoustic properties of marine species. A large amount of data has been accumulated by experiments measuring acoustic energy backscattered to an echosounder. This data is known as target strength (TS), power target or dispersion cross-section in its linear expression .(Foote 1989)

Study of the acoustic properties of marine species has been carried out in parallel to the development of transducers for these applications. Transmission power, transducer aperture and operation frequency are key factors in the study of fish school characteristics. It is of vital importance to develop a specific acoustic transducer for each type of study.

Furthermore, work has been done on biomass estimation in marine aquaculture (Knudsen, F., Fosseidengen, J., Oppedal, F., Karlsen, Ø, Ona, E. 2004) (Moszynski 2002) including

TS characterization of Mediterranean species in marine farms (Soliveres 2015). It has been found that the distance ranges in floating cages condition the application of the echosounding techniques commonly applied in fisheries acoustics. First, the detection of single specimen and TS measurements for fish sizing are limited by different problems associated to field diffraction effects and by the small acoustical beam diameter compared to fish size, as well as by high fish densities. Second, the application of the linear superposition principle to estimate fish density has been questioned because of the high densities. Backscattered energy per unit volume must be proportional to the density of scatterers (fish). High densities can provoke the acoustical extinction of the beam and also multi-scattering effects; therefore estimation of energy impinging on each fish is not trivial and depends on fish densities, fish size and acoustic frequency (Feuillade and P Raveau n.d.; Foote 1990; Foote, Ona, and Toresen 1992).

The need for sustainable fishing also requires enhanced capabilities to differentiate size and species. One of the emerging technologies dedicated to tropical tuna fisheries are satellite buoys for fishing aggregating devices (FADs) localisation and monitoring. Earlier these devices were mere GPS trackers of FADs (Fonteneau, Chassot, and Bodin 2013), but current satellite buoy technology includes a single beam echosounder with one or more frequencies capable of performing echo integration and biomass estimations. Echosounders associated to drifting devices are proposed as instruments to evaluate relative abundances of FAD-associated fish (like tropical tuna species) using catch-independent data, and there is a clear need to improve their ability to discriminate species and size (Lopez et al. 2014).

One of the techniques in underwater acoustics that has undergone a remarkable development due to its multiple applications is the nonlinear generation of sound. The devices based on this principle were specially developed during the Cold War and are

known as parametric acoustic arrays (in the Western literature) or parametric antennae (in Soviet references)(Oleg A,G. and Palmer R,D 2008).

This power effect, originated in the propagation medium allows the generation of lower frequencies inside the emitted beam of higher frequencies excited on the acoustic transducer, resulting in a beam with lower absorption and with similar insonified volumes.(Hamilton et al. 2008) These insonified volumes have been proposed as a key tool in bathymetries or oceanic floor and sub-bottom classification and, more recently in species classification, (Foote 1989; Godø and Foote 2010)

Research work developed in the present thesis deals with the design, construction and characterization of an acoustic transducer, which is considered part of a parametric echo sounder device. Our aim was to study the application of parametric techniques in the range of distances involved in aquaculture, very shallow waters or the upper layer of oceans where echosounders associated to drifting devices operate. A compromise between beam aperture and the efficiency of parametric generation of sound should be investigated. A wider aperture than the one used in scientific or commercial parametric echosounders is desirable to improve insonified volumes at short distances, but due to their power-dependent character, the gain in parametric generation can be compromised.

During the design process, simulation studies of piezoelectric ceramics, essential constituents of the transducer, have been made, adding all the elements for their optimization such as the impedance matching layer, or the backing necessary for their correct operation. After building prototypes, a measurement campaign was conducted, developing all the necessary software to acquire and analyse the signals. Finally, with the experimental results we proceeded to study the range of applicability for the developed prototypes.

The work contained in this document can be listed schematically according to the following items.

In relation to the acoustic transducer design:

- a) Acoustic transducer design and simulation.
- b) Development and prototyping.
- c) Acoustic transducer characterization (in linear regime).
- d) Simulation of non-linear acoustic field generation by the developed transducer.
- e) Non-linear measurement campaign.

With the results obtained in section e) the viability of the transducer was studied for use in a non-linear regime (parametric acoustic array) :

- a) Sound pressure level from the parametric generation has been considered, calculating, depending on expected TS for different species, the viability of the transducer under different distance conditions.

2

Ultrasound theory

This chapter provides a short description of ultrasound physics, to review general concepts of ultrasonic wave propagation. A brief introduction to non-linear propagation and to the corresponding equations is also provided. Considering that the field of application of the present Thesis is the field of fisheries acoustics, ultrasonic propagation in water, mainly sea water, has been specifically addressed.

2.1. ACOUSTIC WAVES

Sound is a mechanical perturbation. It consists in pressure fluctuations propagating through elastic bodies, fluids and gases and it is not produced in a vacuum. In sound propagation, particles move with compression and expansion through a material, with no displacement of mass.

Different parameters are required to describe a sound wave. The most important are described below.

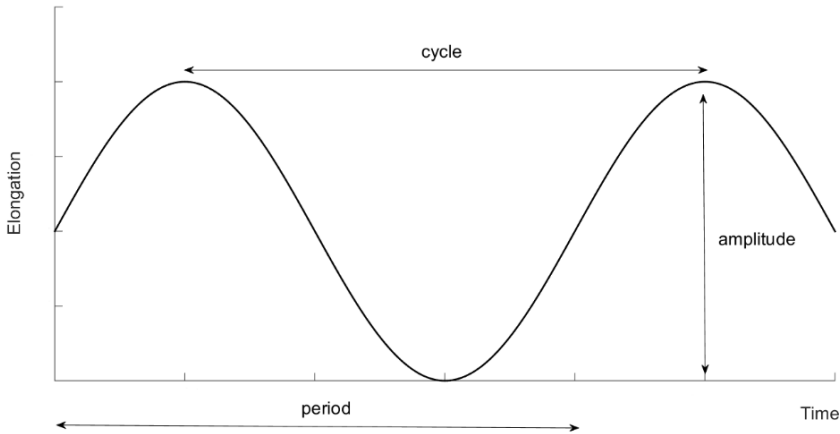


Figure 2.1. Waveform parameters

- Frequency: frequency is defined as number of cycles that take place in a second.

$$f = \frac{1}{T} \quad (2.1)$$

Where f is the frequency in hertz (Hz) and T is the period in seconds (s).

- Period: the elapsed time between two equivalent points of the wave. The period (T), is a reciprocal magnitude of frequency and the unit is seconds (s).

- Wavelength: Distance between two nodes of the wave. Its international unit is the meter (m). In isotropic materials, wavelength is the ratio between propagation velocity and frequency.

$$\lambda = \frac{V_L}{f} \quad (2.2)$$

Two other important features in the study of acoustic waves are propagation velocity and acoustic impedance.

Propagation velocity is defined as the speed at which acoustic vibrations pass through materials. It depends on the elastic properties of the material and the type of vibration. Generally, sound travels faster in liquids and solids than in gas. In all materials, propagation velocity varies inversely with the square root of the density. Velocity also varies proportionally to the square root of elasticity represented by Young's Modulus (E). For example, in water, longitudinal propagation velocity is about 1500 m/s at ordinary temperatures, but greatly increases with increasing temperature. In steel, which is more elastic, sound travels at about 5000m/s; its spread is very efficient.

Another factor that also affects propagation velocity is Poisson's ratio. For example, in an ultrasonic transducer, the main component is the active element, explained in the following chapter. It is usually a piezoelectric ceramic. When traction is applied to a certain ceramic, elastic elongation occurs and deformation in the direction of the applied load (which we arbitrarily call the z direction). As a result of this elongation, constrictions will occur in the lateral directions (x and y) perpendicular to the direction of voltage application. From these contractions, compression deformations S_x and S_y can be determined.

The ratio between the lateral and axial deformations is Poisson's ratio

$$\nu = -\frac{S_x}{S_z} = -\frac{S_y}{S_z} \quad (2.3)$$

The negative sign is included in the expression for which "v" is always positive. For longitudinal ultrasound waves, the propagation velocity expression taking into account the relationship of these three factors (E, ρ, and ν) is as follows:

$$V_L = \sqrt{\frac{E}{\rho} \frac{1-\nu}{(1+\nu)(1-2\nu)}} \quad (2.4)$$

Where:

V_L = Longitudinal propagation velocity [m/s]

E = Young's modulus [Pa]

ρ = Density [kg/m³]

ν = Poisson's ratio

Closely related with this property is acoustic impedance. Acoustic impedance describes the propagation conditions of ultrasonic waves through a particular medium. It is commonly denominated by the letter Z and its unit is Rayls. In plane waves, it is equal to the product of medium propagation density and longitudinal propagation velocity

$$Z = \rho_0 V_L \quad (2.5)$$

When a wave travels from one medium to another with different impedance reflection occurs. Great differences between two media can reflect almost all the wave, without the wave being spread in the second. For that reason, acoustic impedance is important for determining acoustic transmission and reflection at the boundary or border between two materials with different impedances. In transducer design, it is an important parameter as well, to choose the different materials involved in the design and the correct dimensions for them. In fisheries acoustics, the echo of the swimbladder is used to estimate the

biomass of most species or detect them. The swimbladder is a membranous sac in fish under the spine and its capacity to fill with gas is used to improve buoyancy. Due to the impedance difference between the sea and the gas, the swimbladder produces the most energy reflection back to the transducer for analysis.

The shape of the acoustic wave depends on the source and is described by the shape of the wavefront. Paradigmatic wave shapes are considered plane, spherical or cylindrical waves. When a wave is observed far away from the source, it can be considered a plane wave. As an idealization, plane waves propagate in an ideal medium with no loss of energy in the direction of wave propagation. Spherical waves, on the other hand, have an energy decay in an ideal medium that follows a spherical law : energy decreases with the inverse of the distance square (Cheeke, 2002). There may be other local conditions and sound waves can also propagate as cylindrical waves, or with other decay factors.

Material state in which the acoustic wave is transmitted also defines the local motion of the perturbation. Longitudinal and transversal waves, known as body waves can exist from within material. In longitudinal waves, also called compressional waves, displacement and wave propagation direction are parallel. In the case of transversal waves, displacement is perpendicular to the wave propagation direction. (Kinsler et al., 1999). . The difference between the two is illustrated in Fig 2.1. In solids, both waves are possible as well as other surface propagations such as Rayleigh and Love waves. However, in fluids or gases, only longitudinal waves are possible. .

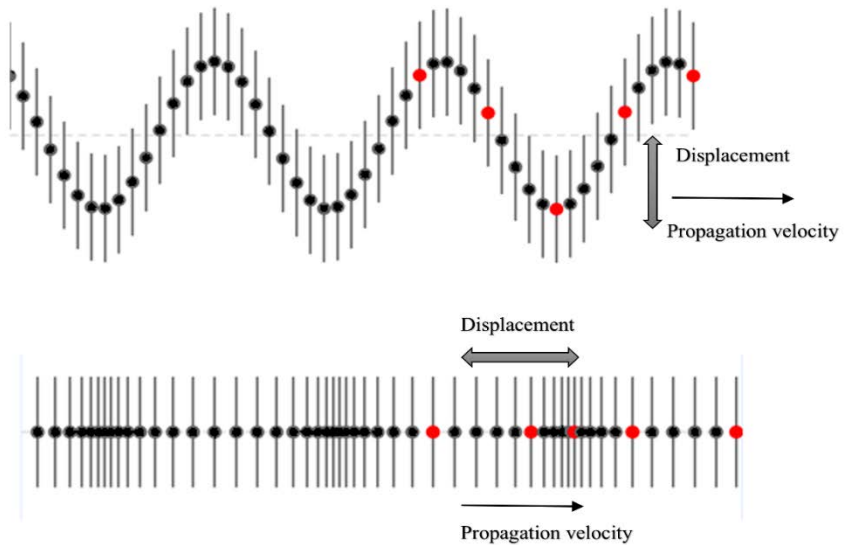


Figure 2.2. Transversal and longitudinal wave propagation.

Finally, there is another sound classification into different ranges depending on frequency. The audible range defined by human beings hearing goes from 20Hz to 20KHz. Below 20Hz, the infrasound range is defined. Up to 20 kHz starts the ultrasonic range. 0 to 20Hz and above 20 kHz are ultrasounds waves.

As noted above, ultrasounds are high frequency sounds. Ultrasonic waves are usually longitudinal but it is possible to find ultrasonic shear waves in some solids like piezoelectric ceramics as explained below in the section on piezoelectric theory.

This thesis focuses on the generation of ultrasound by a piezoelectric disc transducer and ultrasonic propagation in water. Due to the working dimensions and distances spherical propagation is considered. As the propagation medium is nonviscous fluid (water), only longitudinal waves are present.

2.2. LINEAR ACOUSTIC WAVE EQUATION IN FLUIDS

Acoustic wave propagation through fluids has obviously been a matter of interest in underwater acoustics. In the linear regime, with small intensities and perturbations, it is defined by the linear acoustic wave equation.

Section 3.4 describes the ultrasonic transducer properties of acoustic pressure, velocity, frequency, intensity and attenuation, among others.. Most of them are obtained from solving wave equations.

Conservation of mass (2.6) and momentum (2.7), from fluid dynamics, provides the basis for developing an acoustic wave equation in gases and liquids. (Eckert 2007)

$$-\frac{\partial \rho}{\partial t} = (\rho \bar{u}) \quad (2.6)$$

$$\rho \left(\frac{\partial \bar{u}}{\partial t} + (\bar{u} \cdot \nabla) \bar{u} \right) = -\nabla p' \quad (2.7)$$

where \bar{u} is particle velocity, ρ is density, ∇ is the spatial gradient operator, t is time and p' is the acoustic pressure at any point as defined by $p' = P - P_0$ where P is the instantaneous pressure at any point and P_0 the constant equilibrium pressure in the medium.

Acoustic wave equation governs the propagation of acoustic waves through a material medium. The form of the equation is a second order partial differential equations:

$$\nabla^2 p' = \frac{1}{c^2(x, y, z)} \frac{\partial^2 p'}{\partial t^2} \quad (2.8)$$

Where $c(x, y, z)$ is the local velocity.

This equation is valid for small amplitude perturbations in a homogenous and isotropic fluid.

2.3. NON-LINEAR REGIME: PARAMETRIC SOUND GENERATION

When sound waves have sufficiently large amplitudes, a non-linear regime should be considered. One of the most important non-linear effects is parametric sound generation. Nowadays this technique in echosounders, has been used in both open sea and shallow water. Shallow water requires certain characteristics in terms of biomass estimation and species characterization. These characteristics are the utilization of wider beams to insonify full fish schools and the generation of collimated beams with free side-lobe in order to avoid reflective interfaces as much as possible. Apart from that, other important features to ensure good results are the possibility of taking multifrequency measurements in the same insonified area as well as to go through the fish school without screening. Therefore parametric echosounders are chosen as a good work tool. Although there are parametric commercial echo sounders (Neil 1992; Wunderlich 2003), experiments in the field of fisheries acoustics are scanty (Godø and Foote 2010), as their main purpose is sub-bottom profile characterization.

The aim of this section is to provide a general overview of parametric sound generation.

2.3.1. HISTORICAL BACKGROUND

To discuss the parametric effect we must return to non-linear acoustics. Until now, the approximations of linear acoustics models largely simplified constitutive equations, facilitating the modelling of concrete physical phenomena. However, many other processes could not be described linearly such as cavitation and radiation force, among

others. (Bjørnø 2017). Based on the work by Euler, for fluid dynamics, and Lagrange many models have been proposed to describe non-linear acoustic phenomena.

Parametric effect was the first non-linear acoustic effect of interest for practical applications. It was suggested by Westervelt in 1963(Westervelt 1963). This effect consists in a high power modulated sound beam. The non-linear properties of sound propagation in the medium cause such a beam to act like a distribution of sources for modulation frequencies, and as a result the sound at these frequencies is radiated as from an end-fire directional array. If the primary beam is a compound of two waves of frequencies f_1 and f_2 , respectively, the sound beam generated in the medium will have new spectral components like sum frequencies (f_1+f_2), difference frequencies (f_2-f_1), and other higher order harmonics ($2f_1, 2f_2$, etc.). Sound absorption limits the propagation range of primary waves which are proportional to the frequency squared, except for the difference frequency sound that will be absorbed at much slower rate than primary sound, and will therefore propagate farther than the primary beam. These spectral components will acquire primary beam directional properties giving several frequencies with the same beam radiation pattern. In addition, unwanted side lobes are considerably reduced in most cases.

A broader and more precise development both theoretically and experimentally was published by H. O. Berktaay in 1965(Berktaay 1965), extending Westervelt's results by generalizing the primary waves to cylindrical and spherical waves. In addition, Berktaay extends the analysis of two pure tones to the case of the emission of a primary wave modulated in amplitude to a low frequency (envelope), producing the effect that the medium itself demodulates the original signal and the low frequency (parametric) appears. This process is known as self-demodulation of the medium.

From that point until now, numerous investigations have been developed in this field both in water and air (Yoneyama 1983), contributing to a better knowledge of the effect, observing for example the effects caused by divergence of the Primary beam in the radiation pattern of spectral components, (Hobæk and Vestrheim 1977), defining optimal ratios between primary and secondary frequencies.

In underwater acoustics parametric arrays have been used extensively because of their unique features. They are generally used as a wide band sonar system for direct measurement of environmental parameters in shallow waters, in fisheries, and in bottom area sounding when reverberation is a problem (Woodward et al. 1994). Having a beam pattern with significantly reduced side lobes, as in the case of the parametric array, prevents interference due to boundary interactions in shallow waters. Parametric arrays can also be used in sub-bottom and seismic profiling and in hydrophones because with only one single transducer, wide band frequency can be achieved (Radulescu et al. 2003)

2.3.2. PARAMETRIC ARRAY: OPERATING REGIMES

Summarizing the previous section, the main difference between a linear and a nonlinear system is the creation of additional harmonics due to the interaction of primary waves. Transfer of energy that occurs in the primary harmonics causes frequency combinations to appear. (Figure 2.3)

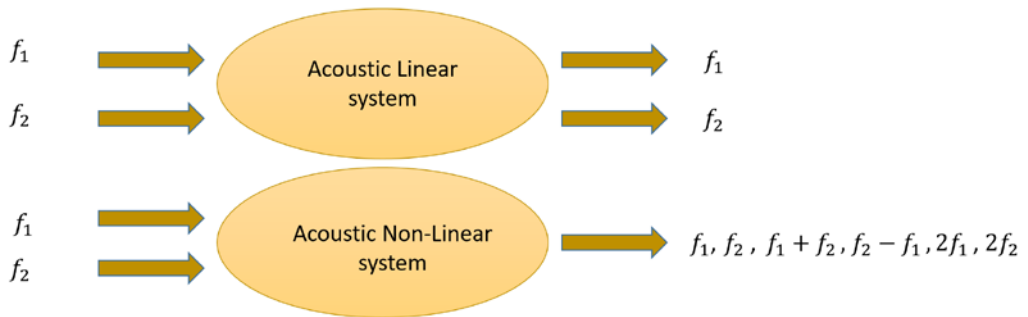


Figure 2.3. Harmonic frequency generation in a non-linear acoustic system

Within the parametric array, which is the non-linear system under study, three operating regimes can be defined depending on the factors taken into account in the study.

In the Westervelt approximation, (Westervelt 1963) it is assumed that primary waves are perfectly plane collimated waves and the interaction region is limited by viscous absorption whereas non-linear absorption is neglected. The area of the beam is negligible compared to the wave length of the ultrasonic frequency (Berktay 1965). Therefore, virtual sources created along the axis due to nonlinear interaction do not intervene in the directivity pattern of the new spectral components. This case is called *Absorption limited* (Kopp et al. 2000).

Spreading limited was the model that Bertkay developed later on, where beam aperture effects were included, as well as absorption effects. In this model, extra attenuation due to the formation of shock waves is discarded.

Shock waves are produced by the behaviour of the non-linear medium. This non-linear conduct causes changes in sound speed as a function of wave amplitude. If, for example, a high-amplitude sine wave signal is propagated by a medium, wave peaks would begin

to travel faster than wave thoughts, causing the signal to transform into a saw-tooth wave (Figure 2.4)

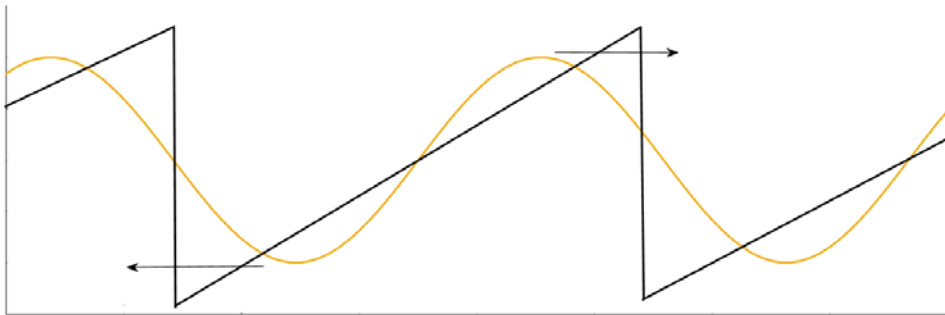


Figure 2.4. Sine wave transformation in saw-tooth wave

Thus some energy is converted into high harmonics and is no longer available on the primary frequency for longer. This is referred to above as extra attenuation. The model named Shock-wave limited was introduced by Mellet and Moffet (Moffet n.d.).

To define the operating regime in a specific problem, three characteristic distances must be defined. These are:

- Rayleigh distance: As mentioned in section 3.3, an emitter transducer has two types of field. The near field and the far field. In the far field, spherical divergence begins to act and the wave attenuates progressively. In the near field, however, waves are kept contained in a cylinder where interference phenomena can affect their amplitude. The length of this cylinder is called the Rayleigh distance (R_F)

$$R_F = \frac{d^2}{\lambda_p} \quad (2.9)$$

Where d , is the source diameter

λ_p , is the primary mean frequency $(f_1+f_2/2)$ wavelength.

- **Absorption distance:** Also called interaction distance, it depends on the medium absorption for the primary frequencies and how it limits the nonlinear generation of new spectral components, as shown in Figure 2.5

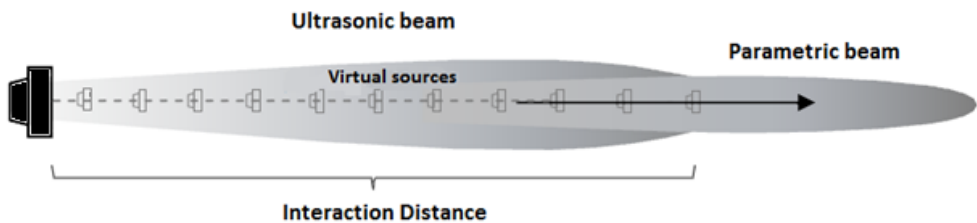


Figure 2.5. Source virtual representation depending on interaction distance

This distance is inversely proportional to the medium absorption at the mean primary frequency (α)

$$R_A = \frac{1}{\alpha} \quad (2.10)$$

- **Shock wave distance:** the distance at which the shock waves explained above are formed. It is equal to:

$$R_s = \frac{1}{\beta k M} \tag{2.11}$$

Where M , is the acoustic Match number $M = v/c_0$

β , is the non-linear parameter $\beta = 1 + B/2A$

k , is the wavenumber at the primary mean frequency.

Depending on the relationship between these three distances we will be in a certain operating range that will present its own characteristics. Figure 2.6 shows the different combinations.

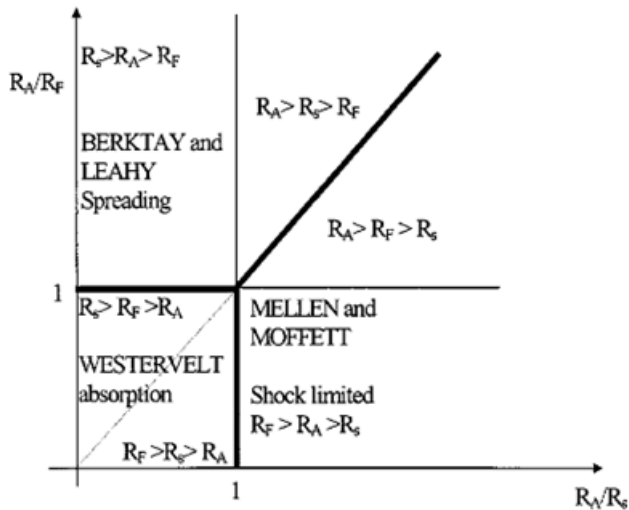


Figure 2.6. Validity model regions for parametric arrays. ((Kopp et al. 2000))

2.3.3. NONLINEAR ACOUSTIC MODELS

Since the whole process takes place in a fluid medium, the starting point will be the fundamental equations of fluid dynamics explained in Section 2.2. The combination of these and a particular state equation provide the set of equations necessary to raise the acoustic problem that solves non-linear acoustic problems, with different validity ranges.

2.3.3.1. WESTERVELT EQUATION

Westervelt equation is the simplest equation to describe the parametric array. It describes the evolution of progressive waves in a non-linear medium (Bjørnø 2017). This equation does not have to take into account non-linear absorption and beam divergence.

$$\nabla^2 p' - \frac{1}{c^2} \frac{\partial^2 p'}{\partial t^2} = -\frac{\beta}{\rho c^4} \frac{\partial^2 p'^2}{\partial t^2} \quad (2.12)$$

2.3.3.2. BURGERS EQUATION

When dissipation effects are not negligible, it is possible to use Burgers equation, which describes the evolution of flat progressive waves in a non-linear and viscous medium (Landajuela 2011)

$$\frac{\partial p'}{\partial x} = \frac{\beta}{\rho c^2} p' \frac{\partial p'}{\partial \tau} + \frac{\theta}{2\rho c^3} \frac{\partial^2 p'}{\partial \tau^2} \quad (2.13)$$

θ is the dissipation factor.

τ , is the spatial coordinate : $\tau = x - ct$

2.3.3.3. KZK EQUATION

One of the most complex expression is the paraxial approach developed by Khokhlov, Zabolotskaya and Kuznetsov and is known as the KZK equation (Roanova-Pierrat 2006), which describes focused acoustic beams, considering the nonlinearity effect, dissipation and diffraction in parabolic approximation. KZK model can be modified to take into account other absorption phenomena such as relaxation processes, or heterogeneities in propagation velocity.

$$\frac{\partial^2 p'}{\partial \tau \partial x} = -\frac{\beta}{2\rho c^2} p' \frac{\partial^2 p'^2}{\partial \tau^2} + \frac{\theta}{2\rho c^3} \frac{\partial^3 p'}{\partial \tau^3} + \frac{c}{2} \nabla_r^2 p' \quad (2. 14)$$

∇_r^2 Laplacian operator transversal to propagation direction. $\nabla_r^2 = \frac{\partial^2}{\partial x^2} + \frac{\partial^2}{\partial y^2}$

2.4. PROPAGATION MEDIUM

The transmission type of ultrasonic waves depends largely upon on the medium in which they propagate. This section describes different acoustic properties defined by the transmission medium and the effects that are encountered when ultrasonic waves propagate by the sea, as a particular case for this thesis.

2.4.1. ACOUSTIC MEDIUM PROPERTIES

All measurements carried out in this thesis are made in pure water although prototype transducers are ultimately designed to work in sea water. In both cases, propagation velocity and therefore acoustic impedance, depend on temperature, salinity (sea water) and the working depth. The literature contains different equations for obtaining the correct values, such as Mackenzie (Mackenzie 1981)

$$\begin{aligned}
 V(T, S, D) = & 1448.96 + (4.591T) - (5.304e - 2T^2) + (2.374e - 4T^3) + \\
 & (1.340(S - 35)) + (1.630e - 2D) + (1.675e - 7D^2) \\
 & - (1.025e - 2T(S - 35)) - (7.139e - 13TD^3)
 \end{aligned} \tag{2. 15}$$

T = temperature in degrees Celsius

S = salinity in parts per thousand

D = depth in meters

With a range of validity for temperature of 2 to 30 °C, salinity 25 to 40 parts per thousand, and depth 0 to 8000 m

Or Coppens equation(Coppens 1981), orientated for lower salinity values:

$$\begin{aligned}
 V(t, S, D) = & (V(0, S, t) + (16.23 + 0.253t)D + (0.213 - 0.1t)D^2 + \\
 & [0.016 + 0.0002(S - 35)]tD
 \end{aligned} \tag{2. 16}$$

$$V(0, S, D) = 1449.05 + 45.7t - 5.21t^2 + 0.23t^3 + (1.333 - 0.126t + 0.009t^2)(S - 35) \tag{2. 17}$$

t = T/10 where T = temperature in degrees Celsius

S = salinity in parts per thousand

D = depth in kilometres

With range of validity: temperature 0 to 35 °C, salinity 0 to 45 parts per thousand, depth 0 to 4000 m.

In the tests carried out during this work, considering temperature about 18°, salinity equal to 0 and depth equal to 0.5metres, propagation sound velocity acquires a value around 1475 m/s according to Coppens equation.

Another important acoustic medium property to take into account is absorption. This characteristic is one of the parts that make up the transmission losses of ultrasonic waves. The other part, by which the major part of energy is lost, is geometrical spreading (see the following chapter) which depends on the type of acoustic source.

Absorption, in the particular case of seawater, is considered to be the sum of three contributions from pure water, magnesium sulphate, and boric acid (ionic relaxation of chemicals)

The commonly used Francois-Garrison model calculates absorption coefficient α in units of dB/km based on depth, salinity, temperature, and frequency (Francois and Garrison 1982)

$$\text{Total absorption} = \text{Boric Acid Contribution} + \text{Magnesium Sulphate Contribution} + \text{Pure Water Contribution}$$

$$\alpha = \frac{A_1 P_1 f_1 f^2}{f_1^2 + f^2} + \frac{A_2 P_2 f_2 f^2}{f_2^2 + f^2} + A_3 P_3 f^2 \quad (2. 18)$$

where pressure dependencies are given by P1, P2 and P3, relaxation frequencies are f1 and f2 and A_1 , A_2 and A_3 are empiric constants related with each chemical process. Pure water contribution, A_3 is an analytical expression function of water viscosity. The other two can be obtain from Figure 2.7

François and Garrison estimate their model to be accurate to within about 5%. For frequencies of 10-500 kHz (where the MgSO₄ contribution dominates), the limits of reliability are:

$$-2 < T < 22 \text{ } ^\circ\text{C}$$

$$30 < S < 35 \text{ ppt}$$

$$0 < D < 3.5 \text{ km}$$

Further analysis by Ainslie and McColm (A&M) was published in 1997, but is based on the same data set.(Ainslie and McColm 1998). Figure 2.7 shows attenuation as a function of frequency taking into account all these factors.

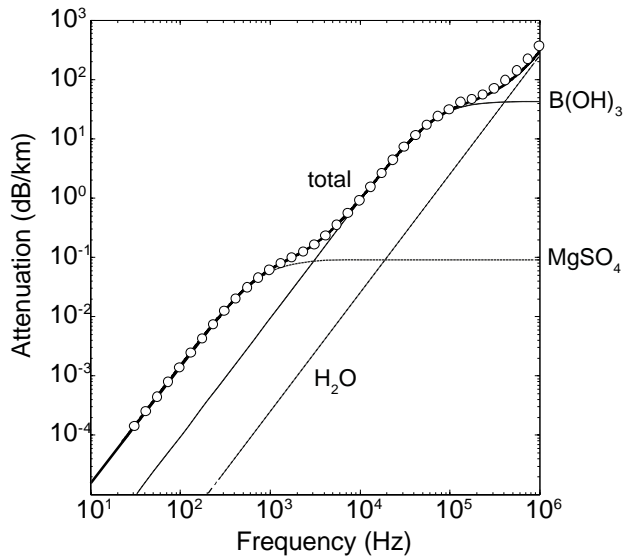


Figure 2.7. Frequency dependent attenuation, for the relaxation processes of oxygen and nitrogen in air, and magnesium sulphate and boric acid in seawater.

For the aim of this thesis, studies of relaxation effects in short distances (20m<) have been carried out neglecting any modification in the ultrasound acoustic wave.

To conclude, other additional losses may occur during the propagation of ultrasonic waves. In the sea, ultrasound experiences phenomena of reflection and refraction. These effects can provoke extra absorption or reverberation.

Definition of both effects are:

- Reflection: Change in direction of a wave at an interface between two different media so that the wave returns to the medium from which it originated.
- Refraction: Change in direction of a wave due to a change in its speed.

For layered media (layers of ocean water with differing properties), Snell's Law relates the angles of incidence and refraction at a layer boundary.

Surface and sea bottom, as well as any submerged object of considerable size, provoke sound reflection, whereas the layers that form sea water are responsible for changes in propagation velocities, diverting wave direction and giving rise to refraction.

In areas where temperature remains constant with depth, there is no refraction of sound waves; when temperature decreases, they refract towards the bottom; and where the temperature increases they refract towards the surface. When there is refraction down, the sound that eventually reaches the sea bottom will undergo absorption, but will reflect as a "bottom echo" towards the surface to refract again.

Isolated, regular objects of greater size than an ultrasonic wavelength on which a ultrasound emission arrives, reflect the strong and well defined sound, which is recognized as echo; But objects that are small, irregular and numerous give rise to many weak echoes that are repeated successively propagating in all directions and overlapping to cause the so-called reverberation of sound.

Knowledge of the characteristics and propagation of ultrasonic waves in the sea, has helped to further progress in the development of echo sounders for measuring depths and distances and more recently, as matter of interest in this thesis, for biomass estimation, applied to fisheries acoustics.

A transducer is a device that converts one form of energy to another. Generally, transducers are used to convert a physic quantity, (pressure, vibration, motion...) into an electric signal as well as the reverse. There is a transducer classification depending on the conversion type that is produced. Ultrasonic transducers are classified as electroacoustic. Electroacoustic transducers, working as transmitters or receivers, play a major role in underwater communication systems, using a variety of different transduction materials or mechanisms to transform electrical energy into sound and vice versa. (Urick 1985).

The aim of this Thesis is to design an ultrasonic transducer to be used, as a future application, in a scientific parametric echosounder for fisheries acoustics applications. This transducer, called ultrasound transceiver, is a reciprocal one, that is, it is able to perform two functions. First, to convert applied electrical energy into an acoustic pulse transmitted to the medium. Second, when an acoustic pulse is reflected by an obstacle back to the transducer, this is responsible for converting received acoustic energy into an electrical signal that is sent to the receiver (Simmonds,2007)

3

Ultrasound generation: Ultrasonic Piezoelectric Transducer

3.1. HISTORICAL BACKGROUND

Ultrasound generation began in 20th century. In 1880, piezoelectric effect was discovered by Jacques and Pierre Curie. Some piezoelectric minerals such as Quartz, Rochelle salt, or Ammonium Dihydrogen Phosphate (ADP) develop an electric charge between two surfaces when the crystal was mechanically compressed, and they expanded and contracted in size in the presence of an applied electrical field. These early devices, built with these crystals, were inherently fragile due to the weak nature of piezoelectric materials used in their construction and rudimentary adhesive bonding technology. In the 1930's, as there was an effort to utilize ultrasonic energy more extensively, piezoelectric technology then available, fell short of the need for reliable, robust ultrasonic devices.

Introduction of different types of materials, an operation modes develop this technology applying nowadays in multitude of applications.

Currently there are different ways to produce ultrasonic transduction. Among other it can be remarked: magnetostriction, capacitance or piezoelectricity. Magnetostrictive and piezoelectric transducers are the most common. The former utilize the magnetostrictive property of a material to convert the energy in a magnetic field into mechanical energy (Massa n.d.). The magnetic field is provided by a coil of wire which is wrapped around the magnetostrictive material. Piezoelectric transducers use piezoelectric effect, previously explained.

In the 1930 magnetostrictive technology, eclipsed piezoelectric technology as the “motor” for ultrasonic devices including early ultrasonic cleaning systems. Magnetostrictive devices of that period were unquestionably more reliable than their piezoelectric partners. All of that began to change, however, with the development of new piezoelectric ceramics for use in SONAR applications during World War II. New, stronger, man-made ceramics replaced naturally occurring “crystals” as the source of vibration. In addition, ways were found to pre-stress the new piezoelectric materials. These ceramic materials, such as Barium Titanate and Lead Zirconate Titanate, are often referred to as piezoelectric ceramics and also produce an electric charge when a mechanical stress is applied, and vice versa. However, they must have an internal polarizing electric field established in order for transduction to occur. Their popularity is due to relatively low cost, coupled with the ability to be fabricated into a wide variety of shapes and sizes. During the 1950’s other improvements were reached, including better coupling with the medium or extra layers in order to obtain different qualities. This technology continues to advance to this day (Relaño Iborra 2014).

So, although there was a period in time when magnetostrictive transducers ruled the world of ultrasonic transducer and its applications, now it is back toward piezoelectricity as the preferred ultrasonic source. This effect is used in the transducer design presented in this thesis.

In the next sections a theoretical description of ultrasonic generation and transducer design is realized.

First, the bases of piezoelectricity are presented and the main properties and parameters of ultrasonic transducers are described. Secondly, elements that make up a transducer are explained and also a basic definition of what an echo sounder is and which parts has. Next, a brief summary of the linear wave equation, to solve wave's propagation in the water, is made and the active sonar equation is introduced. Sonar equation is extensively used in the targets detection in fisheries acoustics application.

Finally, we explain non-linear generation (the parametric sound generation), the operating principle of future echosounder and the numerical simulation models used both in study of transducer behaviour, within the design, as well as in study of parametric generation.

3.2. ULTRASOUND GENERATION: PIEZOELECTRICITY

Piezoelectricity, as mentioned in section 3.1, it was discover by Curie brothers in 1880(Curie and Curie 1880). Interaction between this effect and acoustic wave propagation, explained in section 3.5, fully characterized the ultrasonic transducer behaviour. This phenomenon has two aspects:

- Direct piezo effect

An electric potential difference (voltage) appears in some crystals when these are subjected to a mechanical deformation

- Inverse piezo effect

When an electric field is applied to certain crystals' surfaces, these suffer mechanical distortions. (Arnau 2008)

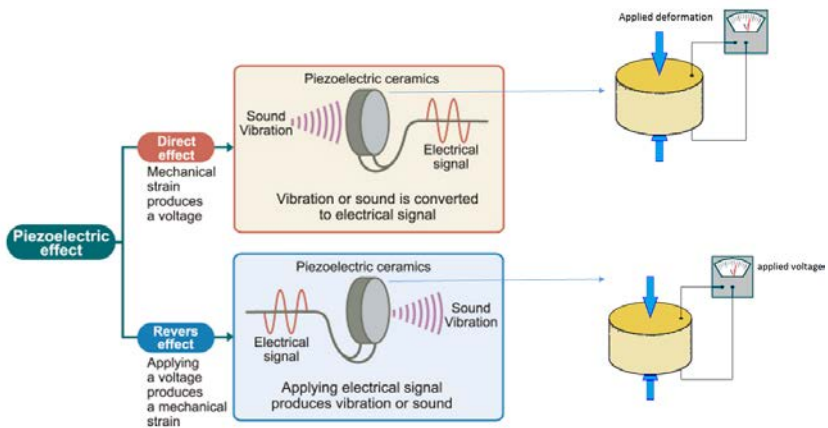


Figure 3.1. Piezoelectric effect in a piezoelectric ceramic.

Honda Electronics CO.LTD source

Piezoelectric effect can only occur in anisotropic materials, meaning materials that lack a centre of symmetry at the unit cell level. This asymmetry in the material allows the dipole generation and the appearance of the piezoelectric effect (direct and Inverse) (Moten 2011).

There are different materials that provide piezoelectric behaviour. The most simple are those with a natural character piezo (Quartz, tourmaline, salt Rochelle ...). Effect usually

occurs in them in a weaker form. In this thesis it is going to use the piezoelectric ceramics, but other materials as thermoplastics like PVDF (Polyviylidenefluoride) or copolymer have shown, in recent years, strong piezoelectric properties.

Piezoelectric ceramic materials are those that naturally contain dipoles, consistent in a positive charge and other negative at a certain distance. The main feature is that, spontaneously, the orientation of the dipoles does not show a particular direction, it is random. Therefore, even if an effort is applied it will show no potential difference, that is, no piezoelectric effect. A ceramic becomes a piezoelectric ceramic when it is subjected to a polarization process.

The process is performed by an external electric field at high temperature. The direction of the applied electric field is equal to the new direction of the dipoles. Once the electric field is removed, the orientation remains even when the material is cooled. Ceramic body has become, permanently, piezoelectric and it can convert mechanical energy into electrical and vice versa. As a precaution, it must not to exceed the Curie temperature of each material. If the material rise this temperature, it can lose polarization and dipoles will be orientated along random directions again. Once polarized, they have better properties than natural crystals. They can adopt more flexible geometries and dimensions. Polarization process is shown in figure 3.2

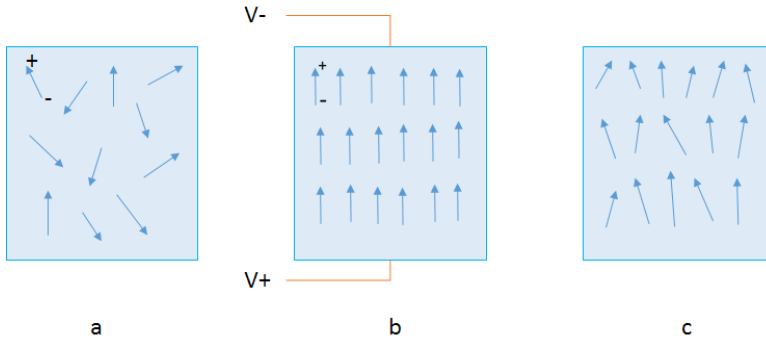


Figure 3.2.-Polarization process. (a)Random dipoles orientation.
Prior polarization. (b) Polarization in DC electric field. (c)
Remanent polarization after electric field

The piezoelectric materials mostly used in industry are barium titanate (BaOTiO_2), and a combination of lead zirconate (PbZrO_3) and lead titanate (PbTiO_3). In this combination, it is called in industry PZT (lead zirconate titanate) and are manufactured by powder compression at high temperature, moulded and baked in an oven.

3.2.1. PIEZOELECTRIC CONSTITUTIVE RELATIONS

Piezoelectricity involves interaction between the electric and mechanical behaviour of a medium. Constitutive equations of piezoelectric materials combine stresses, strains and electrical behaviour and are well defined in the IEEE Standard of Piezoelectricity (Standard 1988).

Taking into account two electrical variables: electric displacement (D) and electric field (E) and two mechanical variables: mechanical stress tensor (T) and strain tensor (S), there are four different ways to write the constitutive relations that define piezoelectricity. These relationships will always define two independent variables of the elastic part and the mechanical part.

One of the way to express the constitutive relations is described in equations (3. 1) and it is the one that is chosen to work in this thesis:

Stress-Charge Form

$$\begin{aligned} T_{ij} &= c_{ijkl}^E S_{kl} - e_{kij} E_k \\ D_i &= e_{ikl} S_{kl} + \epsilon_{ik}^S E_k \end{aligned} \quad (3. 1)$$

Where,

c_{ijkl}^E , elastic stiffness constant tensor at constant electric field [N/m²]

e_{kij}^t , piezoelectric coupling coefficient [C/m²]

ϵ_{ik}^S , dielectric constant tensor at constant strain [F/m]

Being i, j, k, l = 1, 2, 3

This variables will present complex values if elastic, piezoelectric and dielectric losses are introduced (Kocbach 2000a). As shown in equation (3. 1), the subscripts show that elastic and electrical variables are related not only in the direction in which the electric field is applied, but also in the perpendicular directions. Symmetry of the stress tensor enables nine stress components to be reduced to six independent stress components. This also enables the tensor notation to be transformed into pseudo -tensor form. Using this so-called contract Voigt subscript notation (11)→1, (22)→2, (33)→3, (23), (32) →4, (13), (31)→5, (12), (21)→6 . Moreover c_{ijkl} is reduced to $c_{\alpha\beta}$ with (ij) --> α and (kl) --> β . In the same way e_{kij} will become $e_{k\alpha}$. This allows to show an advantage in solving problems

piezoelectric first introduced by Barnet and Lothe (Barnet, D.M and Lothe,J 1975). Matrices would be written as follows:

$$\begin{bmatrix} T_1 \\ T_2 \\ T_3 \\ T_4 \\ T_5 \\ T_6 \end{bmatrix} = \begin{bmatrix} c_{11}^E & c_{12}^E & c_{13}^E & c_{14}^E & c_{15}^E & c_{16}^E \\ c_{21}^E & c_{22}^E & c_{23}^E & c_{24}^E & c_{25}^E & c_{26}^E \\ c_{31}^E & c_{32}^E & c_{33}^E & c_{34}^E & c_{35}^E & c_{36}^E \\ c_{41}^E & c_{42}^E & c_{43}^E & c_{44}^E & c_{45}^E & c_{46}^E \\ c_{51}^E & c_{52}^E & c_{53}^E & c_{54}^E & c_{55}^E & c_{56}^E \\ c_{61}^E & c_{62}^E & c_{63}^E & c_{64}^E & c_{65}^E & c_{66}^E \end{bmatrix} \begin{bmatrix} S_1 \\ S_2 \\ S_3 \\ S_4 \\ S_5 \\ S_6 \end{bmatrix} - \begin{bmatrix} e_{11} & e_{22} & e_{33} \\ e_{11} & e_{22} & e_{33} \end{bmatrix} \begin{bmatrix} E_1 \\ E_2 \\ E_3 \end{bmatrix} \quad (3.2)$$

$$\begin{bmatrix} D_1 \\ D_2 \\ D_3 \end{bmatrix} = \begin{bmatrix} e_{11} & e_{12} & e_{13} & e_{14} & e_{15} & e_{16} \\ e_{21} & e_{22} & e_{23} & e_{24} & e_{25} & e_{26} \\ e_{31} & e_{32} & e_{33} & e_{34} & e_{35} & e_{36} \end{bmatrix} \begin{bmatrix} S_1 \\ S_2 \\ S_3 \\ S_4 \\ S_5 \\ S_6 \end{bmatrix} - \begin{bmatrix} \varepsilon_{11}^S & \varepsilon_{12}^S & \varepsilon_{13}^S \\ \varepsilon_{21}^S & \varepsilon_{22}^S & \varepsilon_{23}^S \\ \varepsilon_{31}^S & \varepsilon_{32}^S & \varepsilon_{33}^S \end{bmatrix} \begin{bmatrix} E_1 \\ E_2 \\ E_3 \end{bmatrix} \quad (3.3)$$

3.2.1.1. PIEZOELECTRIC CERAMIC CASE

Poled ceramics are transversely isotropic material. The isotropy plane is defined as the 12 plane or xy plane. Piezoelectric ceramic therefore exhibits symmetry about 3-axis or (z-axis) with it is the poling axis of the material.

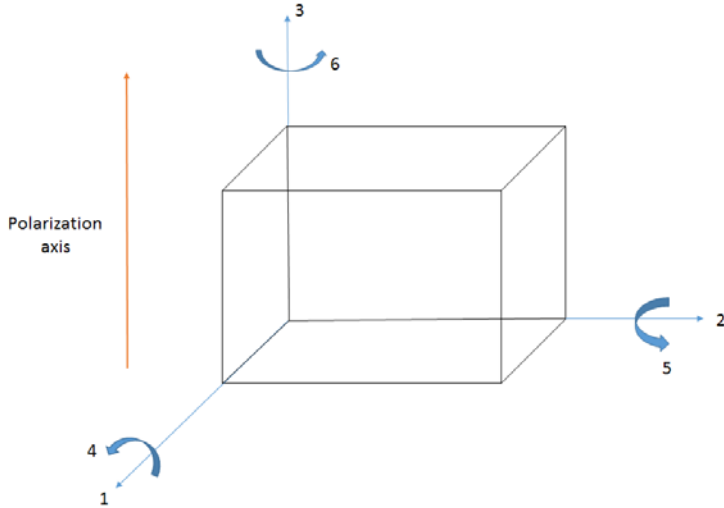


Figure 3.3.-Simmetria axis in piezoelectric ceramic

Due to this Z symmetry, the stiffness constant matrix followed by piezoelectric coupling coefficient matrix and dielectric matrix of equations.(3. 2) and (3. 3) are reduced to:

$$[c^E] = \begin{bmatrix} c_{11}^E & c_{12}^E & c_{13}^E & 0 & 0 & 0 \\ c_{12}^E & c_{11}^E & c_{13}^E & 0 & 0 & 0 \\ c_{13}^E & c_{13}^E & c_{33}^E & 0 & 0 & 0 \\ 0 & 0 & 0 & c_{44}^E & 0 & 0 \\ 0 & 0 & 0 & 0 & c_{44}^E & 0 \\ 0 & 0 & 0 & 0 & 0 & c_{66}^E \end{bmatrix} \quad (3.4)$$

$$c_{66}^E = \frac{1}{2}(c_{11}^E - c_{12}^E)$$

$$[e] = \begin{bmatrix} 0 & 0 & 0 & 0 & e_{15} & 0 \\ 0 & 0 & 0 & e_{15} & 0 & 0 \\ e_{31} & e_{31} & e_{33} & 0 & 0 & 0 \end{bmatrix} \quad (3.5)$$

$$[\varepsilon^S] = \begin{bmatrix} \varepsilon_{11}^S & 0 & 0 \\ 0 & \varepsilon_{11}^S & 0 \\ 0 & 0 & \varepsilon_{33}^S \end{bmatrix} \quad (3.6)$$

Specifications of piezoelectric materials are divided into three properties: electrical, mechanical and electromechanical. Without going to define all the parameters within each of these properties it can be highlight the following described below for their special interest.

- Coupling factor (k): A measure of the material's ability to transform energy from one form to another, it cannot be considered as transducer performance. It does not account for losses but shows the efficiency of the material.

- Loss: Piezoelectric ceramics present losses. They have three loss types: dielectric, mechanic and piezoelectric. The way to introduce them in the calculations is through the use of complex permittivity, stiffness and piezoelectric matrix. In this thesis only mechanical and dielectric losses are going to be use, because there is not reference data for piezoelectric losses. Parameters which determine these losses are the following:

-Mechanical quality factor (Q_m): It determines the material performance and bandwidth. For example, if we want to use a particular material for power applications, high Q factor is desirable due to its few losses and lower bandwidth. However, if what we seek is higher bandwidth it is necessary a small Q factor and considerable losses.

-Dielectrical Dissipation factor, ($\tan \delta_e^T$): quantifies a dielectric material's inherent dissipation of electromagnetic energy.

3.3. ULTRASONIC TRANSDUCER AS A TRANSMITTER.

Ultrasonic beam generation from a piezoelectric disc transducer presents several characteristics that will be explained below.

When an ultrasonic beam is generated there are two regions along the beam propagation that should to be considered: Near field or Fresnel zone and the Far field or Fraunhofer zone.

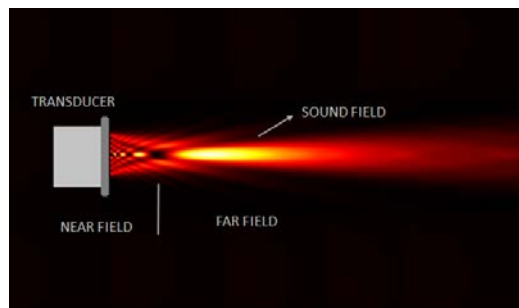


Figure 3.4. Ultrasonic sound beam propagation

According to Huygens principle, a transducer can be considered as a set of separate elements each radiating hemispherical waves forward. Ultrasound intensity along the beam is affected by constructive and destructive wave interference. This wave interference leads to extensive fluctuations in the sound intensity near the source and is known as the near field, where maximum and minimum pressure are presented. Because of acoustic variations within a near field, it can be extremely difficult to accurately evaluate flaws in materials when they are positioned in this region.

However, in the Far field, the wave interference is minimized, the waves are in phase, and pressure decreases inversely with distance from the source, diverging spherically. (Figure 3.5)

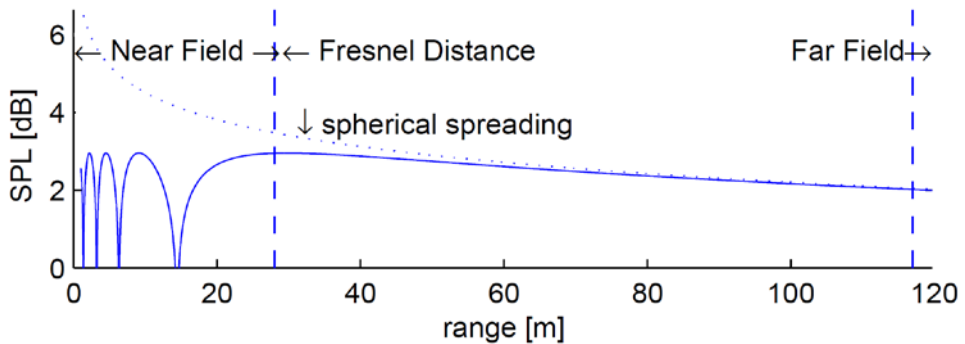


Figure 3.5. On-axis SPL from a circular piston

Fresnel distance is the limit of the near field and is defined as the distance from the source beyond which the amplitude do not oscillate anymore. It is related to the diameter of the transducer and the wavelength of the ultrasonic beam by the following equation:

$$N = \frac{D^2}{4\lambda} \quad (3.7)$$

Where,

N = length near field

D = Transducer diameter (mm)

λ = Transducer wavelength

In the far field region, ultrasound acoustic wave from a transducer diverges spherically, so pressure decreases inversely with distance from the source. Moreover, pressure amplitude wave also decreases exponentially with distance due to the absorption losses of the medium (Section 2.4.1). Considering a harmonic source, the sound pressure, p , in a point located at a distance R from the source, lying on the far field zone, is given by the following expression

$$p(R, \theta, \varphi) = p(R_0, \theta, \varphi) \frac{R_0}{R} e^{-\beta(R-R_0)} e^{-j \cdot k(R-R_0)} \quad (3.8)$$

where R_0 is the reference distance to the source (typically 1 m), $k = 2\pi / f$ is the wavenumber, f is the frequency of the acoustic wave and β is the absorption coefficient of the medium usually expressed in Np / m or Np / km. R , θ and φ are the spherical coordinates of the point of the field relative to the sound source, which is at the origin of the coordinate system (Kinsler et al., 1999).

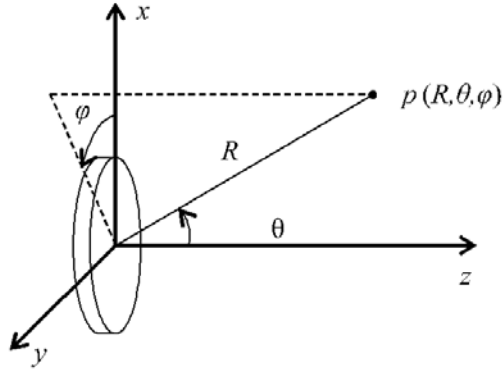


Figure 3.6. Coordinate system used for describing the propagation of an acoustic wave, where the source is a disc centred at the origin of coordinates.

Acoustic pressure can also be expressed in dB by the sound pressure level LP, which is a logarithmic scale of measured pressure at a point relative to a reference pressure, and is defined by

$$LP(R, \theta, \varphi) = 20 \log \frac{p_{rms}(R, \theta, \varphi)}{p_{ref}} \quad (3.9)$$

Where effective pressure of the acoustic wave is p_{rms} being R.M.S equals to root mean square value of pressure and p_{ref} is the reference effective pressure. Underwater acoustic applications usually employ $p_{ref} = 1 \mu\text{Pa}$.

In addition, sound beam carries a certain amount of energy produced by the transducer, per unit time, is what is known as acoustic power. The power unit is the watt (W). The ratio between the power and the beam surface is the intensity (W / cm²). This latter feature is of great importance and it relates the amount of ultrasound energy in every moment into an area.

In far field conditions, ultrasound wave intensity I is proportional to the square of the pressure and can be expressed as:

$$I(R, \theta, \varphi) = \frac{p_{rms}^2(R, \theta, \varphi)}{\rho_0 \cdot c} \quad (3. 10)$$

Where ρ_0 is the medium propagation density.

Like pressure, intensity can be expressed in dB through acoustic intensity level LI, logarithmic measurement of the intensity in a point with respect to a reference intensity and is define as

$$LI(R, \theta, \varphi) = 10 \log \frac{I(R, \theta, \varphi)}{I_{ref}} \quad (3. 11)$$

Being I_{ref} the reference intensity. Relation between LP y el LI comes from

$$LI(R, \theta, \varphi) = LP(R, \theta, \varphi) + 10 \log \frac{P_{ref}^2}{\rho_0 \cdot c \cdot I_{ref}} \quad (3. 12)$$

Usually, intensity reference used corresponds to $I_{ref} = 1 \mu\text{Pa}$ effective pressure of the acoustic wave.

Due to the spherical divergence and medium absorption, intensity decreases when ultrasound acoustic wave propagates through the medium taking into account the distance from the source. Intensity reduction can be obtained from equations 3.8 and 3.10 as

$$\frac{I(R, \theta, \varphi)}{I(R_0, \theta, \varphi)} = \left(\frac{R_0}{R} \right)^2 e^{-2 \cdot \beta (R - R_0)} \quad (3. 13)$$

Where β the acoustic absorption coefficient in Np/m and it is equals to

$$\beta = \frac{\alpha}{8.69}$$

If is consider 1m as a reference distance and knowing water absorption is much lower than 1, can be employ the next approximation.

$$\frac{I(R, \theta, \varphi)}{I(R_0, \theta, \varphi)} \approx \frac{1}{R^2} e^{-2 \cdot \beta \cdot R} \quad (3. 14)$$

As it was mentioned, in section 2.4.1, transmission loss of ultrasonic waves is due to medium absorption and to geometrical spreading. In the far field region geometrical divergence is defined by intensity decreasing with the distance to the source. In homogenous medium, with a small radiating source propagating in all directions, energy spreads spherically. As energy is conserved, the intensity will decrease proportionally to the inverse of the surface

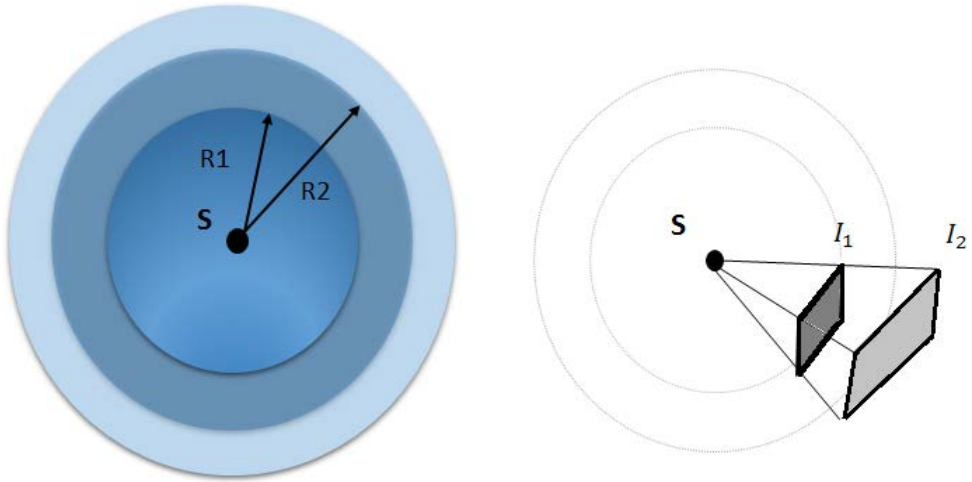


Figure 3.7. Source point propagation with spherical divergence

Hence intensity decreases in $1/R^2$ and pressure in $1/R$. Amplitude dependence was introduced in equation (3.8). The spreading transmission loss can be expressed in dB as

$$TL = 20 \log \left(\frac{R}{R_0} \right) dB \quad (3.15)$$

When losses for medium absorption are added the equation describing the transmission losses is transformed into

$$TL = 20 \log\left(\frac{R}{R_{1m}}\right) - 2\alpha R \quad (3. 16)$$

3.3.1. CHARACTERIZATION OF ELECTROACOUSTIC PARAMETERS.

Taking into account the relationship between the electric and acoustic part of a transducer, electroacoustic parameters are defined. They allow to know in depth the transducer's operation, as well as they are used as a comparison tool between several designs. Moreover they provide a system calibration. This calibration guarantees quality measurement. Depending on the transducer type, it is possible to establish general procedures to calibrate. There are three different kinds of calibration:

- Field calibration:

It is realized in the measurement place using a reference source or calibrated target. It is recommended to carry out before and after the measure. It is the easiest way to check configuration settings, operation, etc.

- Laboratory calibration:

It is not done in free field. It is necessary a stable and controlled environment. It is more precise than field calibration due to the smaller temperature, wind and humidity variability.

- Factory calibration:

Commercial transducers are supplied with a calibration certificate. It guarantees the right behaviour for their application and tolerances proportionated in technical data. These measurements are carried out with certified measurement devices and in laboratory conditions

Measurements performed along this thesis are under laboratory conditions. The different calibration methods will provide each of the parameters considered essential in the characterization of an electroacoustic transducer that will be defined in the following.

Most relate parameters describe both the electrical and mechanical part of the transducer. However, there is an electrical parameter that allows to know quickly, important features about our design as resonance frequency of the system, quality factor, etc. This parameter is the electrical admittance (Y). It measures the ease current flow through the circuit or system. It is defined as the inverse of the electrical impedance (Z). It is measured in Siemens (S).

$$Y = \frac{1}{Z} \quad (3.17)$$

Y is a complex number that can be written in binomic form (real and imaginary parts) as

$$Y = G + jB \quad (3.18)$$

Where,

G is the conductance, B is susceptance and j is the imaginary unit defined by $j^2=-1$

Conductance is in charged in how easily is the energy flow meanwhile the susceptance express how easily the system stores energy.

Efficiency, η , is another important parameter to be considered in any transducer. It is defined as the ratio between the acoustic power radiated by the transducer and the electrical power that is given W_{Tx}

$$\eta = \frac{W}{W_{Tx}} \quad (3. 19)$$

In the linear regime, a transducer radiates an acoustic wave with amplitude proportional to the transmitter sensitivity. In the opposite direction when a transducer captures acoustic waves, the electrical signal is proportional to receiving sensitivity. Transmitter sensitivity, $S_{Tx,v}$ or Transmission voltage response (TVR) is the ratio between the amplitude of the sound pressure, extrapolated backwards from the far field, with a reference distance on the acoustic axis, usually 1m, and the voltage amplitude applied to the transducer terminals

$$S_{Tx,v} = \frac{p_{inc}(R_0, 0, 0)}{V_{Tx}} \quad (3. 20)$$

where p_{inc} is the pressure generated by the source and V_{Tx} is the voltage applied to the transducer. Sensitivity can also be expressed in terms of current $S_{Tx,i}$ as the ratio between

pressure generated at the reference distance on the acoustic axis and the current supplied to the transducer during the transmission I_{Tx} ,

$$S_{Tx,i} = \frac{p_{inc}(R_0, 0, 0)}{I_{Tx}} \quad (3. 21)$$

Relationship between sensitivity defined in voltage and current is given by

$$S_{Tx,i} = S_{Tx,v} \cdot |Z_T| \quad (3. 22)$$

where Z_T is the electric impedance in the transducer terminals.

In the echoes reception, relation between open circuit voltage V_0 and the incident pressure in the front face of the transducer p_{bs} define transducer receiver sensitivity S_{Rx} or open circuit voltage (OCV) as,

$$S_{Rx} = \frac{V_0}{p_{bs}} \quad (3. 23)$$

In reciprocal transducers with spherical propagation, there is a parameter called reciprocity parameter, J . It is the relation between receiver sensitivity and the transmitter sensitivity during the radiation (Urick, 1983), it is defined as

$$J = \frac{S_{Rx}}{S_{Tx,i}} = -j \frac{2 \cdot \lambda \cdot R_0}{\rho_0 \cdot c} \quad (3. 24)$$

where λ is the wavelength. When one sensitivity is known, projector or receiver sensitivity, it is possible to obtain the other by the reciprocity parameter. For spherical waves, the relationship between sensitivities is given by

$$20 \log \frac{S_{Rx}}{1V/\mu Pa} = 20 \log \frac{S_{Tx,i}}{1\mu Pa/A} - 354 - 20 \log f (kHz) \quad (3. 25)$$

Reference distance here is 1m, water density 1000 kg/m³, and reference pressure, 1 μ Pa (Urick, 1983).

In some transducers, as it is the case of transducers used in echo sounders, sensitivity is highly dependent on the acoustic wave direction. For a directive source, pressure in one point can be expressed in terms of the pressure axis at a reference distance, propagation loss and directivity function $D(\theta, \varphi)$

$$p_{inc}(R, \theta, \varphi) = p_{inc}(R_0, \theta, \varphi) \frac{R_0}{R} e^{-\beta(R-R_0)} \sqrt{D(\theta, \varphi)} \quad (3. 26)$$

Directivity function, also called radiation pattern, is defined as the square of the ratio between the acoustic pressure amplitude generated at a reference distance and the pressure

amplitude on the acoustic axis in a distance under interest, considering the axis as the maximum radiation direction

$$D(\theta, \varphi) = \left| \frac{p_{inc}(R_0, \theta, \varphi)}{p_{inc}(R_0, 0, 0)} \right|^2 \quad (3. 27)$$

This parameter describes how transducer radiates depending on the direction. For a reciprocal transducer, receiver directivity is equal to transmission directivity. When transducer operates as a hydrophone, directivity is defined as the ratio to the square of terminals voltage V_{Rx} in the front face transducer from any direction and the voltage from axis transducer direction.

$$D(\theta, \varphi) = \left| \frac{V_{Rx}(\theta, \varphi)}{V_{Rx}(0, 0)} \right|^2 \quad (3. 28)$$

By definition D is equal to 1 in the axis transducer (highest sensitivity) and less than 1 in the other directions. Usually Directivity pattern is expressed in logarithmical scale, D_{dB} according to

$$D_{dB}(\theta, \varphi) = 10 \log D(\theta, \varphi) \quad (3. 29)$$

For a flat circular piston radius r , mounted on an infinite screen and $r \gg \lambda$, directivity function in far field can be calculated according to the following expression

$$D(\theta, \varphi) = \left(\frac{2 \cdot J_1(k \cdot r \cdot \sin \theta)}{k \cdot r \cdot \sin \theta} \right)^2 \quad (3. 30)$$

Being J_1 Bessel function order 1 (Kinsler *et al.*, 1999; Sherman & Butler, 2007).

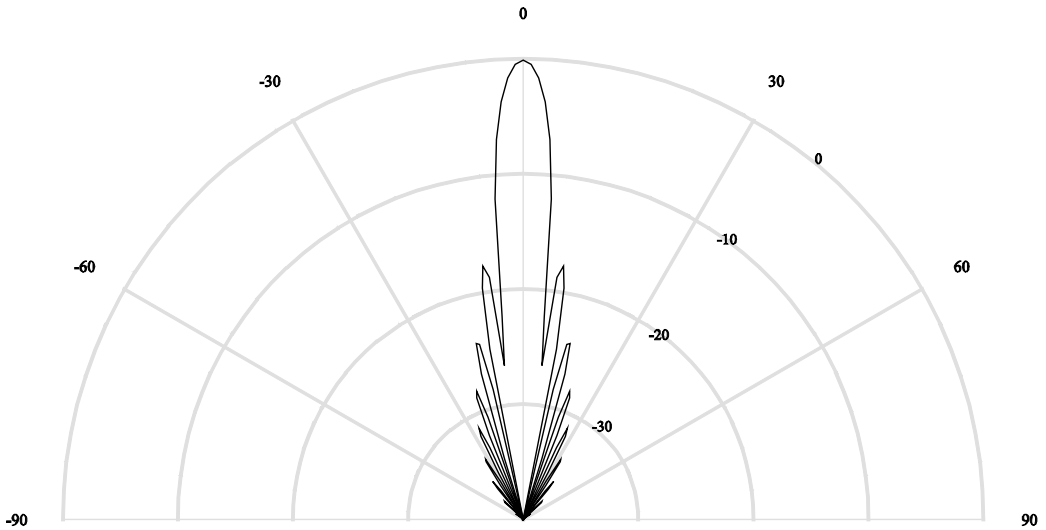


Figure 3.8 represents directivity

Figure 3.8. Circular piston pattern with 4 cm radius, mounted in an infinite screen, at 200 kHz ($kr = 33.5$) radiation of a circular piston with 4 cm radius at 200 kHz.

Acoustic pressure level (LP) can also be expressed using the logarithmic expression of Equation 3.26, so LP anywhere at far field region of the source can be calculated as

$$LP(R, \theta, \varphi) = SL - TL(R) + D_{dB}(\theta, \varphi) \tag{3.31}$$

where SL is the source level, defined as the level of pressure generated by the source on the acoustic axis to a reference distance and far field conditions as defined in equation 3.9

However, sometimes it is more convenient to estimate source level through transmitter sensitivity and rms voltage $V_{Tx,rms}$ in transducer terminals, according to (Moszyński, 2005)

$$SL = 20 \log S_{Tx,v} + 20 \log V_{Tx,rms} \quad (3.32)$$

Another way to express SL is using electrical power supply to the transducer

$$SL = 10 \log W_{Tx} + ID_{max} + 10 \log \eta + 170.8 \quad (3.33)$$

where ID_{max} is the maximum directivity index (Kinsler et al., 1999; Moszyński, 2005; Balk & Lindem, 2011).

Transducer directivity can also be expressed through the directivity factor, Q . It is the ratio between the acoustic intensity in that direction and the intensity that would transmit n isotropic source I_{iso} with equal power

$$Q(\theta, \varphi) = \frac{I(\theta, \varphi)}{I_{iso}} \quad (3.34)$$

It can be expressed in logarithmic scale through directivity index ID. It is defined as

$$ID = 10 \log Q(\theta, \varphi) \quad (3.35)$$

In the maximum radiation direction it is satisfied that

$$Q_{m\acute{a}x} = Q(0,0) = \frac{4 \cdot \pi}{\int_{4\cdot\pi} D(\theta, \varphi) \cdot d\Omega} \quad (3.36)$$

$$ID_{m\acute{a}x} = 10 \log Q_{m\acute{a}x} \quad (3.37)$$

where $d\Omega$ is the solid angle difference. It can be seen than radiation pattern and directivity pattern keep the next relation

$$Q(\theta, \varphi) = Q_{m\acute{a}x} \cdot D(\theta, \varphi) \quad (3.38)$$

Similarly, relationship between radiation pattern expressed in dB and directivity index is given by

$$ID(\theta, \varphi) = ID_{m\acute{a}x} + D_{dB}(\theta, \varphi) \quad (3.39)$$

For a flat circular piston radius r , mounted on an infinite screen and $r \gg \lambda$, $ID_{m\acute{a}x}$ scan be approximated by

$$ID_{m\acute{a}x} \approx 10 \log (k \cdot r)^2 \approx 45.5 - 20 \log \theta_{-3dB} \quad (3.40)$$

where θ_{-3dB} is -3 dB beam aperture expressed in degrees (Urlick, 1983; Kinsler *et al.*, 1999; Sherman & Butler, 2007).

-3 dB beam aperture is defined as the angle in both directions to the main lobe, where pressure level fall off 3 dB respect to the main axis, this means, where $D = 1/2$ (Simmonds & MacLennan, 2005).

For this thesis, it is used a circular transducer and 3dB beam aperture can be expressed as

$$\theta_{-3dB} = \frac{58 \cdot \lambda}{2 \cdot r} \quad (3.41)$$

where θ_{-3dB} is expressed in degrees (Lurton, 2002; Moszyński, 2005; Sherman & Butler, 2007).

3.4. TRANSDUCER ELEMENTS

For the purpose of this thesis, the design of a single-element piston transducer is realized. It is the simplest ultrasonic transducer, with only one active element involved.

These transducers can be designed with two types of configurations: flat configuration and focused configuration. The latter is that whose vibrating surfaces have a certain curvature causing the energy to concentrate at a certain focus point, improving the lateral resolution and adding gain to the system (Peña 2014). For fisheries acoustics application, it is usual to opt for the first configuration, since it is desirable to insonify an entire area equally. However, limitation in the lateral resolution due to the geometric dispersion of the beam with distance must be taken into account.

Main components of a simple ceramic ultrasonic transducer are: Active element, damping block (backing) and a matching layer. The main characteristics and functions of each of them are described below:

- ACTIVE ELEMENT:

Piezo or ferroelectric material that converts electrical excitation energy into mechanical energy. The most commonly used materials are polarized ceramics. These include the PZT (Lead Zirconate Titanate). Due to their relatively high coupling capacities and low dielectric loss have been used in widely electromechanical application. For specific applications, proper piezoelectric materials are chosen according to a number of factors such as their piezoelectric performance, dielectric properties, elastic properties and stability. Piezoelectric materials vibrate sinusoidally after their exposure to an electric field has ended. The frequency of that oscillation is known as the fundamental resonance frequency of the transducer. Depending on which faces of the ceramic electric field has been applied, the frequency will be related to one of its dimensions (Kinsler 2000; Silva and Santos 2006). For this thesis piezoelectric ceramic disc is going to be used. This means, as it was explained in section 3.2.1.1, it has polarization in the Z-axis, exhibiting symmetry and null particle displacement at coordinate $y=0$. Therefore amplitude of oscillation must be a maximum at the ends, where $y=\pm L_T / 2$, being L_T the thickness of the transducer(Arnau 2008). Moreover this condition force that thickness resonance frequency is:

$$F_{nr} = nF_r = n \frac{v_L}{2L_T} \rightarrow n = 1, 2, 3 \quad (3. 42)$$

Where, F_r is the fundamental resonant frequency in the thickness mode and its multiples are called harmonic of the fundamental frequency.

- DAMPING BLOCK

It is usually a non-conductive material that attaches to the element active rear face and it is in charge to absorb the "reverse" ultrasound wave that is transmitted to the back of the piezoelectric ceramic (Rubio and Marrero n.d.). In order to achieve this function, it is played with the acoustic impedances of the materials following the transmission coefficient equation:

$$T = \frac{2Z_2}{Z_1 + Z_2} \quad (3.43)$$

where T is the Transmission coefficient, Z_1 and Z_2 are the piezoelectric ceramic and backing acoustic impedance respectively.

Following this equation, when acoustic material impedance used as backing is more similar to the active element, more energy will be transmitted towards the first, resulting a strongly damped transducer. It will therefore have lower sensitivity and higher bandwidth. In contrast, if the impedance of both differs, more energy will be reflected forward and there will be a low damping, which will improve the transducer sensitivity reducing the bandwidth. In this design, it is sought to obtain a bandwidth, as long as there is a trade-off between maximizing bandwidth with maintaining an acceptable device sensitivity to work over the distance that is needed.

- MATCHING LAYER:

It is a material layer that is inserted between the piezoelectric element and the medium load through which the ultrasonic wave is transmitted. This intermediate layer allows a more effective energy transmission. Piezoelectric ceramics usually have very high acoustic impedances, of the order of $\sim 30\text{MRayls}$, whereas the load medium by which they transmit the waves may be much smaller. For example, the water which is the transmission medium for this work consists of an acoustic impedance of 1.5MRayls . This difference causes that the acoustic energy does not propagate properly and a coupling layer is needed.

In terms of selecting the proper acoustic impedance, several studies have been done. The most extended gives the next expression introduced by (Al-Budairi 2012; Moten 2011):

$$Z_m = (Z_c Z_L)^{1/2} \quad (3.44)$$

Where Z_m is the matching acoustic impedance, Z_c and Z_L are the piezoelectric ceramic and load medium acoustic impedance respectively.

There are other equations that introduce an improvement in the band signal like:

$$Z_m = (Z_c Z_L^2)^{1/3} \quad (3.45)$$

For thickness-mode operation transducer, the optimum thickness for this layer is one-quarter wave length of resonance frequency following $\lambda/4$ transmission line sections in microwave applications. Basically by using this size, a phase reversal occurs, which increases signal performance and strengthens the wave front entering the medium.

Passive elements described are able to provide certain characteristics to the transducer. These characteristics do not only depend on the relationship of impedances but also on the elements thickness. For this reason when designing a piezoelectric transducer, with all its components, we can make use of various tools to know how the global response will be. By one hand these include numerical models described above and by another hand, analytical models, based on piezoelectricity equations, which relate mechanical and the electrical parts of the transducer.

However, it is usually more convenient to use a one-dimensional equivalent electrical circuit, using the fundamental electromechanical analogies. In these analogies, mechanical forces are equivalent to the voltage applied at the transducer terminals and the particle velocity at the electric current.

From them, there were several contributions, the most outstanding being those produced between 1948 and 70, by Mason (Mason 1948) Redwood (Redwood 1961) and Krimholtz, Leedom and Matthaei (Krimholtz, Leedom, and Matthaei 1970).

All of them have been widely used for design and optimization, but the latest (KLM) is consolidated as the most used circuit nowadays. Figure 3.9 shows KLM scheme:

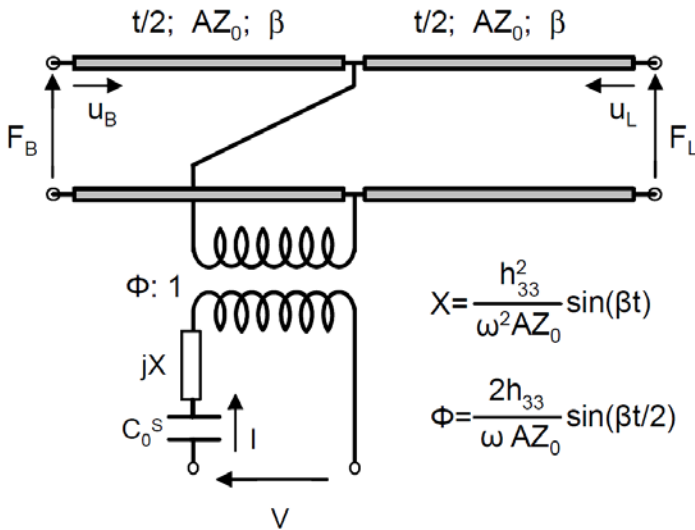


Figure 3.9. KLM equivalent circuit of a thickness extensional piezoelectric transducer(Arnau 2008)

Where

F_B , is the force on the back face

t is the thickness of the piezoelectric plate

u_B , is the particle velocity at the front face

Z_0 , is the characteristic impedance

A , is the area of the electrode

u_L , is the particle velocity at the front face

F_L , is the force on the front face (radiating surface)

X, Reactance

$\beta = \omega / (c_{33}^D / \rho)^{1/2}$ the propagation constant.

C_0 , is a capacitance

Φ , Transformer ratio

Electrical impedance at the transducer terminals $Z_{in}(\omega)$, in the most general case, when the mechanical ports are terminated by back block (Z_B) and load medium (Z_L) can be derived as:

$$Z_{in}(\omega) = \frac{1}{j\omega C_0^S} \left(1 + \frac{k_t^2}{\beta t} \frac{j(Z_L + Z_B)Z_0 \sin\beta t - 2Z_0^2(1 - \cos\beta t)}{(Z_0^2 + Z_L Z_B)\sin\beta t - j(Z_L + Z_B)Z_0 \cos\beta t} \right) \quad (3.46)$$

Apart from these models there are other forms of representation as the two-port networks, for example, based on Transfer matrix coefficients (Arнау 2008)

3.5. SCIENTIFIC ECHOSOUNDER

Transducer, once designed, can be integrated into a larger system. In this work, its design is proposed for its later use within a scientific echo sounder, which is a particular type of SONAR.

SONAR (Sound Navigation and Ranging) system is one of the largest applications in underwater acoustics. It is the general term used to refer to any device that uses sound for detection or remote observation of objects immersed in water. Sonar can be classified into two main groups: passive sonar and active sonar. Passive sonar uses the sound radiated

by the target itself to detect and locate it. However, active sonar detects and processes the echoes received from the acoustic signal that it has radiated itself.

An echosounder is a particular type of active sonar. Basically it is conformed for several components: A transmitter, a transducer, a receiver, and a representation system of detected echoes(Simmonds John 2007).

Transmitter, formed by an electric signal generator and an amplifier, is responsible for generating sinusoidal electric short pulse duration at a given frequency and amplifying its level. Typical frequencies oscillate in a range from 38 to 400 kHz. Low frequencies can detect targets at greater distances, since the absorption of sound in water increases rapidly with frequency, but high frequencies present more resolution. Application definition will give the optimal value for this parameter

Transducer transforms the electric pulse generated by the transmitter into an acoustic pulse, radiating sound in a directional beam. This beam is characterized mainly by the beamwidth and its operation frequency. When acoustic pulse propagating through the water encounters a target it is scattered or reflected, and some of the energy goes back in the transducer direction forming what is called an echo. Transducer detects this echo and converts it into an electrical signal. Time elapsed between pulse emission and echo reception gives information about the distance to which the target is located.

Receiver is in charge to receive the signal by the transducer and displayed on an echogram. After a certain time the transmitter emits another pulse and repeats the entire process, resulting in a two-dimensional representation by connected echo-traces. The echogram is a representation of the target. The horizontal trace position shows the depth to which the echo is. The vertical position shows variations in time if echosounder is in a fixed position,

or variations in space if echosounder is mounted on a moving vessel. Echo amplitude is represented by a colour scale. (Sanchez Carnero 2012; Simmonds 2005)

The simplest echo sounders are primarily used to locate fish schools or determine the sea floor depth. They provide little information on the number of detected target. This problem had now been overcome with the advent of scientific echosounders. They are more sophisticated instruments, built with the same basic components. However, its electronics have been designed with amplitude stability and with some additional features such as filtering and an accurate time-varying gain (TVG) amplifier on the receiver. A signal filtering from the transducer is performed to decrease the noise level present in the signal. The TVG provides compensation due to the losses suffered by the acoustic wave in the expansion beam and the medium absorption, obtaining an echo amplitude independent of the distance to the target. (Marek and Tel n.d.)

As a result, a sufficiently accurate signal is obtained to evaluate different material layers in sub bottom profile application or count individual fish and measure school fish density in fisheries acoustic application. Moreover, for this last application, some echosounder can incorporate an eco-integrator, which provides a signal proportional to the density of fish. As explained below, some transducers are sensitive to target direction and provide a direct measure of target strength (Section 2) when they detect individual fish.

In an echo sounder the beam is directed vertically downwards in most of the devices used for fishing and bathymetry. Nevertheless, it can also be oriented upwards, to take ventral measures for example, or even laterally. It is used mainly in the distances estimation and incidence angles, and in the targets identification and characterization.

Depending on the beam radiation pattern, the following transducers types, standing the echosounders name, are considered:

- Single-beam transducer: The signal provided depends on the direction of the target with respect to the acoustic axis and the target cross-section. It does not provide information on the target direction, so the target power estimation is performed indirectly using statistical methods (Craig and Forbes 1969).
- Dual-Beam transducer: Facilitates direct target power measurement. Transducer ceramic elements are arranged in concentric circles around a central element. If a narrow beam is required, signal is applied to all elements, if the required beam is wide signal is applied only to the central elements. Received signal for the wide and narrow beam is processed separately. The intensities ratio, between wide beam and the narrow beam, provides information with some ambiguities regarding direction. These deviations can be minimized by applying thresholds to the intensities. (Balk and Linderm 2008)
- Split-beam transducer: Performs direct target power measurement, compensating for the transducer radiation pattern. Transducer is divided into four quadrants, determining the target direction, precisely, by comparing phase differences between quadrants (Rudstam et al. 1999). Pulse is emitted by the entire transducer, but the signals received by each quadrant are processed separately.

Prototypes designed are single-beam in this dissertation. Instead of radiation pattern correction, the main matter of interest will be the transducer capacity to operate as a multiple transducer, it indicates, the simultaneous transmission of two frequencies. This transmission, at high power levels, will cause the parametric effect in the medium, which has been explained in more detail in Section 2.3, and thus the obtainment of a parametric echosounder.

3.6. ACTIVE SONAR EQUATION

Thus far, there has been talked about beam properties generated by a transducer, electroacoustic transducer properties, and wave equation that help us to solve the propagation of acoustic waves in a given medium. However, with regard to echo sounder operation, where transducer operates as transceiver, (Section 3.5) another equation has relevance in underwater acoustic field, the sonar equation.

A sonar equation is the equation of energy conservation that relates several parameters described in the previous section, and new ones such as TS that will be explained below. It was originally developed to describe sonar performance and consists in a sum of decibellic magnitudes.

For the particular case of the echo sounder where two paths are considered, it would be like:

$$\underbrace{SL - 2TL + TS - NL}_{\text{ECHO LEVEL}} > DT \quad (3.47)$$

Where:

SL , is the source level. It is defined as the pressure level at particular distance (Equation 3.32).

TL , is the transmission loss (spreading divergence and medium absorption)

TS , is the target strength. This new concept introduced in brief in chapter one is a logarithmic measure of backscattering and can be defined as the proportion of incident energy that disperses back to the transducer.

$$TS = 10 \log \frac{I_{bs}}{I_{inc,r=1m}} \quad (3.48)$$

Depends on shape, orientation and size of target

NL , is the noise level present in the medium

DT , is the detection threshold.

Threshold detection, DT , is the value by which the echo level must exceed the detected noise level in order to discriminate target.

This equation is used in fisheries acoustics to obtain the echo level produce by a target, e.g. single fish or fish aggregations (fish schools).

4

Numerical Simulation Methods

Numerical models have become, nowadays, powerful design tools at engineering level. Through them, you can simulate systems under study and know the behaviour of these a priori.

This chapter presents the different numerical models used, both for design and characterization of the selected prototypes, as well as to study the nonlinear generation that occurs with parametric effect

4.1. TRANSDUCER DESIGN AND WAVE PROPAGATION

The first numerical method for describing transducer behaviour is the finite element model (FEM). FEM is a extensively used numerical technic to approximate solutions of partial

differential equations. Due to these equations, it is possible to solve engineering and mathematical physics problems.

When these problems involve complicated geometries, loadings, material properties, etc. mathematical analysis to clear the unknown variables is sometimes impossible. The basic concept about FEM is to approximate the unknown variables' solutions only in a discrete number of elements. These elements cover the entire continuum and are interconnected between them for a series of points called nodes. The equations governing the behaviour of the continuum also govern the elements' behaviour (Nikishkov 2004).

Based on this, it is derived from a complex system with infinite degrees of freedom (DOF), governed by a differential equation or system of differential equations, a system with a finite degrees of freedom whose behaviour is modelled by a system of equations.

4.1.1. BRIEF HISTORICAL BACKGROUND

This section provides a brief overview of the most important events done in the history of FEM. Although it is a fairly current method, it can be said that the first progress in this area were by Isaac Newton and Leibniz in the XVII century, laying the foundations of infinitesimal calculation. With it is possible to analyse, precisely, functions with continuous domains.

Later, in 1909 a theoretical physicist, Walter Ritz (Leissa 2005) developed an effective method to approximate solutions for mechanical deformations in solids.

However, was not until 1940s, when this technic, following specifically the mechanic field, acquire an important developing due to Hrennikoff (Hrennikoff 1941) and McHenry works..

That same year,1943, the mathematician Courant propose an especial method distinct from that submitted by Ritz. He used polynomic functions for the formulation of elastic problem in triangular subregions.

In 1947, Levy (Levy,1947.), gave his contribution developing a strength and flexibility method. Due to its effort to solve the problems by hand,it was not popular until the advent of digitize computers.

Not until 1960, the term “finite element” is introduced formally. People who introduced the method as it is known at present were Turner, Clough, Martin and Trom (Clough 1960). They implemented stiffness matrix, triangular and rectangular elements for stress analysis etc.

Over the years, this technic get an extension in three-dimensional problems by Gallagher et al and Zienkiewicz (Zienkiewicz, Watson, and King 1968).

From 1963 until nowadays, new formulations have been registered to apply them in several applications as Aerospace, Civil and Automotive engineering, Structural/Stress Analysis, Fluid flow, Heat transfer, Acoustics, etc. Within the latter, we can found authors that have been simulating through the years, ultrasonic transducer, (Abboud 1998),(Hossack and Hayward 1991). Some of them focus in the internal behaviour (piezoelectricity theory) and others about all the concern to ultrasonic transducer propagating in the acoustic medium.

4.1.2. MAIN CONCEPTS AND PROCEDURE

As mentioned above, the idea of FEM method is to discretize a continuum in a series of elements connected each other, via points called nodes. At each node, a set of unknown variables are established for later resolution. These unknown variables are called degrees of freedom (DOF). DOF, therefore, are variables that determine the node status and / or node position. The infinite system is now a finite system to work with.

In any system to be analysed must be differentiated the following:

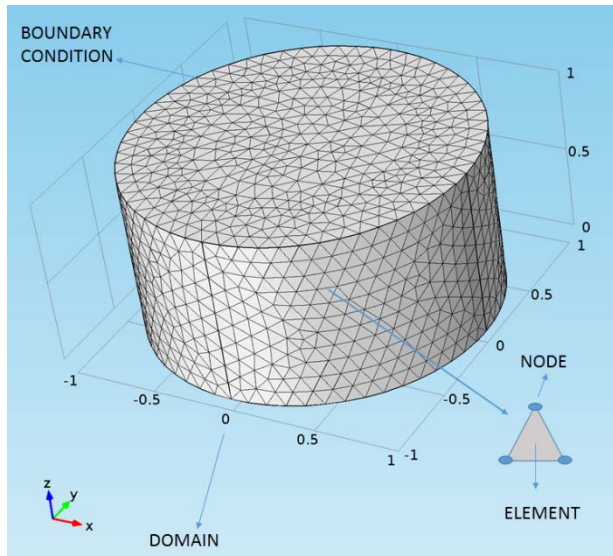


Figure 4.1.-Substructural division by Finite element method

Domain: Geometrical space where system is analysed (material properties)

Element: Substructures that divide the domain. They could be either points (one-dimensional case), lines in the bi-dimensional case or surface in the three-dimensional case.

Node: Connecting point between different elements. In each one, the system' unknown variables are solved.

Boundary conditions: Known variables. They determine the system behaviour. (Loads, displacements, stress...)

Once this is clear the way to face a problem can be separated in four different stages. These are:

1. Knowledge of the problem: Describe the problem with all the available tools (Engineering drawings, conceptual design, unknown variables definition...) In this stage should be able to simplify the problem into a problem that can be solve by FEM.

**PRE-
PROCESSING**

2. FEM model: Defined the domain to apply the analysis. Discretize (mesh the solid, define material properties and apply boundary conditions.
3. Analysis specifications: Select type of analysis and solve the problem.

PROCESSING

4. Results: Obtain, visualize and interpret the results (graphical representation, movies...)

**POST-
PROCESSING**

4.1.3. MATHEMATICAL DESCRIPTION

The mathematics behind Finite element method is an extensive topic, and will not be presented in detail here but there is a plenty of literature in this topic (Qi 2006)(Tura and

Dong 2012). However a brief outline in the analytical mechanics and the matrix formulation will be given.

Once the domain is discretized and degrees of freedom for each node are defined, they can be collected in a column vector called u . This vector is called state vector. For each degree, using analytical mechanics, there is the corresponding conjugate. These conjugates represent the system boundary conditions. They determine if the system changes in one way or in the other and they are known variables. All of them are called forces and they are collected in other column vector called f .

Relationship between these two variables is assumed to be linear and homogenous, but not always happens and system can present inhomogeneity.

Through this expression both of them are related:

$$Ku = f \tag{4. 1}$$

Where K is called stiffness matrix, even in other applications that not involve structural physics.

On the other hand, physical significance of these vectors depends on the application problem. For example, in solid mechanics application u represent displacement and f mechanical force but in electrostatics u is the electric potential whereas f represents charge density.

Another mathematical concept to take into account working with FEM is the shape function. The shape function is used to interpolate the solution between the discrete values obtained at the mesh nodes.

In general terms, a finite element, e , is defined by several nodes, i, j, k , etc. and boundary lines. Degrees of freedom collected for each node are represented in the state vector, u . This state vector at any point within the element can be approximate in a column vector \tilde{u} , by the following expression:

$$u = \tilde{u} = \sum_m N_m q_m^e = [N_i, N_j \dots] \begin{bmatrix} q_i \\ q_j \\ \vdots \end{bmatrix} = Nq^e \quad (4. 2)$$

N_i is the shape functions of node i and q^e represents the nodal solutions for a particular element.

4.1.4. CONSIDERATIONS

When a problem is modelled by finite element various factors should be taken into account to ensure accurate and consistent results with the physics of the problem.

Ultrasonic transducers modelling involves equations in piezoelectric theory and in acoustic wave propagation through a medium described in sections 3.2 and 2.2.

To obtain an accurate approximation of the real problem that involves characteristics such as damping, surrounding medium etc. certain considerations must be established. (Kocbach 2000a)

4.1.4.1. LIMITATIONS IN THE SPATIAL DISCRETIZATION

Model resolution is defined by the mesh size. Simulation of an ultrasonic transducer transmitting in a particular frequency bandwidth must ensure the correct discretization of the highest frequency to obtain a good result. It corresponds to the smaller wavelength. In the literature, it is recommended that at least two degrees of freedom per wavelength but experience over the years, positions this value to at least 12. (Medina et al. 2003). This spatial discretization is closely linked with the convergence model that will be explained below.

4.1.4.2. MODEL CONVERGENCE

Models often have complex geometries or artificial boundary conditions which can destabilize the model. When mesh size is reduced, number of element increase. A convergence tendency should be obtained to ensure the model is stable.

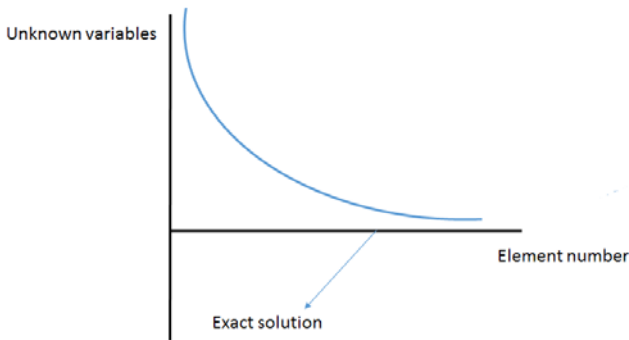


Figure 4.2.-Model convergence tendency

4.1.4.3. MODEL SIMPLIFICATION

The translation from the physical problem to the mathematical model can be complicated in some cases. However, conditions of symmetry in the structure under study can reduce the degrees of freedom of the system and therefore save a lot of computational resources. This is the case of the prototypes built in this thesis. Its cylindrical geometry allows the use of an axial symmetry as shown in the following figure:

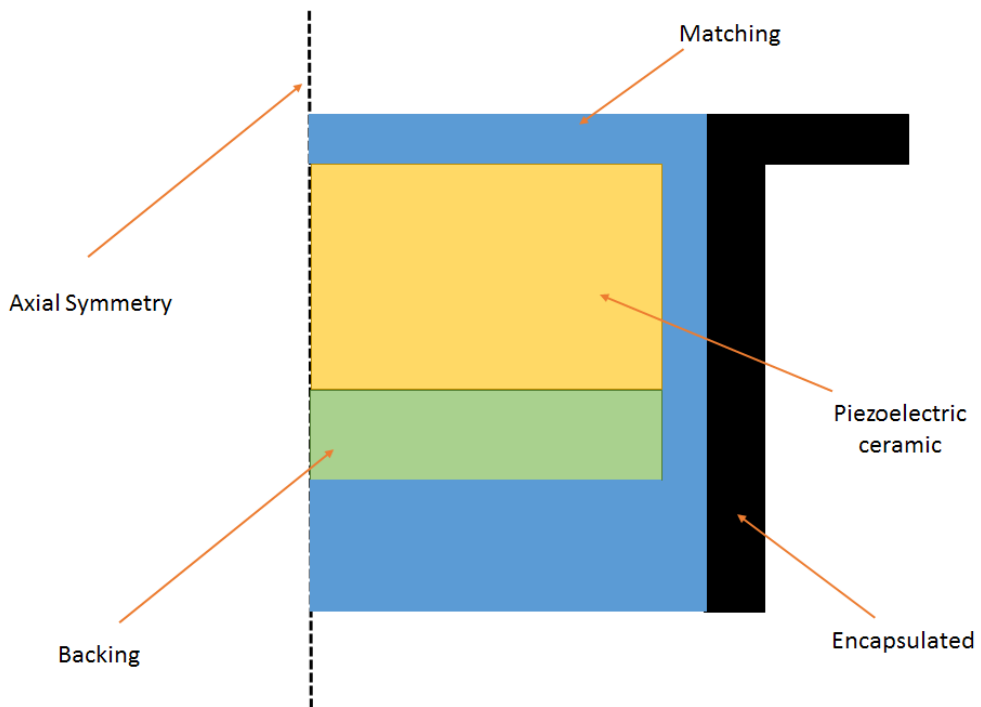


Figure 4.3.-Model geometry with axial symmetry

Figure 4.3, is represents a piezoelectric disc transducer geometry with axial symmetry. In it, all transducer elements are represented: Matching, backing, active element... They were explained deeply in section 3.4

4.1.4.4. ARTIFICIAL BOUNDARY CONDITION

On some models, it is necessary to know the behaviour of a system or find the system solution at a given point a fair distance from him

In ultrasonic transducer simulations, there are two important matters. On the one hand, to understand and to have knowledge of the internal behaviour gives important information about vibrational modes of ceramics, resonant frequency, etc. This behaviour changes depending on the surrounding medium. It must be ensured by artificial boundary conditions that reduction or dimensions adaptation not influence the system causing unwanted reflections. There are several types PML (Perfect Matching layer), Infinite elements, Radiation condition, etc.

On the other, to model scattered wave from a system into elastic media can be important to the observation of the acoustic wave in far-field (section 3.2.2). For this purpose it is used Kirchhoff Helmholtz integral theorem (Schleicher et al. 2001)

4.1.5. FINITE ELEMENT SOFTWARE

In this part, a brief description of the software used for simulation during the ultrasonic transducer design is made. These programs are used to obtain some parameters in the materials characterization section and also approach the model with the current system behaviour to validate them. Once they are validated, they can be applied for improvements in the design.

The two programs based on the finite element method are COMSOL Multiphysics software V.4.4 and 5.1 FEMP software.

The first, COMSOL, is commercial software that provides an easy user interface. It has predefined physics models where you just have to enter the data, while math problem are already scheduled. Its application range is wide. Disciplines go from acoustic propagation to electromagnetics for example (Comsol 2010). Furthermore it allows the coupling of different physical problems, in the same model, approaching interactions that occur in real life.

On the other hand, FEMP (Finite element modelling of Piezoelectric structures) is a free program created by Jan Kocback in 2000 during his Masters and PHD Thesis (Kocbach 2000a) at the University of Bergen (Norway). Thanks to a collaboration of three months, different works with version 5.1 were developed. This version includes enhancements of other contributors as Magne Aanes (Aanes 2013).

The working platform is MATLAB program based on C ++. Its scope is the modelling of piezoelectric transducers exclusively. There is No pre-processor like COMSOL and the user is responsible for programming the structure under study, as well as the parameters to be solved, nodes, elements, etc. Through pre-programmed .mat files (MATLAB files) , system is solved and the results are stored in files .TXT for later post-processing (FEMP version 3.5 - Documentation n.d.)

The main difference between both (COMSOL and FEMP)is the computational cost. Both are based in the same equations, but FEMP due to work in MATLAB platform reduce considerably the computational time to solve the models, particularly in water. In figure 3.12 is represent a full piezoelectric transducer in water (axial symmetric model) for both programs.

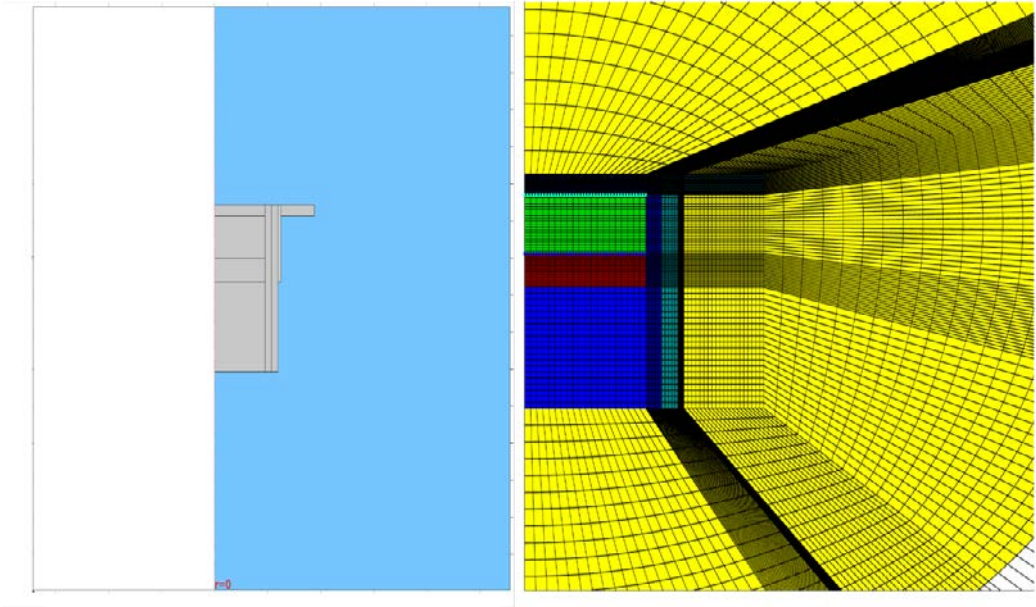


Figure 4.4.-Example of model geometry from COMSOL and FEMP respectively.

4.2. K-SPACE PSEUDO SPECTRAL METHOD

In this point the numerical model to simulate parametric array behaviour used in this thesis is described.

K-space pseudo spectral method is the numerical method used for K-wave MATLAB toolbox. This toolbox solves time domain simulation of acoustic wave fields in 1D, 2D or 3D. It works for both linear and nonlinear wave propagation system. It has been developed since 2009 by Bradley Treeby and Ben Cox (University college of London). There is a

C++ version driven by Jiri Jaros (Brno University of Technology). (Treeby, Cox, and Jaros 2016)

The equations governing the K-wave method are the first-order differential equations based on the conservation equations of mass, momentum and pressure density. As mentioned previously, in acoustics, the relation between these allows arriving at a particular second-order equation called the wave equation (section). The K-wave does not solve this second order equation but the first order differential equations. This is due to different reasons:

1. Introduction of fluids in a simpler way
2. Use of special anisotropic layers PML

On the other hand in the acoustic medium, heterogeneous absorption losses are introduced.

To model parametric acoustic array, the nonlinear parameter should be introduced by modifying the three main equations. Adding this parameter, together with the absorption and dispersion of the medium, gives a generalized form of Westervelt equation.

K-space pseudo spectral method combines spectral analysis of spatial derivatives (using Fourier method) with a temporal propagator expressed in the spatial frequency domain k-space.

Advantages are:

- Fourier amplitude component can be calculated efficiently using fast Fourier Transform (FFT).

- Theoretically grid required, for a sinusoidal wave, is reduce to two nodes rather than 6 or 10 for other methods.

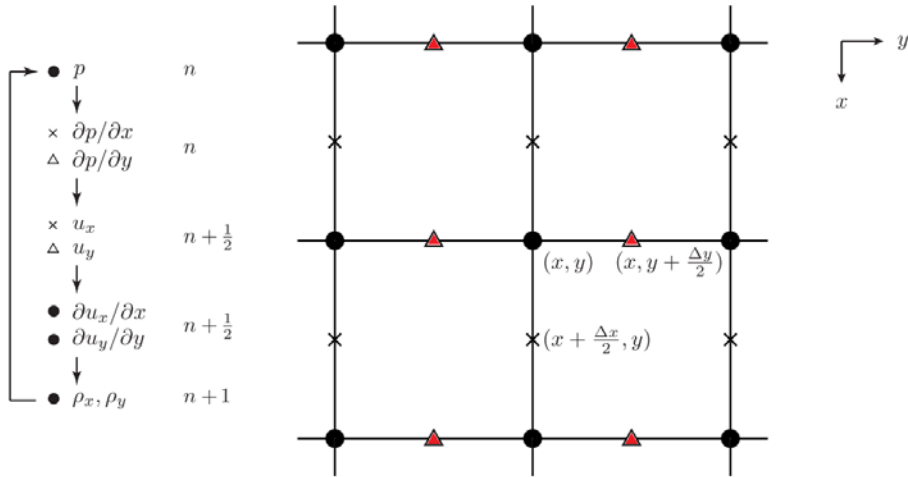


Figure 4.5. Schematic showing the computational steps in the solution of the coupled first-order equations using a staggered spatial and temporal grid in 2D. Here $\partial p / \partial x$ and u_x are evaluated at grid points staggered in the x-direction (crosses), while $\partial p / \partial y$ and u_y evaluated at grid points staggered in the y-direction (triangles)(Treeby, Cox, and Jaros 2016).

K-space pseudo spectral method will be used first to carry out a previous study with which to fix working range of certain experimental set-up parameters like input pressure required for parametric generation and optimum measurement distance between Transducer and hydrophone. Secondly it will be a comparative model between the experimental results obtained from the transducers under study and those obtained by an ideal simulation model of a flat piston with dimensions equal to experimental one.

5

Ultrasonic Transducer Design

5.1. INTRODUCTION

Demand for ultrasonic transducers has grown in the last decades due to the increase of its use in diverse applications. As mentioned in section 3.1, it was, from World War I, that ultrasound began to take hold after the French physicist, Pau Langevin, invented Sonar. It was used in both the marine and aviation areas (Kino GS 1987; López 2014). However, it was not until the end of the Second World War that its development began in other fields, such as medicine, mainly to ultrasonic diagnosis, which now extends to numerous

applications such as non-destructive analysis (NTD) of materials, positioning systems, ultrasonic cleaning, sonochemistry, etc.

Traditionally, ultrasonic transducer design has always been done through “rules of thumb” and fundamental theoretical understanding (Moten 2010). Design, is the process whereby the optimal solutions for the execution of a system, oriented to a particular application, are found. This includes obtaining optimal values for variables that determine materials and dimensions of mechanical and piezoelectric elements, which minimize or maximize different objectives, such as system sensitivity, electric power, resonance frequency etc.

Transducers were originally designed by the use of one-dimensional analytical models and the prototype manufacturing. This procedure, although it is still used at the present time, display a number of disadvantages(Al-Budairi 2012).

- In certain situations, the analytical resolution form can be complex.
- Experimental method of making prototypes may require too much time and money

With the technological developments occurred in recent years, application of numerical methods, in engineering, has allowed the development of prediction models to approximate systems' behaviour. These allow to make a feasible and more efficient design with lower cost for a particular application. (Acosta Aparicio et al. 2010).

These models are equations systems whose unknown's variables represent key magnitudes that allow to discover the system behaviour. These magnitudes, in terms of the ultrasonic transducers design, can form a broad list. Among the most important we highlight the following:

1. Operating range
2. Sensitivity
3. Frequency response and Resonance frequency
4. Beamwidth
5. Use and robustness
6. Materials and its parameters

The most relevant aspects that will be taken into account in the ultrasonic transducer design considerations presented in this chapter will be the following:

- Central operation frequency and bandwidth that will determine the system resolution for echo-impulse applications.
- Beam-width, the one in charge of giving information about the insonified area by the transducer and consequently by the acoustic wave.
- Projector and receiver sensitivity. These characteristics will give information on the source levels that the transducer is able to transmit and to discern.

This chapter presents several sections: First, we introduce the active element characterization (piezoelectric ceramic), as well as, the passive materials characterization that conform mechanical parts of the transducer. Once characterized, the optimum materials were chosen and a full transducer finite element modelling is described. Steps of transducer set-up are shown and experimental measurements were carried out in terms to characterize the full transducer behaviour. Last stage is the comparison between experimental data and simulations, to validate finite element modelling for future design improvements

5.2. ACTIVE MATERIALS CHARACTERIZATION

Next two sections describe how characterization of various materials has been carried out to use them, in the different elements that make up the ultrasonic transducer, and which have been explained above. (Section 3.4)

This characterization is divided into two blocks: Active element characterization and Passive materials characterization. This is due to the fact that the parameters under study, in each of them, are different and therefore the whole experimental process is different and needs to be covered separately.

Part of the work carried out in this thesis, is part of a collaboration agreement with Zunibal S.L., a Spanish company that develops technological tools for the marine sector. Its technology is oriented to fisheries and more specifically to the use of acoustics for achieving more efficient and sustainable fishing. The quantification of fish schools and the classification of species in the first 100 m of the water column are the main objectives. Due to this, certain design premises were established a priori:

- Resonance frequency was established in 120 kHz. This particular frequency have been used for several years in fisheries research to analyse different pelagic fisheries resources. (González 2015; Skaret et al. 2015)
- Materials available were selected only for the company providers.
- Transducer geometry and final dimensions had to be adapted for the possibility of future incorporation in a bigger system.
- Projector sensitivity should be at least 150dB (ref 1uPa/V) to obtain proper SNR (Signal to noise ratio) over short and long distances.
- Beamwidth (-3 dB) must be between 15° and 20°.

5.2.1. PARAMETERS UNDER TEST

As described in Chapter 3 and more specifically in Section 3.4, the used active elements are ceramic materials that present the piezoelectric effect. Characteristics of this energy conversion are given by the constitutive relations of the interplay between piezoelectric and elastic phenomena, and piezoelectric coupling factors and dielectric constants matrix are derived from them. Together with them, there are losses, which are intrinsic to each material, they allow to describe completely the active element behaviour and how it will affect the total system.

In piezoelectric ceramic processing there are four important steps: powder preparation, machining, electroding and poling. The latter being responsible for orienting dipoles inside the material and induce piezoelectricity along one axis. In the case of PZT (Lead Zirconate Titanium), piezoelectric ceramic under interest, the powder is a mix between lead oxide, titanium oxide and zirconium oxide as the main compounds. Nevertheless it is common to use dopant materials to modify its characteristics. (Jordan and Langley 2001).

Although in the material type reside the main properties, once the powder is done, this can be matching in different shapes and sizes. After cutting, electrodes are applied and start the polarization process. Depending on which direction exhibits the polarization, symmetry can be obtained in one particular axis and, as it was explained in the theoretical introduction, a constant matrix reduction is derived. For our design purposes, ceramics with polarization along the Z-axis were chosen, and the resultant coefficients are shown in table 5.1

Elastic Constants	$c_{11}^E, c_{12}^E, c_{13}^E, c_{33}^E, c_{44}^E$
Piezoelectric Coupling Coefficient	e_{31}, e_{33}, e_{15}
Dielectric Constants	$\epsilon_{11}^S, \epsilon_{33}^S$

Table 5.1. Material properties under characterization for a piezoelectric ceramic with polarization along Z axis

To determine these fundamental constants, direct measurements have to be done through different methods (resonant method, capacitance measurement etc.) (Brissaud 1991)(Standard 1988). Moreover, to obtain all of them a series of measurements on samples of various shapes and poling orientations are required. Processes to measure or calculate one parameter from the coupling of other parameters is fully described in IEE Standards of Piezoelectricity(Standard 1988) and it is not going to be a matter of interest in this thesis.

The present study on piezoelectric ceramics is based on the parameters provided by the manufacturer of each material. These data contain both, the coefficients collected in Table 5.1 as well as the mechanical losses (and the dielectric losses ()). The first of them are accompanying the elasticity matrix and the last one to the dielectric matrix. Both are independent for each coefficient and may have different values(Aanes 2013; Kocbach 2000b). Piezoelectric losses are neglected on this work due to the fact that there are not reference data to start with. In order, to properly characterize the ceramic behaviour, we used a finite element simulation tool. The objective is, by means of the comparison with

real electric measurements, to adjust coefficients and their losses provided to the simulation tool; the selected ceramics being completely and accurately described.

Once the parameters have been adjusted, a resonance study as a function of ceramic dimensions is carried out, with the purpose to observe the most predominant vibratory modes in each material. On the other hand, within the materials characterization, acoustic impedance values are obtained. This will be, in the design, a key factor to select the rest of materials involved in the setup of the transducer.

5.2.2. MATERIALS AND METHODS

Two piezoelectric ceramics are selected to study their characteristics as active element. Both of them present a circular disc geometry with a 38mm outer diameter due to the company conditions. In Table 5.2 is shown a short summarize description.

Manufacturer	Description	Dimensions (mm)	Resonant Frequency (kHz)
Meggit 	PZ37	38 X 12.25	120
PI ceramics 	PIC255	38 X 15.06	125

Table 5.2. Piezoelectric ceramic general description

The first piezoelectric ceramic is Pz37 from Meggit PLC, British engineering company. PZ37 is a new PZT ceramic generation. It is a porous ceramic that allows to decrease acoustical impedance, thus improving transfer of acoustic energy to the load medium. Its low mechanical quality factor makes it present a greater bandwidth and that is optimal for transducers used in both transmission and reception (Ferroperm n.d.).

Alternatively PIC255 is a modified soft PZT material with high coupling factor, high permittivity and extremely high Curie temperature. This material have been optimized for actuator applications under dynamic conditions and high ambient. As the same as its partner, PIC255 is suitable for broad-band systems (PI Ceramic GmbH n.d.). Table 5.3 collect the piezoelectric properties available from manufacturer for both ceramics.

<i>Manufacturer data</i>	Meggitt (PZ37)	PI ceramics (PIC255)
$c_{11}^E [10^{11}\text{N/m}^2]$	7.23	1.23
$c_{12}^E [10^{10}\text{N/m}^2]$	4.17	2.226
$c_{13}^E [10^{10}\text{N/m}^2]$	3.34	7.67
$c_{33}^E [10^{10}\text{N/m}^2]$	4.63	9.71
$c_{44}^E [10^{10}\text{N/m}^2]$	1.53	7.025
$e_{31} [\text{C/m}^2]$	1.11	-7.15
$e_{33} [\text{C/m}^2]$	11	13.70
$e_{15} [\text{C/m}^2]$		11.90
$\epsilon_{11} [10^{-9}\text{F/m}]$		930
$\epsilon_{33} [10^{-9}\text{F/m}]$	689	857
$\rho [\text{kg/m}^3]$	6470	7800
Q_M	127	80
$\tan\delta$	0,015	0.020

Table 5.3. Manufacturer piezoelectric ceramic properties for Pz37 and PIC255 respectively

5.2.2.1. ACOUSTIC IMPEDANCE

In ultrasonic transducer design, acoustic materials impedance play a very important role, since through them, it can be adjust the transmission and reception characteristics suitable for our application scope. Although it is necessary a trade-off between theory and design premises, it is important to obtain the acoustic impedance values for each element involve in the design.

Acoustic impedance defined in equation(2. 5) is directly related to the propagation velocity and material density. In circular disc piezoelectric ceramics working in thickness mode, propagation velocity will correspond to the longitudinal velocity along the Z axis as shown in figure 5.1:

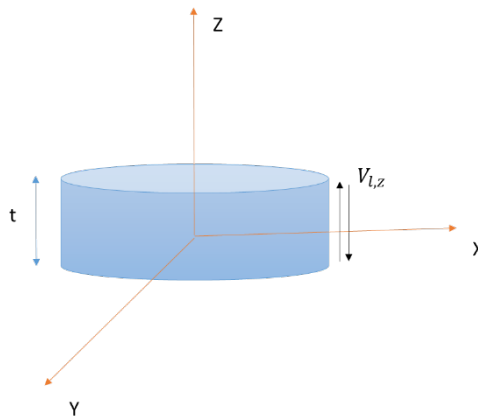


Figure 5.1. - Piezoelectric ceramic scheme

This propagation velocity can be obtained theoretically or experimentally. For the active element case, and in particular piezoelectric ceramics, theoretical calculation is obtained

through the Christoffel's equation which relates the stiffness constant along Z-axis to the density of the material.

$$V_l = \sqrt{\frac{c_{33}^D}{\rho}} \quad (5. 1)$$

where c_{33}^D , in the thickness stiffness constant under constant Displacement.

For the experimental calculation the eco-impulse ultrasonic testing technic (Hellier 2012; Valencia Ilarregui 2009) is used which will be described next

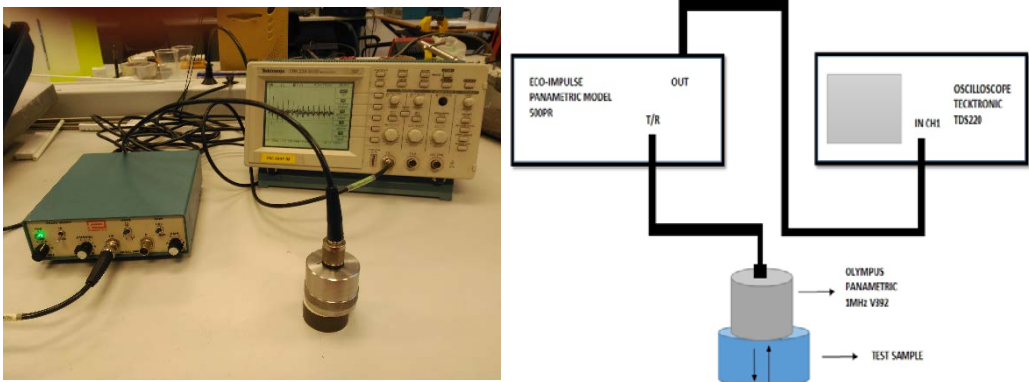


Figure 5.2.-Longitudinal sound speed measurement.
Experimental set-up (left side) and blocks diagram (right side)

Experimental measurement configuration is shown is figure 4.2. The equipment involve in the measurement is:

- PANAMETRIC Model 500PR Ultrasonic pulse-receiver
- TECKTRONIC oscilloscope TDS 220

- PANAMETRIC V392 0.5MHz ultrasonic transducer

- Test sample

In the pulse-echo method, an ultrasound transducer generates an ultrasonic pulse and receives its echo. The ultrasonic transducer functions as both transmitter and receiver in one unit. An electronic pulse is generated using the piezoelectric effect. A short, high voltage electric pulse (less than 20 Ns in duration, 100-200 V in amplitude) excites a piezoelectric crystal, to generate an ultrasound pulse. Transducer broadcasts the ultrasonic pulse at the surface of the specimen. The ultrasonic pulse travels through the test sample and reflects off the opposite face. The transducer then listen to the reflected echoes. Ultrasound pulse keeps bouncing off the opposite faces of the specimen, attenuating with time. The time between any two echoes is the length of time required for the pulse to travel through the sample and back to the transducer. The attenuation (amplitude decay) is exponentially with time.

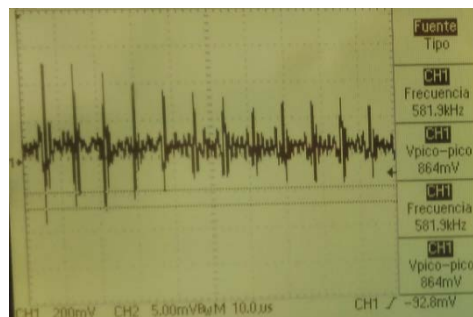


Figure 5.3.-Oscilloscope signal detail. Receive transducer signal from piezoelectric ceramic eco-impulse test

The speed of sound in the solid can be calculated from the observed difference time, Δt , and the test thickness, t :

$$V_l = \frac{2t}{\Delta t} \quad (5.2)$$

To obtain this value, 5 measurements have been made with the echo impulse, giving as an optimal result the arithmetic mean of them plus its associated error. Obtaining the propagation velocity is an indirect measure through two magnitudes (sample thickness and the time difference between echoes when measuring with the echo impulse). For both, instrumental error, $1e-3m$ and $1e-6s$ respectively, is less than the aleatory error produced in the measurement. Therefore, following the Gauss theory, we take as the best estimate of the error, the so-called quadratic error defined by:

$$\Delta x = \sqrt{\frac{\sum_1^n (x_i - \langle x \rangle)^2}{n(n-1)}} \quad (5.3)$$

Where n , number of measurement

x_i the value for each measurement and $\langle x \rangle$, the arithmetic mean defined by:

$$\langle x \rangle = \frac{x_1 + x_2 + \dots + x_n}{n} = \frac{\sum_1^n x_i}{n} \quad (5.4)$$

Therefore the result of the experiment will be expressed as:

$$\langle x \rangle \pm \Delta x \quad (5.5)$$

Δx is an absolute error, the relative error will be as follows:

$$e = \frac{\Delta x}{\langle x \rangle} \quad (5.6)$$

Once propagation velocity is calculated, density values are taken from the manufacturer data and acoustic impedance is obtained.

5.2.2.2. PIEZOELECTRIC PROPERTIES ADJUSTMENT

In order to adjust the piezoelectric coefficients a FEM simulation model is used and also an electrical measurement. The process followed is described below.

Electrical admittance is the reference measure to adjust the properties under interest. This variable show, in the piezoelectric ceramic case, the resonant frequencies present due to specimen dimensions and geometry. It is divided in real and imaginary part. Both are called conductance and susceptance respectively and their unit is Siemens (S)

Experimental set-up is shown in figure 5.4. Impedance analyser (WAYNE KER 6500PR) is connected to the piezoelectric ceramic applying and electric potential, around 1V, in

test sample terminals. Through LabVIEW system, impedance analyser is controlled and electrical admittance and impedance are obtained as an output data with .txt format

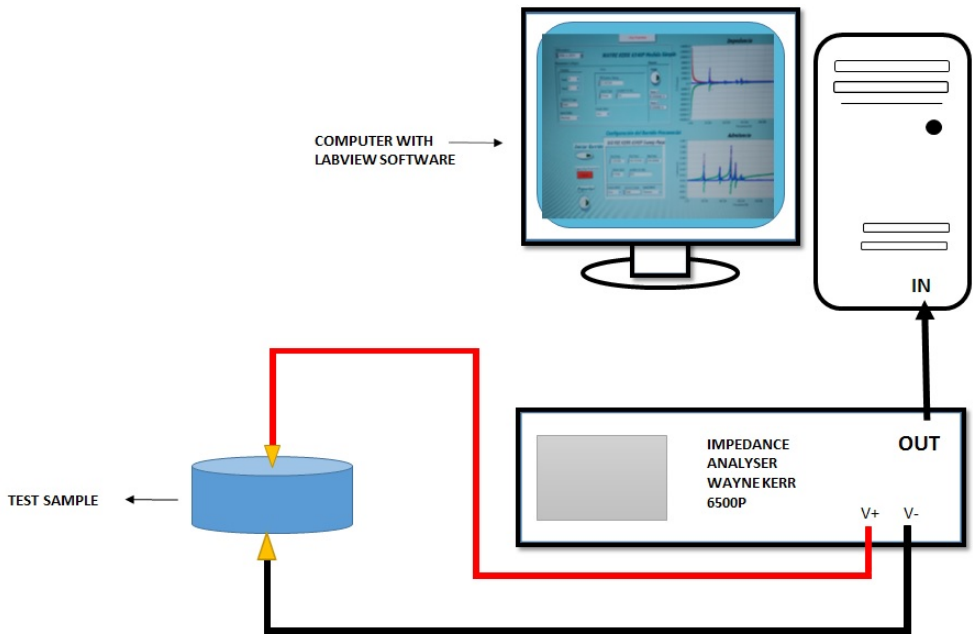
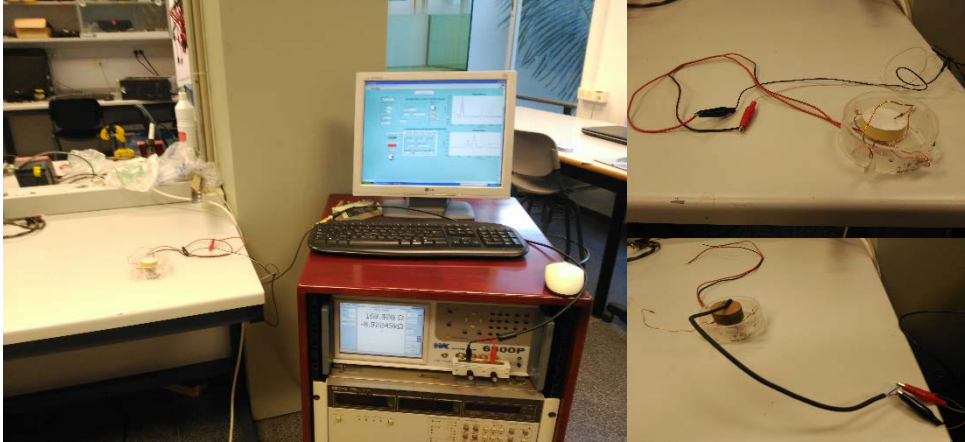


Figure 5.4.-Electrical admittance measurement set up.

Once electrical admittance is measured, next step is to create the finite element model. 2D axisymmetric model is carried out in two different Finite Element software, COMSOL and FEMP, described in section 4.1

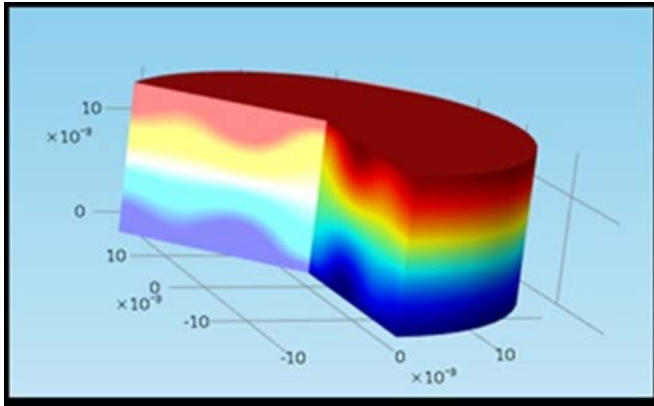


Figure 5.5. - Piezoelectric ceramic FE modelling detail.

The goal of this simulation is to obtain in a theoretical manner, the value of electrical admittance measured experimentally. Once the model has been designed and the analysis performed, it serves as a tool to approximate coefficients until theoretical result approaches to real one. Several simplifications are produced in the finite element model so that the analysis execution time is reduced to the maximum without interfering with the physical characteristics of the problem under study. Steps to follow in both software are the same with small discrepancies that will be discussed below.

- Model definition:

When FE modelling was introduced to simulate piezoelectric ceramics. 1D modelling was the most used. This simplification treats the piezoelectric ceramic disc as if it were a flat piston radiating the same way across the surface (Acosta Aparicio et al. 2010). Later studies showed that it was only valid for piezoelectric ceramics where their radiant surface, corresponding to the largest dimension (ceramic diameter), was much larger than the remaining dimension (ceramic thickness). For piezoelectric ceramics, with finite dimensions it is necessary to make use of 2D or 3D models. In the present work, due to the cylindrical geometry of the sample under test, axial symmetry can be introduced along the polarization axis. In this case, piezoelectric ceramics are polarized in the Z-axis. Although 3D model have been discarded due to computational cost, a 3D piezoelectric ceramic disc have been realized to check the axisymmetric model results validity.

On the other hand, experimental measurement have been done in air while for the FE simulation, vacuum is chosen. By not using air it is avoided to define an external medium where the ultrasonic waves propagate, avoiding an increase of meshing and therefore computational cost. The physics of the problem is also simplified. In the vacuum model, only material piezoelectric properties and its behaviour due to the boundary conditions are taken into account. Instead, when we introduce a propagation medium apart from properties mentioned, it must include the piezo-acoustic interaction that occurs due to the propagation of the ultrasonic waves by a medium with different physical properties.

- Analysis type selection

Direct harmonic analysis is selected for this model. Piezoelectric ceramic is evaluated over a range of frequencies from 40 kHz up to 160 kHz in 100Hz steps.

- Geometry design

COMSOL and FEMP have different procedure in this point. In COMSOL it is possible to import an AutoCAD design or to use the drawing tools available in the program. For this model, thanks to the axial symmetry, a simple rectangular is drawn. In contrast, in FEMP, the user is in charge of define all the geometry manually. Firstable it is defined the vertex points and after that, all the areas involves in the geometry

Dimensions selected are those corresponding to the thickness of each ceramic:

	Thickness (mm)
PZ37	12.25
PIC 255	15.02

Table 5.4. Thickness ceramics values

And half of the ceramic diameter disc due to axial symmetry (19mm).

- Materials properties

Elastic, piezoelectric coupling coefficient and electrical permittivity matrix are manually introduced for each material. These properties are introduced in a complex way adding the mechanical and dielectric losses independently for each coefficient. Along with density, all properties are stored in a materials library present in each simulation software. From the model, this library is accessed and associated with the geometry designed.

- Boundary conditions

Four boundary conditions are established following the outline of Figure 5.6.

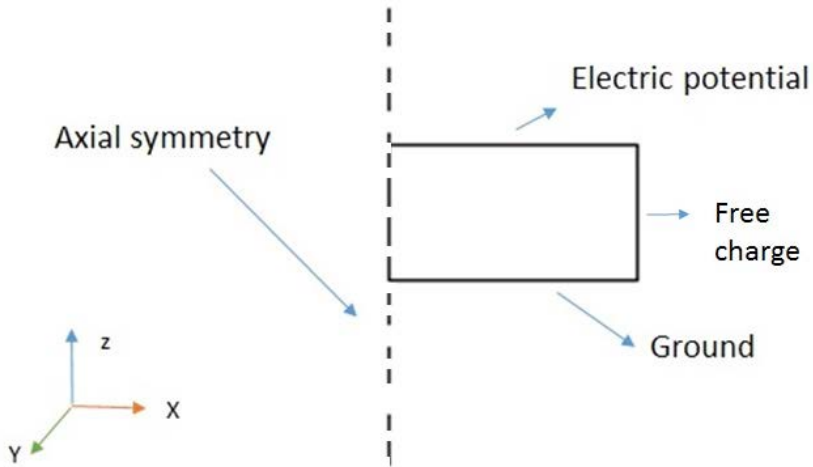


Figure 5.6. – Boundary conditions scheme for a piezoelectric ceramic disc

Electric potential: Apply 1V on the radiant surface of the ceramic (surface perpendicular to the polarization axis)

Ground: Imposes 0V on the back side where the electrical potential is defined. Thereby establishing a potential difference and thus achieving the piezoelectric effect.

Axial symmetry: Condition available only on the axis of rotation of 2D axis-symmetric models ($r=0$). Solution is revolved about the axis. Symmetry boundary will act like rigid wall. The pressure derivate will be zero on the symmetry boundary.

Free: This boundary condition implies free movement without any constraint

- Mesh

Mesh is defined in both programs in a rectangular shape. The element size is established by the relation between the wavelength of the maximum frequency under study and the number of divisions (N) that are made following equation

$$Elementsize = \frac{\lambda_{f_{max}}}{N} \quad (5.7)$$

If the model is well defined but does not have an appropriate mesh, solution obtained is not valid. In this thesis, convergence studies has been made for the different models. The process is to increase the elements number until the solution remains stable.

Size element for this models are shown in next section, when convergence results are presented.

- Output variable

Electrical admittance is the variable under interest. For FEMP simulations, admittance is an output variable already programmed that can be used by the user. Here the voltage is set to 1V. Then the frequency range for the admittance is collected from the model file (inn-file), if no frequency vector is given, the frequency range for the direct harmonic analysis is used. (FEMP version 3.5 - Documentation n.d.)

However in COMSOL, admittance should be define in the variables section through the following equation:

$$Y = (\text{int op}(pzd.nJ / I[V])) \quad (5.8)$$

Where $pzd.nJ$ is the current density.

Admittance is the ratio between an integration along the surface where electric potential is applied and the voltage value.

Furthermore to establish an optimal number of divisions per wavelength, and therefore the mesh element size, that finite element simulation model must have, it is necessary to perform a convergence study.

The convergence study is carried out using the simulation models of piezoelectric ceramics in the vacuum, for each material. Study is performed in the FEMP software and results are applied to the two software used in order to have the same parameters to be able to compare both models.

With this study, it is intended to achieve a solution that remains stable regardless of the mesh element size.

Each model is executed seven times by changing only the number of divisions per wavelength. Variable used as reference is the conductance value at the thickness resonance frequency in the piezoelectric ceramics. 124 kHz for PIC255 and 120 kHz for PZ37.

This variable is chosen, since it is the only available experimental data to characterize the materials. Measurements made for both, active element and passive materials explained in the next section, are performed in air. The modelling in the vacuum is due to the fact

that only piezoelectric behaviour is interesting and not the acoustic interaction with the medium. Simplification is done by reducing computational cost

Table collect the results by defining the following parameters: Number of divisions per wavelength (N), model run time and conductance amplitude in the resonance frequency.

PIC 255

Number of divisions (N)	Conductance Amplitude	Model run time
5	0.003522	21s
7	0.003640	28s
9	0.003702	42s
12	0.003715	76s
15	0.003718	89s
18	0.003719	139s
21	0.003720	190s

PZ 37

Number of divisions (N)	Conductance Amplitude	Model run time
5	0.006217	34s
7	0.006172	39s
9	0.006150	45s
12	0.006138	53s
15	0.006135	82s
18	0.006134	109s
21	0.006134	140s

Table 5.5. Convergence study results

Figure 5.7 show graphically the convergence results, where the stability is shown more clearly.

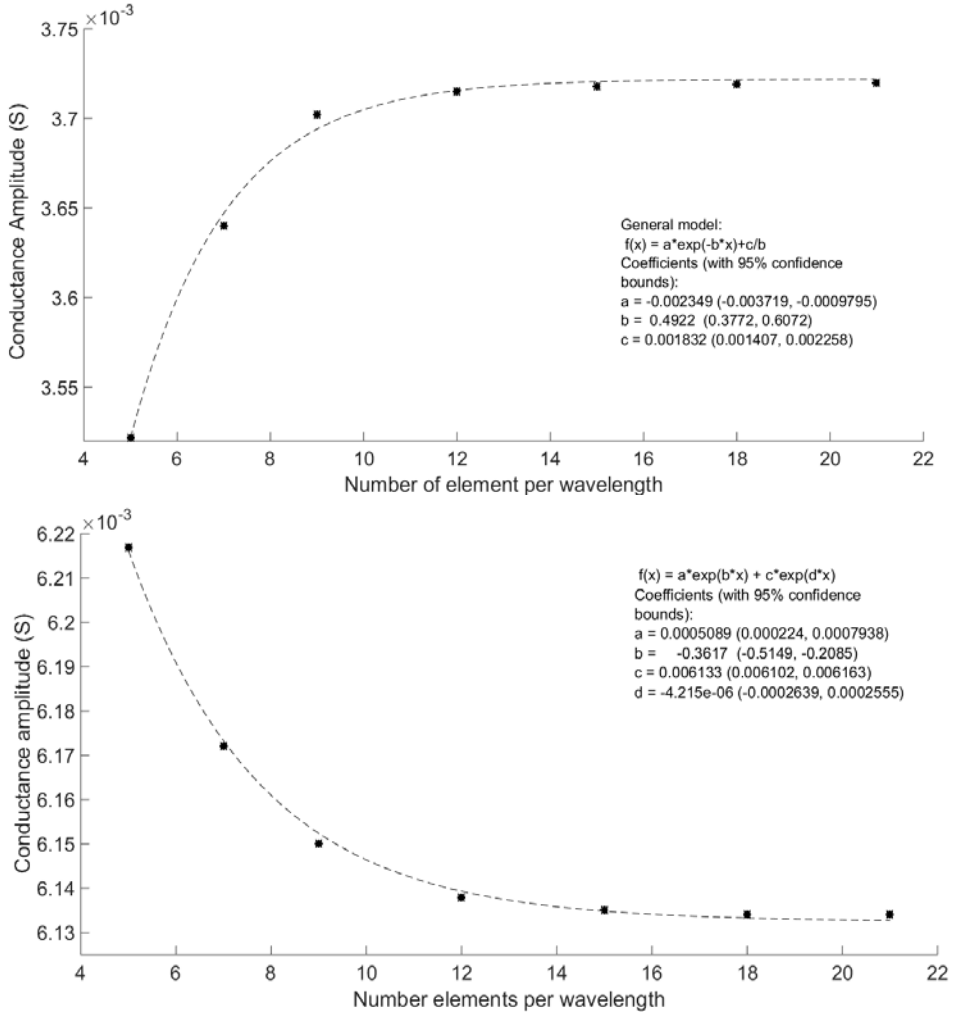


Figure 5.7. – Convergence graphic results for PIC255 and PZ37 ceramic respectively

From results it is observed that in both cases, from 16 elements, solution remains stable. Therefore the value selected be 16 divisions obtaining a mesh element size for each piezoelectric ceramic of:

	PZ37	PIC255
$\lambda_{f_{\max}}$ (160kHz)	0.021625	0.02803125
N	16	16
Element size	0.001352	0.001751

Table 5.6. Mesh element size for each piezoelectric ceramic depending on simulations parameters

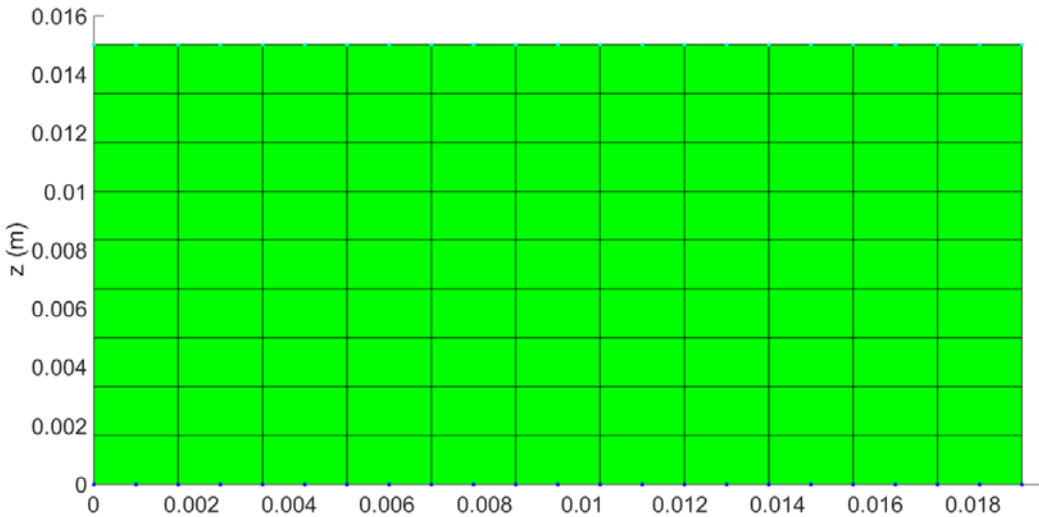


Figure 5.8. –Detail geometry PIC255 ceramic, in FEMP model, with 16 elements wavelength

5.2.2.3. RESONANCE FREQUENCY STUDY AS FUNCTION OF DIAMETER/THICKNESS RATIO

Resonant frequency study has been realized based on the work carried out in the Jan Kocbach thesis with title: "Finite Element Modelling of Ultrasonic Piezoelectric Transducer" (Aanes 2013; Kocbach 2000a).

His work pointed out the importance of resonance frequency spectra of circular piezoelectric ceramic disc to evaluate their behaviour taken into account different parameters: Poisson ratio, geometry etc. (Kocbach, Lunde, and Vestrheim 2001)

Kocbach focus in particular on observing the vibrational modes according to the ratio between the diameter and the thickness of the ceramic. From their study, it was concluded that for ratios > 10 , the vibrational modes are more independent of each other and as this value ratio decreases, they increase their dependence provoking strong perturbations that can affect the final design.

The ceramics present in this thesis present ratios below 5. Therefore it is considered an extra tool to understand the behaviour of these ceramics and possible perturbing problems.

The study is carried out with the FEMP simulation tool, perform a modal analysis in which resonance frequencies up to 200 kHz are extracted. Resonance and Eigen modes are calculated with complex losses.

Due to the polarization apply, only symmetric vibrational modes are studied. They have been classified for different authors, and 7 different types of vibrational model have been identified: R, L, E, A, T, TS, TE (Aanes 2013; Kocbach 2000a)

In Jan Kocbach thesis there is a definition for each of them but this thesis is focused in only two:

- Radial mode (R): Resonance at the lowest frequency that corresponds to motion in the largest dimension of the ceramic, which in this case is in the radial direction. Often, several harmonics will also be seen at higher frequencies. Radial mode will be study in the next chapter for parametric application along with the extensional thickness mode
- Thickness Extensional mode (TE): Oscillation is across disc faces so will be higher in frequency. Is the most used in transducer applications and it is the frequency under interest in the present transducer design.

5.2.3. ACTIVE MATERIALS CHARACTERIZATION RESULTS

This point collects all the results obtained within the active element characterization. It is divided in three parts: Acoustic impedance characterization, results of the piezoelectric coefficients adjustment and the study of resonance frequency spectra due to the ratio between diameter and thickness for each material.

5.2.3.1. ACOUSTIC IMPEDANCE

Table 5.7 shows the values of propagation velocity measurements for both ceramics. Table also shows the mean value, absolute error and relative error associated with the measurement.

Table 5.8 shows the acoustic impedance values for both piezoelectric ceramics. In the table are collected both the theoretical and experimental results. There are small differences between them. In both materials the values of the experimental results are greater than those theoretically calculated

	PZ37	PIC255
x_1 (m/s)	3462	4487
x_2 (m/s)	3454	4484
x_3 (m/s)	3458	4479
x_4 (m/s)	3461	4491
x_5 (m/s)	3466	4486
$\langle x_i \rangle$	3460	4485
Δx	2.38	2.01
e	6.9e-4	4.5e-4

Table 5.7. Propagation velocities experimental results and associated error

Material	PZ37		PIC255	
	THEORY	EXPERIMENT	THEORY	EXPERIMENT
Densidad (kg/m ³)	6470	6470	7800	7800
c _L (m/s)	3198	3460 ± 2.4	3954	4485 ± 2
Z(Mrayls)	20	22	30	35

Table 5.8. Acoustic Impedance Theoretical values & Experimental results

5.2.3.2. PIEZOELECTRIC COEFFICIENTS ADJUSTMENT

The adjustment of piezoelectric coefficients was done following the work of Rune Fardal (Fardal 2002). In this work, a relation was established, taking into account the dependence between the amplitude of the most outstanding vibrational modes, R1 and its second harmonic R2 and TE1, with the real and imaginary part of some piezoelectric coefficients. These include elasticity matrix, piezoelectric coupling factor and dielectric permittivity.

Figures 5.9 and 5.10 graphically represent the final fit obtained for both materials. Table 5.9 and 5.10 shown the modification of the piezoelectric coefficients offered by the manufacturer

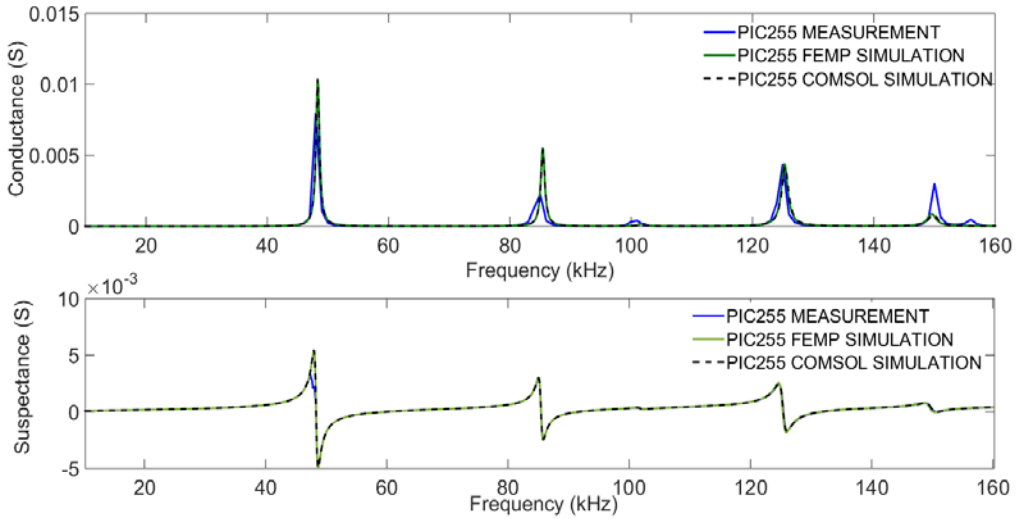


Figure 5.9. – Electrical admittance for Pic255 Piezoelectric ceramic: FE modelling & Experimental measurement

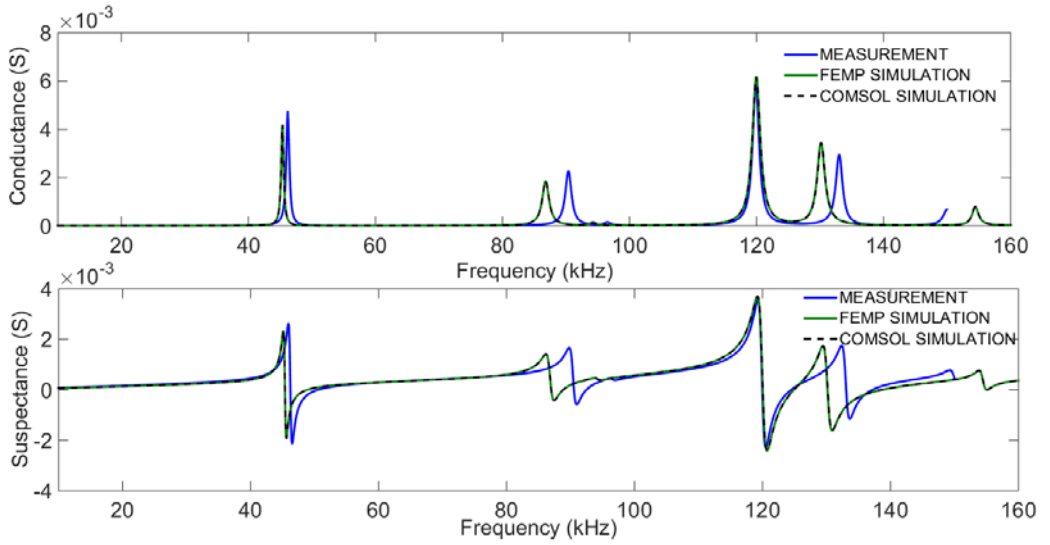


Figure 5.10. - Electrical admittance for Pz37 Piezoelectric ceramic: FE modelling & Experimental measurement

<i>PZ37</i>	Meggitt	Adjusted (FE simulation)
c^E_{11} [10^{10}N/m^2]	7.23	7.23(1+i/187)
c^E_{12} [10^{10}N/m^2]	4.17	4.17(1+i/187)
c^E_{13} [10^{10}N/m^2]	3.34	3.34(1+i/127)
c^E_{33} [10^{10}N/m^2]	4.63	4.55(1+i/67)
c^E_{44} [10^{10}N/m^2]	1.53	2.20(1+i/187)
e_{31} [C/m ²]	1.11	1.11
e_{33} [C/m ²]	11	11
e_{15} [C/m ²]		9
ϵ_{11} [10^{-9}F/m]		889(1-i/67)
ϵ_{33} [10^{-9}F/m]	689	689(1-i/67)
ρ [kg/m ³]	6470	6470
Q_M	127	Not used
$\tan\delta$	0,015	Not used

Table 5.9. Manufacturer piezoelectric ceramic properties for Pz37

<i>PIC255</i>	PI ceramics	Adjusted (FE simulation)
c^E_{11} [10^{11}N/m^2]	1.23	1.229(1+i/58.6)
c^E_{12} [10^{10}N/m^2]	2.226	7.66089(1+i/58.6)
c^E_{13} [10^{10}N/m^2]	7.67	7.1178 (1+i/80)
c^E_{33} [10^{10}N/m^2]	9.71	9.7056 (1+i/145)
c^E_{44} [10^{10}N/m^2]	7.025	2.35 (1+i/120)
e_{31} [C/m ²]	-7.15	-7.8417
e_{33} [C/m ²]	13.70	13.5583
e_{15} [C/m ²]	11.90	11.244
ϵ_{11} [10^{-9}F/m]	930	930(1-i/50)
ϵ_{33} [10^{-9}F/m]	857	857(1-i/50)
ρ [kg/m ³]	7800	7800
Q_M	80	Not used
$\tan\delta$	0.020	Not used

Table 5.10. Manufacturer piezoelectric ceramic properties for PIC255

PZ37 ceramic presents more variations than PIC255. The adjustment of R1 and TE1 mode has been given greater importance, since they are in which the design is focused.

Coefficients modification has always been done respecting the dependence relations in the matrix that define piezoelectric behaviour.

5.2.3.3. RESONANCE FREQUENCY STUDY AS FUNCTION OF DIAMETER/THICKNESS RATIO

Both ceramics have a low ratio, 2.52 for PIC255 and 3.15 for PZ37. Results are shown in Figure 5.11 and 5.12

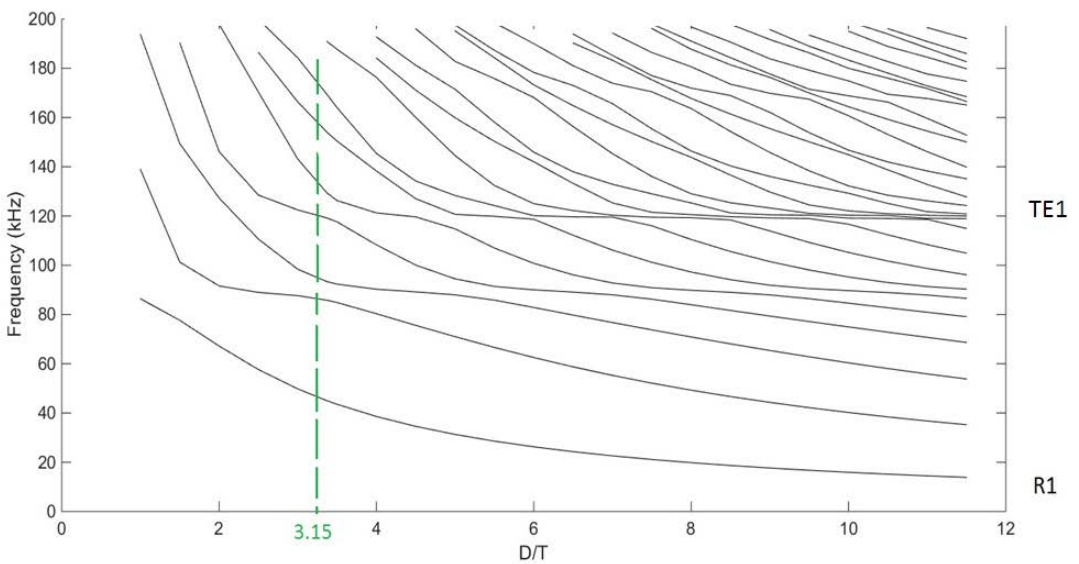


Figure 5.11. – PZ37 Resonant Frequencies depending on the ratio between its diameter and thickness

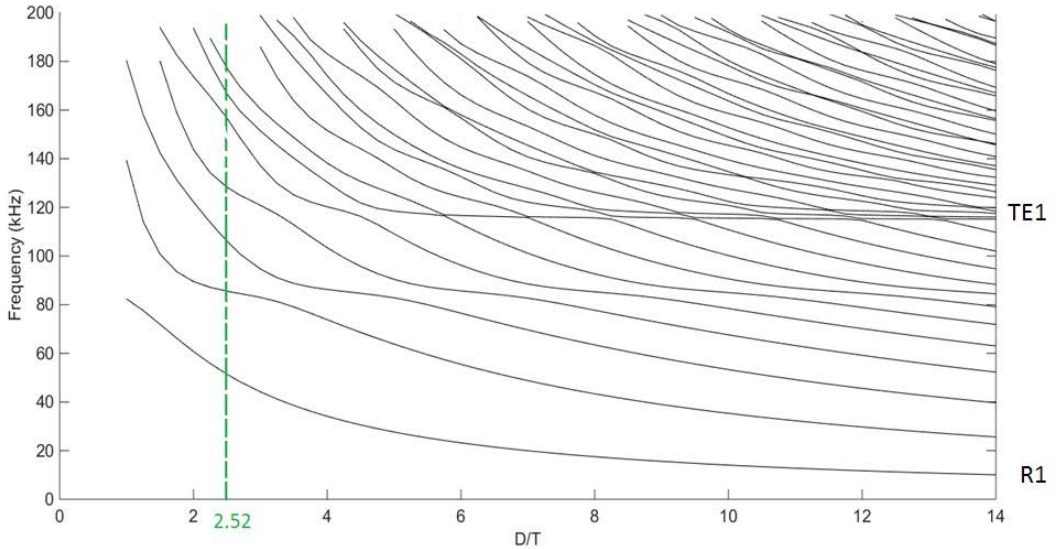


Figure 5.12. – PIC255 Resonant Frequencies depending on the ratio between its diameter and thickness

Due to this low ratio, vibrational modes are more dependent between them. Comparing both graphics, Thickness Extensional mode (TE1) which is the frequency of interest (120 kHz-125 kHz) is less strong in PIC255 than in PZ37. This can affect in the transducer sensitivity, therefore it is important to take it into account in the transducer design.

5.3. PASSIVE MATERIALS CHARACTERIZATION

Once active element materials are characterized, next step is to characterize materials that compound the different elements within the ultrasonic design. These materials are called non-piezoelectric materials or passive materials.

As described, in section 3.4, each element of the transducer has a function and according to the dimensions and physical material properties will behave in one way or another.

Although these thumb rules must always be taken into account in order to select the right material, sometimes the economic or manufacturing limitations provide to have a compromise between the desired ultrasonic transducer performance and the materials available for its manufacture.

Materials under study have been provided by the Spanish company suppliers with which the collaboration is maintained. From different materials provided, have been only selected two. They are the best adapted for the design and that greater ease of manufacture and better cost.

5.3.1. PARAMETERS UNDER TEST

In section 3.4, it was mentioned that the most important characteristics for materials used for both *Backing* and *Matching* are the following: Acoustic Impedance, attenuation and dimensions material.

Characterization is divided in two parts: Acoustic Impedance Characterization and adjustment, through FEM simulation, of transversal propagation velocity and mechanical loss factor.

The former is done through longitudinal velocity experimental measurement and density.

With longitudinal velocity value it is also going to establish *Matching* dimensions (Section 3.4) trying to increase the energy transference between piezoelectric ceramic and load medium when its thickness is equal to quarter-wavelength (thickness mode).

Second characterization allows to obtain, through simulation, approximate values of transversal propagation velocity and mechanical loss factor by means of the adjustment with experimental measurement that will explain in the following point.

When introducing the physical properties of passive materials in the simulation model can be introduced in two different ways:

- First option: Direct input of velocity values (longitudinal and transversal), density and mechanical loss factor

- Second option: Introducing the Young and Poisson ratio coefficients, density and mechanical loss factor

Young modulus and Poisson ratio values can be more easily achieved through the manufacturer. However, in this case only the density is the known parameter and the rest of them must be obtained experimentally.

Nevertheless, prior to these measures a theoretical estimation of these values is made thanks to material database of various sources in order to obtain a certain range of values with which to validate the experimental results.

5.3.2. MATERIALS AND METHODS

Two materials, have been electrically and acoustically characterized. Table 5.11 give an overview of them, differentiating by materials for matching and backing

Material	Manufacturer	Type
<p>Matching material (EL217C)</p> 	<p>ROBNORRESINS</p>	<p>Polyurethane resin</p>
<p>Backing (CORK TD1049)</p> 	<p>Amorim T&D</p>	<p>Cork composites</p>

Table 5.11. Matching and Backing materials investigated.

EL217C from ROBNOR Company (Robnor ResinLab Ltd.), is the material selected to be used as matching layer. It is an epoxy, usually for electronic and electrical application, requiring a highest protection against toughest environment such as sea water for example. It allows enhanced adhesion and its density is 1100kg/m³. It is chosen to give high protection to the ceramic and improve the energy transfer

Cork TD1049, it is a porous material supply by AMORIM T&D Company(AMORIM Cork Composites). It is going to be the back block element in the transducer design. This porous material has intercommunicated channels that will penetrate the ultrasonic wave reflected by the piezoelectric ceramic rear face and by dispersion will cause its attenuation (Andersen et al. 2000). This material will allow to reduce back propagation and increase bandwidth.

5.3.2.1. ACOUSTIC IMPEDANCE

In this section another method to measure longitudinal propagation velocity is described.

During the course of this thesis has been held a collaboration in the physics department of the University of Bergen (Norway).

In this period, passive materials characterization is carried out by means of the contact method (Ramadas, Leary, and Gachagan 2009). The advantages of this method over the eco-impulse method are as follows:

- Transmitted signal can be controlled. (Number of cycles, amplitude, shape)
- Transducers available are Panametrics of 0.5MHz with a bandwidth large enough to be able to perform measurements around 120 kHz and characterize the materials at the final work frequency of the system.

- As the working frequency decreases, the wavelength is larger, so it will penetrate further into the samples under test, reducing possible attenuation problems

In Fig.5.13 the experimental setup is shown and the equipment used

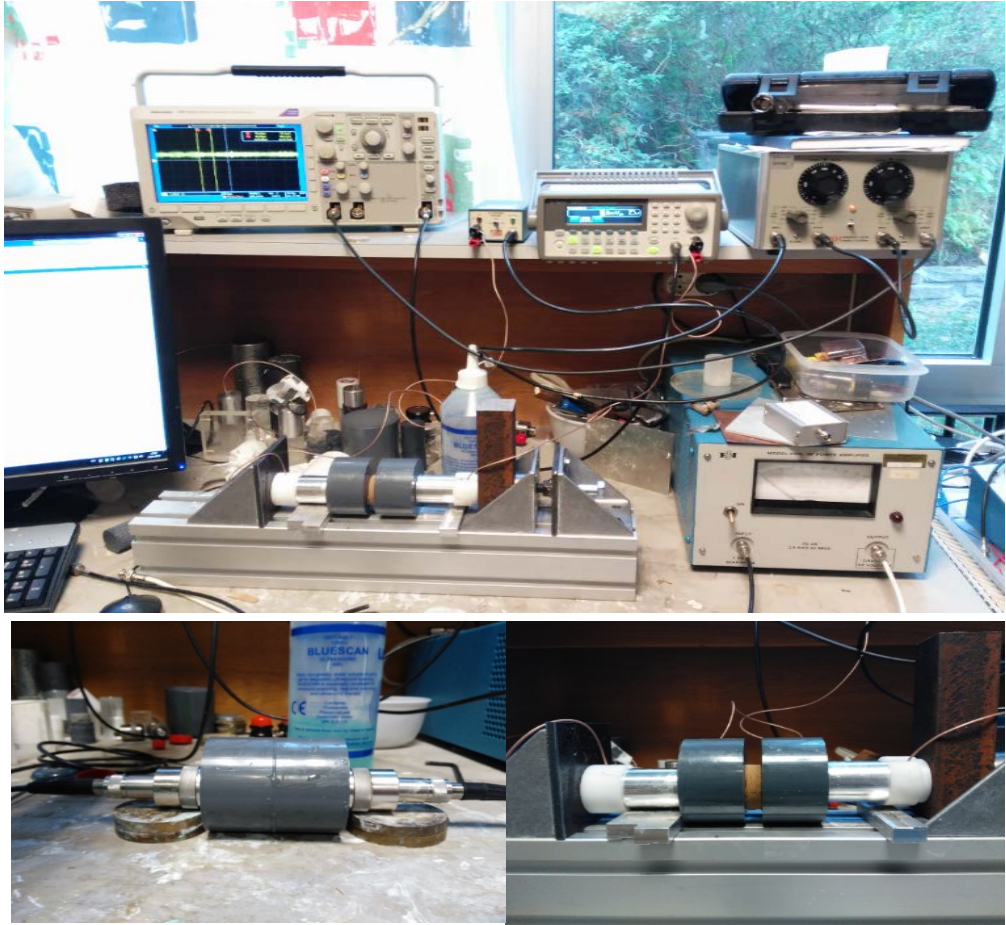


Figure 5.13. – Contact method experimental set-up

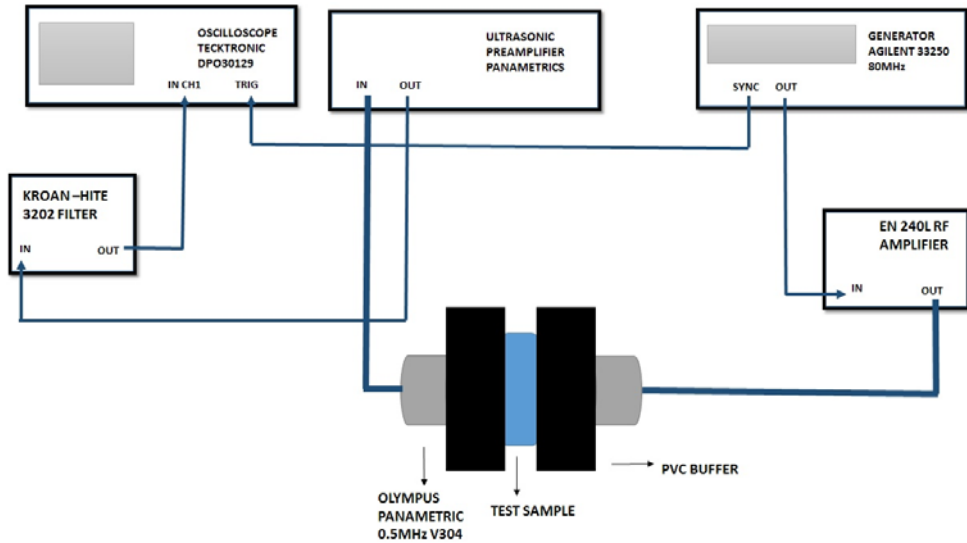


Figure 5.14. – Contact method diagram block

Experimental measurement configuration is shown in figure 4.14. Equipment involved in the measurement is:

- Oscilloscope: Tektronix DPO30129
- Ultrasonic pre-amplifier: Panametrics
- Function generator: HP AGILENT 331250A
- Filter: KROAN-HITE 3202 Filter
- Transducers : Panametrics V304 0.5MHz/1" 654055
- PVC buffer
- Samples
- RF amplifier : EN240L

Process is as follows: A 10 cycles burst at 125 kHz is transmitted. The voltage used in the transmission was different depending on test sample attenuation. This varied from 100mVpp for EL217C material up to 2Vpp for cork TD1049. A first measurement is performed transmitting the signal through the PVC buffer. The received signal, at the transducer receiver is recorded on the oscilloscope. Then, a second measurement is made,

repeating the process but this time by introducing the sample under test between PVC buffers. Delay time differences between the two received signals and the samples thicknesses give the longitudinal propagation velocity values. MATLAB program is used to obtain that values by zero-crossing method. The zero-crossing is the instantaneous point at which there is no voltage present. In a sine wave or other simple waveform, this normally occurs twice during each cycle. In zero-crossing method, this points are compare in the two received signals giving a number of delay time differences. From them, an average is performed and the mean value is obtained which with the sample thickness will give us the material propagation velocity

Highlight that the samples and the PVC buffer are attached to the transducer structure by means of a screw. The force exerted by him is recorded and applied to all measures so that there are no repeatability errors.

Bluescan ultrasound gel is used as a link between transducer and test sample. It facilities the ultrasonic transmission.

This measurements as it was in the active element characterization have their associated error.

5.3.2.2. TRANSVERSAL SOUND SPEED AND ATTENUATION COEFFICIENT EXPERIMENTAL ADJUSTMENT

Electrical measurement are realized as in section 5.2.3.1 . Due to passive materials are non-conductive materials. They have to be attached to piezoelectric ceramics and observe their behaviour through them.

PIC255 ceramic is chosen due to its closer piezoelectric coefficients adjustment with the experimental results. Sample dimensions adhered to the ceramic are listed in the table below:

Test Sample	Description	Dimensions (mm)
	EL217C	38 X 3
	CORK TD1049	38 X 8.5

Table 5.12. Materials samples dimensions for electrical admittance measurement

Simulation models performed to characterize passive materials have the same methodology as those made for the active element.

They are 2D-axymmetric models in the vacuum. A harmonic frequency analysis is performed between a range of 40 kHz and 160 kHz.

Models have two domains. One domain is the piezoelectric ceramic and the other the material under study. The first one presents the same boundary and meshing conditions as in section 5.2.2.2. The latter has free boundary conditions and its mesh element is shown in Table 5.13

	EL217C	CORK TD1049
$\lambda_{f_{\max}}$ (160kHz)	0.0091875	0.0040625
N	16	16
Element size	0.000574	0.000254

Table 5.13. Mesh element size for each material under test

5.3.3. PASSIVE MATERIALS CHARACTERIZATION RESULTS

5.3.3.1. ACOUSTIC IMPEDANCE

Like for active material characterization, five measurements of longitudinal propagation velocity has been made. Results obtained for each material are shown in table 5.14. In table 5.15 final experimental values for acoustic impedance are collected with also density values.

	EL217C	CORK TD1049
x_1 (m/s)	1464	657
x_2 (m/s)	1482	643
x_3 (m/s)	1465	650
x_4 (m/s)	1472	662
x_5 (m/s)	1468	640
$\langle x_i \rangle$	1470.2	650.4
Δx	3.26	4.13
e	0.0022	0.0064

Table 5.14. Materials acoustic properties measurements

Material	EL217C	CORK TD1049
Densidad (kg/m ³)	1100	950
v_L (m/s)	1470±3.26	650±4.13
Z(Mrayls)	1.61	0.598

Table 5.15. Materials acoustic properties measurements

5.3.3.2. TRANSVERSAL SOUND SPEED AND ATTENUATION COEFFICIENT ADJUSTMENT

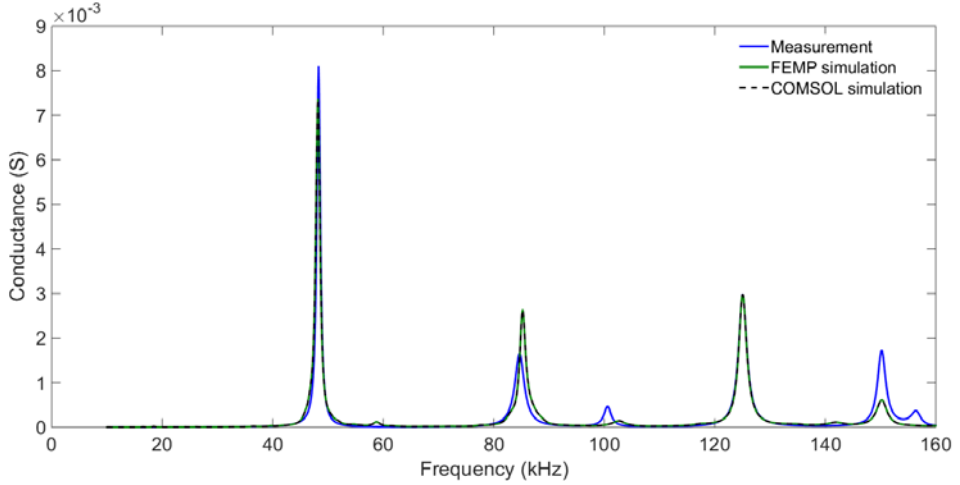


Figure 5.15. – Conductance comparison between simulation and measurement. PIC255 piezoelectric ceramic + 6.5 mm of TD1049 backing material

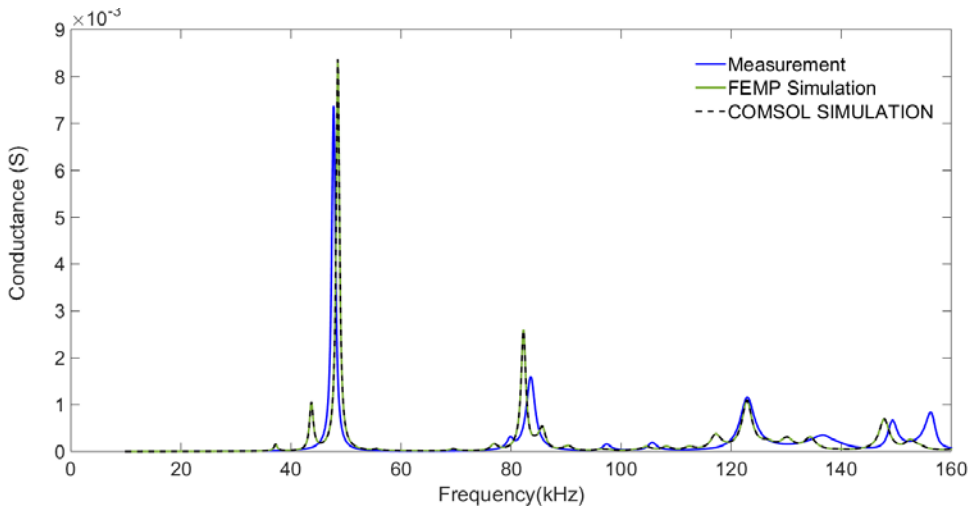


Figure 5.16. – Conductance comparison between simulation and measurement. PIC255 piezoelectric ceramic + 3mm of EL217C front layer material

Figures 5.15 and 5.16 graphically represent the final fit obtained for both materials. Theoretical estimations data for matching and backing material are collected in Table 5.16 and experimental results in

Table 5.17

Material	EL217C	CORK TD1049
Densidad [kg/m ³]	1100	950
E[Pa]	2e8	8.4e7
V	0,44	0,4
v _L [m/s]	1248	513
v _S [m/s]	255	178
Z[Mrayls]	1.4	0.487

Table 5.16. Materials acoustic properties Theoretical estimation

Material	EL217C	CORK TD1049
Densidad [kg/m ³]	1100	950
v _L [m/s]	1470±3.26	650±4.13
v _S [m/s]	485	265
Z[Mrayls]	1.61	0.598
Q	45.61	39.7

Table 5.17. Acoustic material properties adjusted

Experimental and theoretical estimation present a low deviation, having bigger values the experimental results.

EL217C selected as a matching material have an acoustic impedance of 1.61MRayls. This value is below the recommended to maximize the energy transfer. Following equation (3.44), Front layer acoustic impedance value, should be for a proper energy transmission in water (1.5MRayls), around 5.74 MRayls for PZ37 and 7.24 MRayls for PIC255.

5.4. PROTOTYPE MODELLING AND IMPLEMENTATION

Characterized the materials wrapped in the design, next is to proceed to the realization of a simulation model that includes the full transducer in water. Several models have been realized and two have been selected, one for each prototype. The prototypes present the same material configuration except for the piezoelectric ceramics. Both of them, operates around 120 kHz and its general description is as follows:

Prototype 1:

PIEZOELECTRIC CERAMIC: PIC255 (PI CERAMICS)

CASING: ABS

MATCHING: EL217C (3mm)

BACKING: TD1049 (6.5mm)

Prototype 2:

PIEZOELECTRIC CERAMIC: PZ37 (FERROPERM)

CASING: ABS

MATCHING: EL217C (3mm)

BACKING: TD1049 (6.5mm)

This section describes the simulation model carried out with its main characteristics. On the other hand, prototypes once constructed and characterized are compared with simulation results in order to verify that the estimated behaviour approaches or not as measured experimentally.

This model simulation is carried out only by FEMP software due to the bigger resources and computer cost required by COMSOL when a surrounding medium, around transducer, is introduced with the technical capabilities available.

The main features are:

- 2D axisymmetric model with a harmonic analysis is realized. Electrical admittance, directivity pattern and projector sensitivity (*TVR*) at 1 m are the direct output variables obtain from simulation.
- Receive sensitivity (*OCV*) is extrapolated from projector sensitivity by using reciprocity equation.
- Geometry elements are defined trough points, areas command from FEMP. Due to circular disc geometry and axial symmetry, elements are described as a simple rectangles with origin in the revolution axis.
- 3 mm is stablish as EL217c matching layer thickness to achieve the $\lambda/4$ wavelength.
- Electric potential is define in ceramic boundaries. Its value is setup in 1V.
- Casing material is added. It is ABS plastic material(www.ndt.net n.d.). It has not been characterized but its acoustic properties have been taken out from a material library. The properties values are collected in Table 5.18

Material	ABS
Densidad [kg/m ³]	1050
v_L [m/s]	2250
v_S [m/s]	1120
Z[Mrayls]	2.36
Q	72.52

Table 5.18. ABS acoustic properties

- A water medium is introduced with a radial geometry. Radius is defined to 0.1meter, 10 times bigger than the maximum frequency wavelength. The properties are listed below

Material	WATER
Densidad [kg/m ³]	1000
v_L [m/s]	1485
α [dB/m]	0

Table 5.19. Water acoustic properties

- The impossibility to model an infinite surrounding medium or bigger enough to obtain values in far field provoke the introduction of an INFINITE ELEMENT layer(Comsol 2010; Kocbach 2000a). It avoids undesirable boundary reflections

and the possibility to obtain results from far field regime. Infinite element thickness layer is set to 100 mm

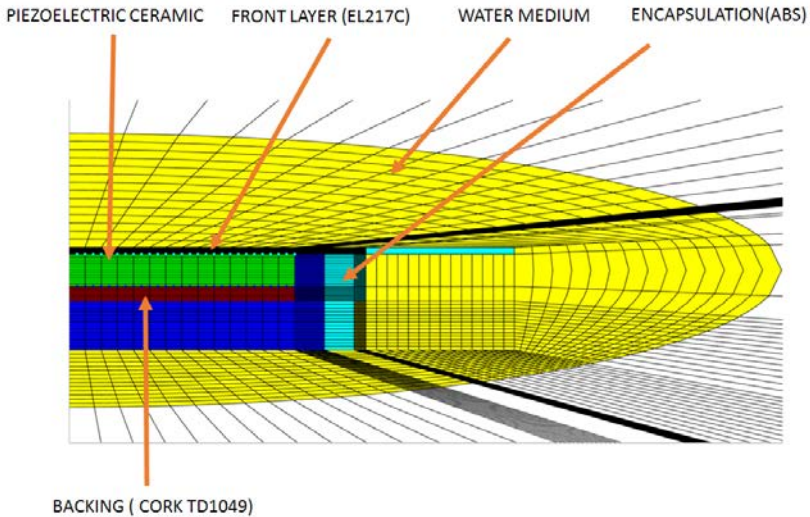


Figure 5.17. – FEMP simulation model: Full transducer in water

Elements per wavelength is setup at 20 after a convergence study for each material except in the infinite element that is set to 1 as a FEMP recommendation. Plot diagram with geometry dimensions in mm is shown in figure 5.18

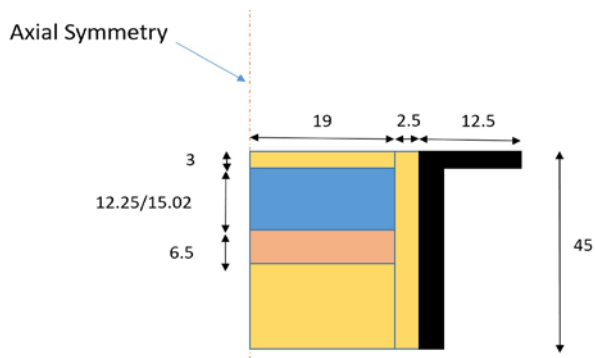


Figure 5.18. – Geometry dimension

The construction process for the two prototypes is graphically described in figure 5.19.

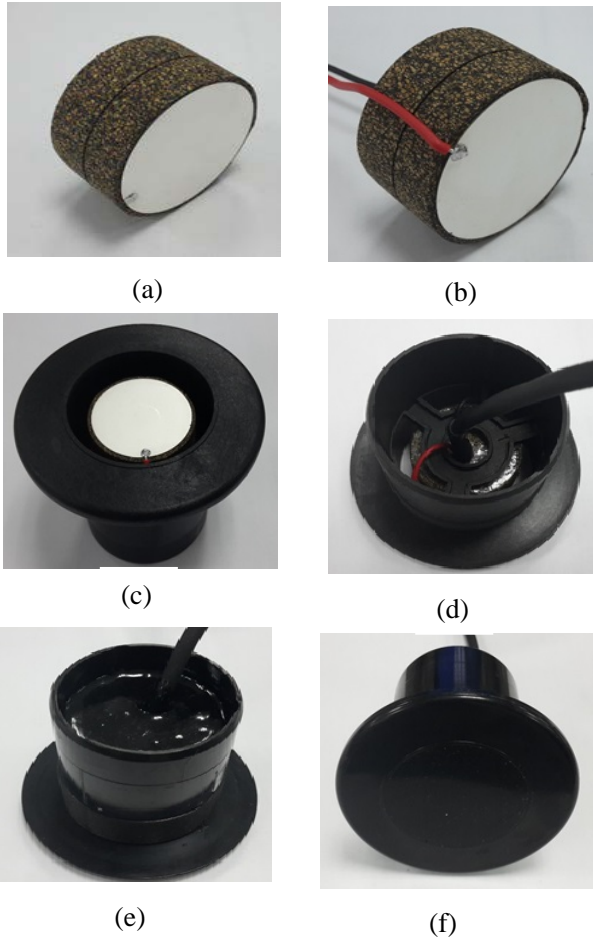


Figure 5.19. – Transducer construction steps. (a) Backing adhesion, (b) Piezoelectric ceramic wired (c) Housing introduction, (d) Matching filling, (e) Elements encapsulation and (f) Transducer finalized

The steps are the following:

1. Backing adhesion

Cork TD1049 disc with 6.5mm thickness is added to piezoelectric ceramic through a transparent epoxy glue.

2. Piezoelectric ceramic wired

Two wires are soldered to the front and rear piezoelectric ceramic faces. These faces are pre-metallized with the silver oxide varnish. In the piezo ceramic rear face where backing is attached, small slot is done to facilitate the process.

3. Housing introduction

ABS Housing presents an internal grate. Block compound by ceramic plus backing is fixed to the grate leaving 3 mm space at the top. This space will be filled with EL217C as a matching layer.

4. Matching filling

Top housing face is collocated towards the table and EL217C mix is verted until the 3 mm are filled.

5. Elements encapsulation

At the same time matching layer is obtained, all the elements transducer are also covered with EL217C mix until achieve a proper encapsulation.

6. Final Transducer

The full transducer set-up is drying for two days and final results is obtained.

5.5. TRANSDUCER CHARACTERIZATION

In this section, we proceed to the two prototypes characterization. In this characterization, the four parameters obtained in the simulation are measured: Electrical admittance, projector and receiver sensitivity, *TVR* and *OCV* respectively, and directivity at frequency of interest.

Following sections describe the experimental set-up and the methodology used to obtain each parameter.

Finally, results obtained for each transducer will be presented. These results will be used in section 4.8 for the complete transducer simulation model validation in water.

5.5.1. MATERIALS AND METHODS

Methodology of measurement is divided into two blocks. The method used for the electrical measurement and the method used for the acoustic characterization. Both are described in detail below.

5.5.1.1. ELECTRICAL ADMITTANCE MEASUREMENT.

Measurement procedure for obtaining the electric admittance is the same as described in the active element and passive materials characterization.

In this case, measurements have been made in both air and water. Measuring equipment and configuration remain the same. Unique variation is the transmission medium. Figure 4.20 shows the transducer arrangement detail according to the loading medium.

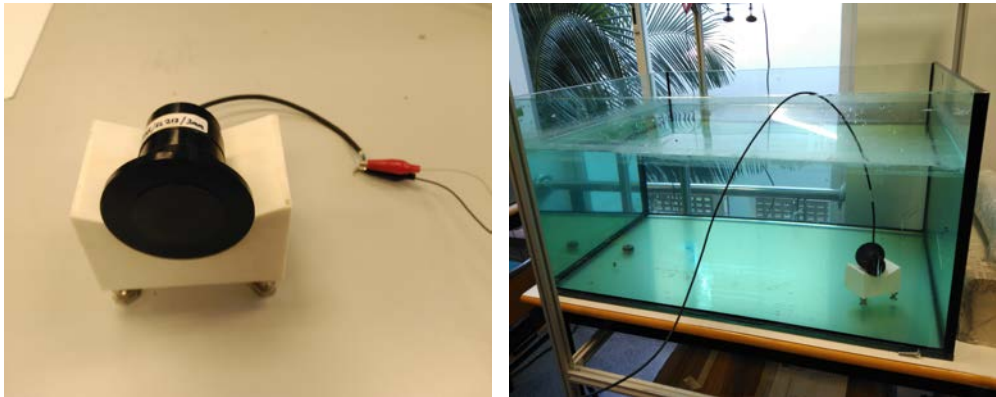


Figure 5.20. – Transducer prototypes placement for electrical admittance measurements. Air and water measurements respectively.

5.5.1.2. SENSITIVITY AND DIRECTIVITY MEASUREMENTS

Directivity and Sensitivity measurements for single nude transducers have been performed in a calibration tank (10 X 5 X 1.5 m³) at the UPV facilities at the Gandia Harbour. A picture of the positioning system is shown in figure 5.21.

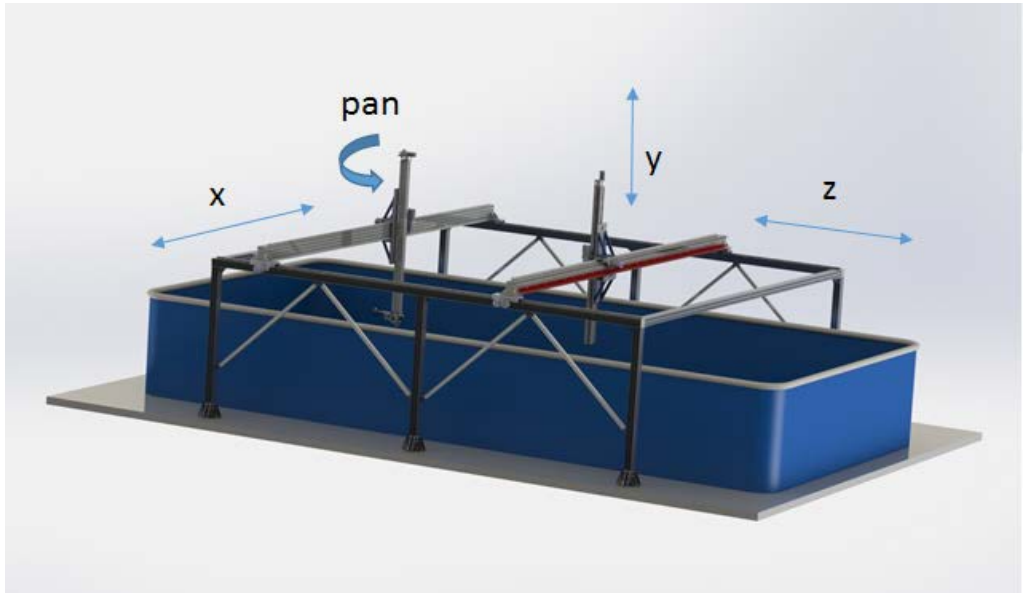


Figure 5.21. – 3D AutoCAD diagram for UPV positioning system.

Six axis are available with three movement directions (X, Y and Z). Another motor is available with PAN movement with 360° rotation.

The tank was filled with fresh water at temperature of approximately 18 Celsius degree yielding a sound speed of $c=1475\text{m}\cdot\text{s}^{-1}$ calculated from Coopens equation (2. 16).

A low-cost but reliable system is implemented for transducer calibration. This calibration system is based in a Red Pitaya device (redpitaya n.d.), an open-source project based in a FPGA card that includes 2x 125MS/s RF input and 2x 125MS/s RF outputs, with 50MHz analogue bandwidth. The default software of the FPGA of the Red Pitaya includes oscilloscope, spectrum analyser, signal generator, LCR meter, and 50MHz 2x2 MIMO PID controller. It can be re-programmed to become other devices, as all the IO ports are

connected to a common FPGA. There are also auxiliary ADC (250kS/s) and digital IO. It has three USB 2.0 ports, Wi-Fi, Ethernet connector. Internally, it uses Linux as operating system. Before measurement its emission and acquisition properties have been calibrated.

A computer controlled a Transmitter/Receiver USB TCP/IP card generate a 1V peak (20 cycles) sine burst. The necessary high voltage for nude transducer excitation will be provided by a linear 55dB (gain) RF AMPLIFIER ENI 1040L. With him 12 V_{peak} are transmitted. At a distance of 1m, a TC4034 RESON hydrophone is used to detect the signal. The recoding the signal and it is digitized using the Transmitter/Receiver USB TCP/IP card input channel. Measurements were made over the frequency range 40 kHz to 160 kHz. Figure 5.22 shown the configuration.

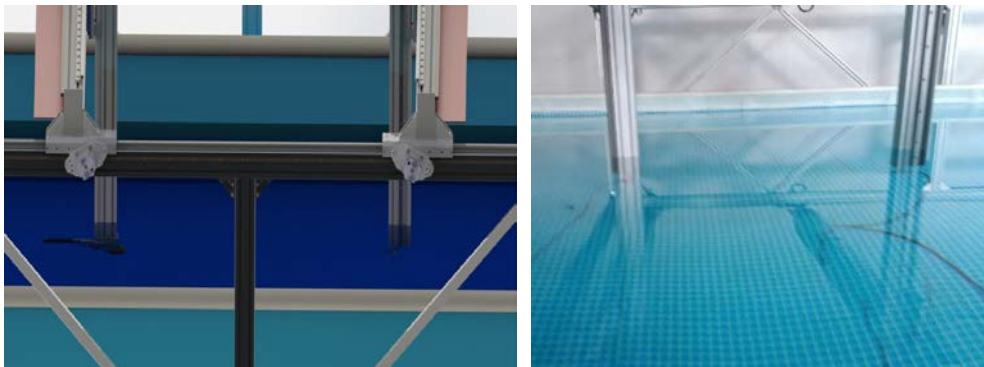


Figure 5.22. – Transducer and hydrophone measurement disposition. 3D AutoCAD representation and real image respectively.

Methodology for sensitivity measurements setup have been performance following the next configuration. On-axis transducer measurements have been taken with distance between the hydrophone and the device active face of 1m.

Frequency range is set up as in the electrical admittance: From 40 kHz to 160 kHz.

Both receiving and projector sensitivity have been calculated using own-implemented scripts in MATLAB following the equation (2.5)

To apply such relationship the sensitivities as projector or as receiver of the reference hydrophone should be well known.

In case of Projector Sensitivity, TVR , ($\mu Pa/V$), a sinusoidal pulse with a particular amplitude ($12 V_{peak}$) is sent by the transducer and the signal received by the hydrophone is recorded and analysed (Figure 5.23). Based on the hydrophone receiving sensitivity and the recorded signal, the received pressure at the active face of the reference hydrophone is obtained. Thus, applying the inverse of equation (3.20) with range compensation p_0 is calculated and the sensitivity could be then obtain with the knowledge of the applied Voltage.

and the device active face of 1m. In this case, transducer is fix to a rotation motor. Only one frequency is measured at time. Transducer move for 0° to 180° in steps of 1.8° . Signal is detected for the hydrophone and by MATLAB post-processing signal amplitude for each degree is saved. The result is a diagram plot for this frequency depending on the angle.

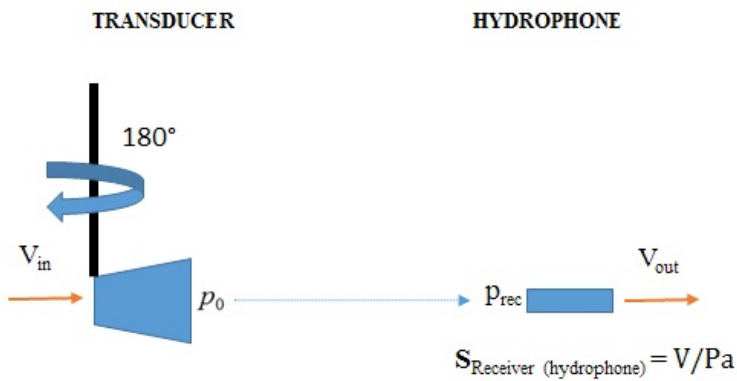


Figure 5.25. – Procedure for the Directivity measurements

5.5.2. RESULTS

Results obtained for the two prototypes are compared. Figure 5.26 shows the electric admittance. As shown for Prototype 1, with PIC255 ceramic, it presents a radial mode stronger than prototype 2 while the frequency corresponding to the thickness mode appears to little bit shifted. The value in prototype 1 is 124 kHz while the 2 is 119 kHz.

On the other hand quality factor (Q) for both prototypes are 23.52 and 17.39 respectively. This agrees with the higher bandwidth show for prototype 2.

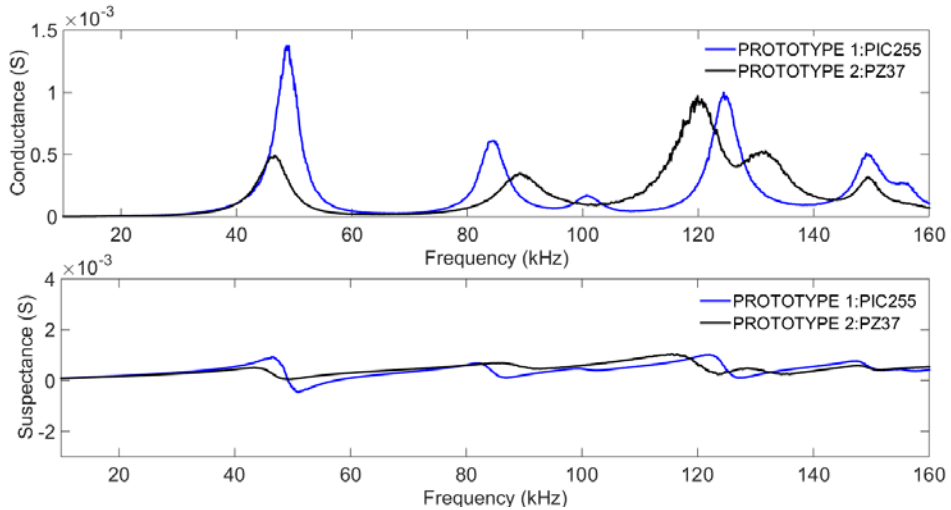


Figure 5.26. – Admittance measurement comparison between prototype 1 and prototype 2.

As for the projector and receiver sensitivity, it is observed that the prototype 2 presents greater sensitivity in the resonance frequency as well as bandwidth. On the other hand, prototype 1 has a higher sensitivity at lower frequency (radial mode), than can be useful for parametric applications, as will be discussed in chapter five.(Figure 4.27 and 4.28)

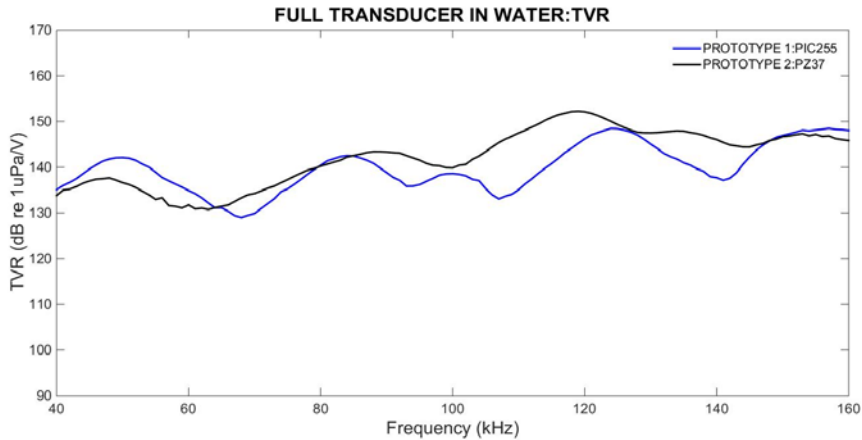


Figure 5.27. – TVR measurement comparison between prototype 1 and prototype 2.

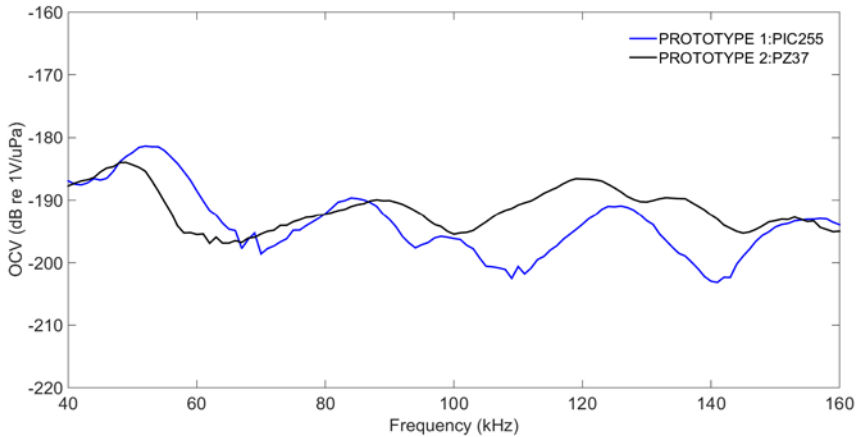


Figure 5.28. – OCV measurement comparison between prototype 1 and prototype 2

TVR and OCV values for both prototypes are collected in Table 5.20 at the frequency of interest, 120 kHz

FREQUENCY (kHz)	TVR (dB re 1uPa/V)		OCV (dB re 1V/uPa)	
	PROTOTYPE 1: PIC255	PROTOTYPE 2: PZ37	PROTOTYPE 1: PIC255	PROTOTYPE 2: PZ37
120	146.7	152.1	-193.9	-186.6

Table 5.20. TVR and OCV values at 120 kHz for both prototypes.

Results shown that prototype 2 with PZ37 arrives to the projector sensitivity requirements (150dB) while prototype 1 with Pic255 ceramic presents -3dB less than the desirable value. In terms of receiver sensitivity this difference increase up to almost 6dB.

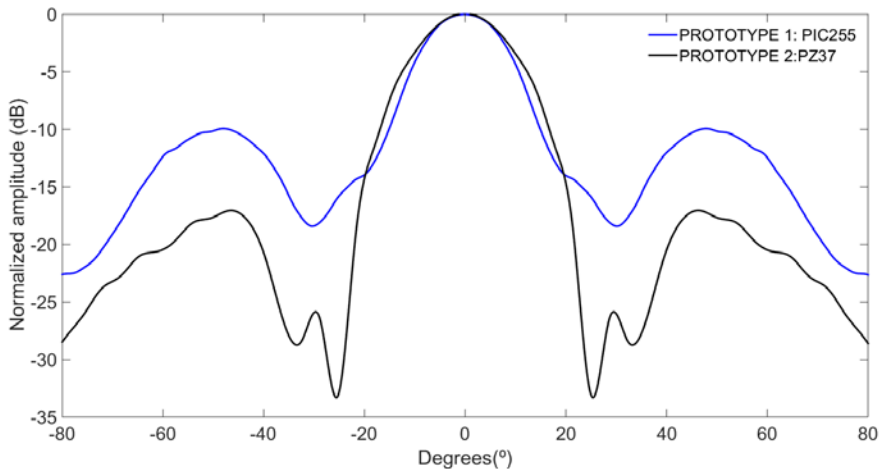


Figure 5.29. –Directivity measurement comparison between prototype 1 and prototype 2 at resonance frequency.

Finally, it is noteworthy, in terms of directivity (Figure 5.29), both transducers have a similar beam aperture, 17° for prototype 1 and 19° for prototype 2. However side lobe

values, reach higher values in prototype 1, with about -10dB, compared to the -18dB of prototype 2 with pz37.

5.6. FEM MODELLING VALIDATION AND DESIGN OPTIONS

Results obtained experimentally in the two prototypes characterization and FEM simulation model for the full transducer in water are compared.

The objective is to verify if the behaviour estimation of numerical model approaches the real behaviour.

On the other hand, once validated, it is used as a design tool without the need to manufacture more prototypes. Various modifications and their comparison, with the current model, will be presented.

5.6.1. FEM MODELLING VALIDATION

Numerical models are nowadays a very active tool in transducer design. The reliability of the results extracted from them depends on many factors (correct description of the materials, meshing, etc.)

In this case, due to the approximation of the acoustic properties of some materials, idealizations in the assembly and model simplifications, a comparison is made with experimental measurements to proceed to the validation of the method.

The comparisons of the two prototypes are shown below.

5.6.1.1. PROTOTYPE 1: PIC255

Four parameters obtained from the simulation are compared with their corresponding measurements

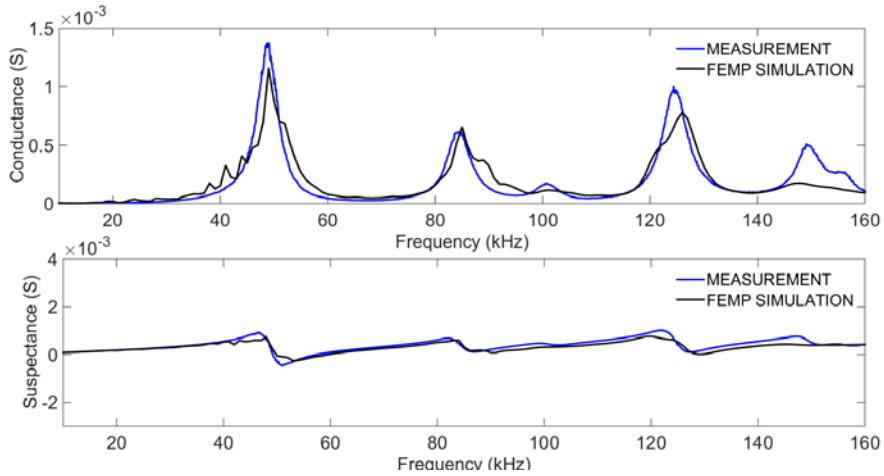


Figure 5.30. –Prototype 1: Electrical admittance comparison between FEM simulation model and measurement

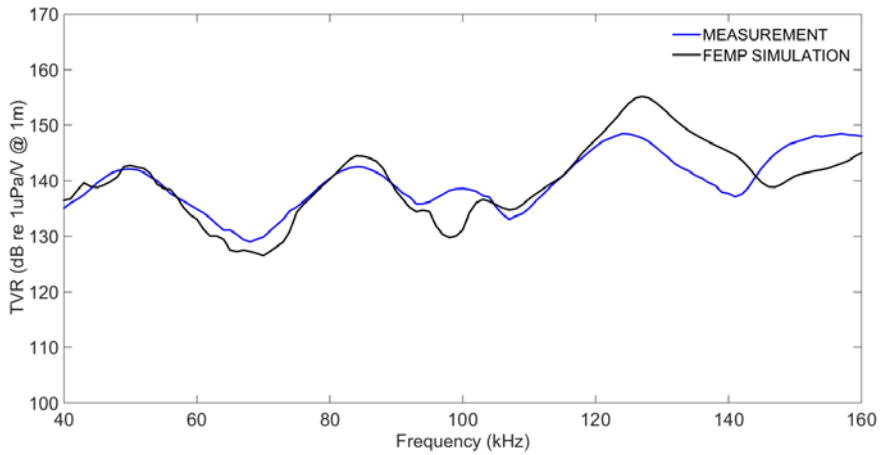


Figure 5.31. – Prototype 1: Projector sensitivity comparison between FEM simulation model and measurement

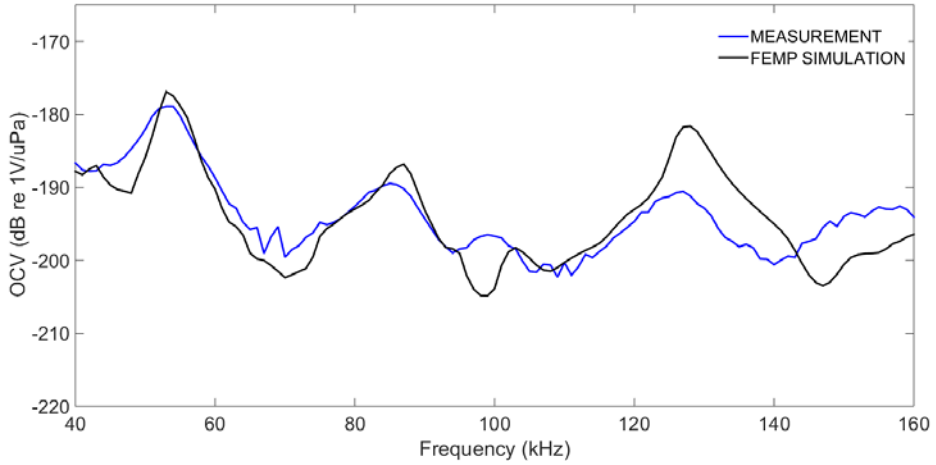


Figure 5.32. – Prototype 1: Receiver sensitivity comparison between FEM simulation model and measurement.

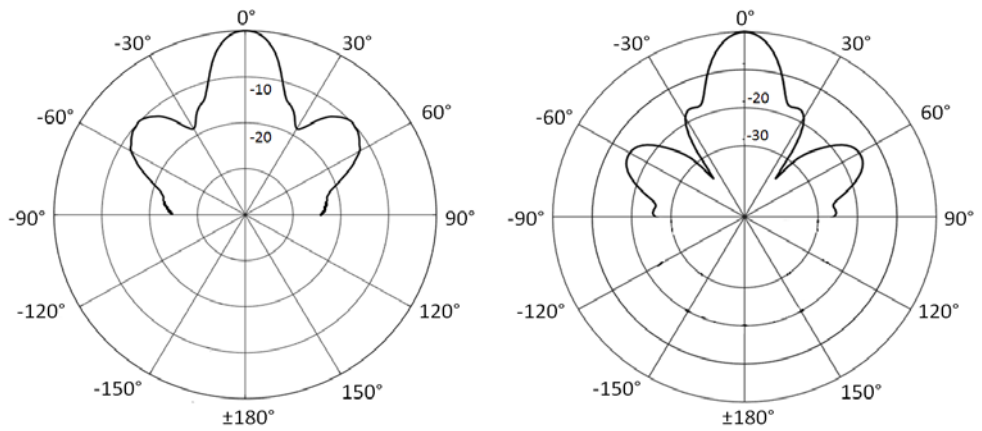


Figure 5.33. – Prototype 1: Directivity comparison between measurement and FEM simulation model respectively.

Simulation model behaviour follows the trend of experimental measurements with deviation at 120 kHz, not larger than 0.8%.

The vibration modes are clearly represented although the simulated values always overestimate the real value.

5.6.1.2. PROTOTYPE 2: PZ37

Same procedure is performed like with prototype 1.

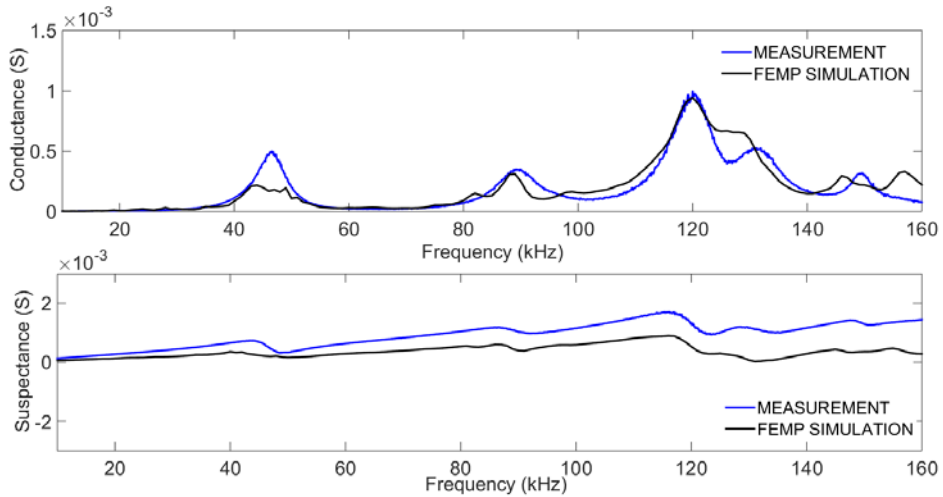


Figure 5.34. – Prototype 2: Electrical admittance comparison between FEM simulation model and measurement.

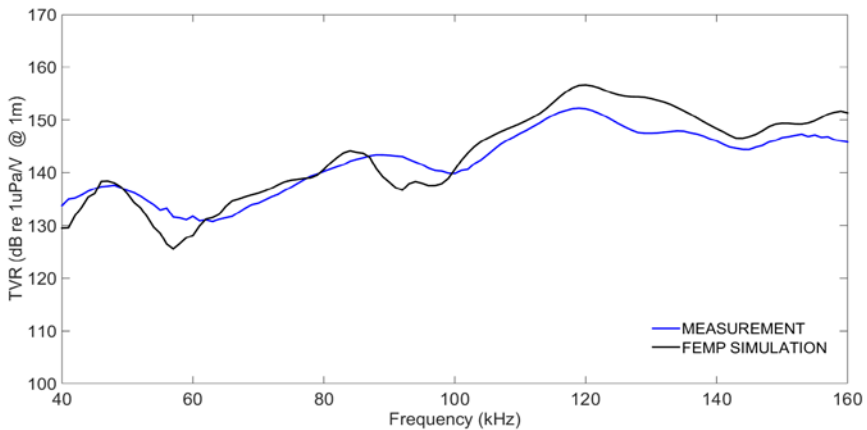


Figure 5.35. – Prototype 2: Projector sensitivity comparison between FEM simulation model and measurement

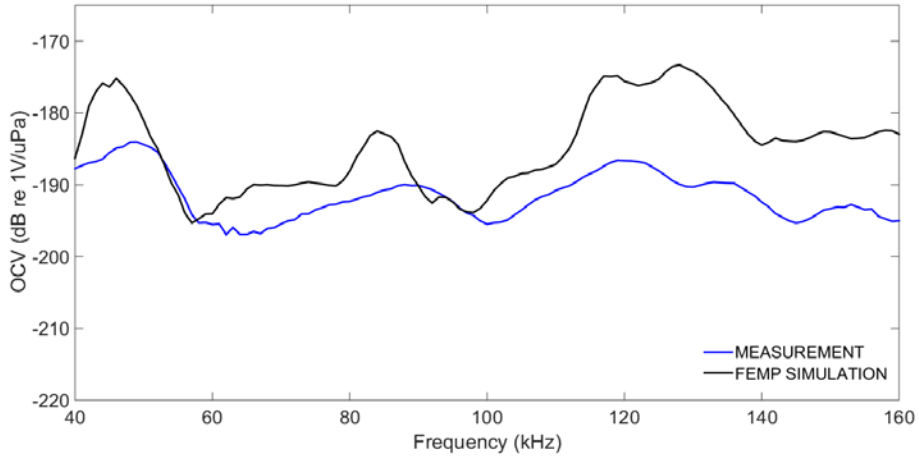


Figure 5.36. – Prototype 2: Receiver sensitivity comparison between FEM simulation model and measurement

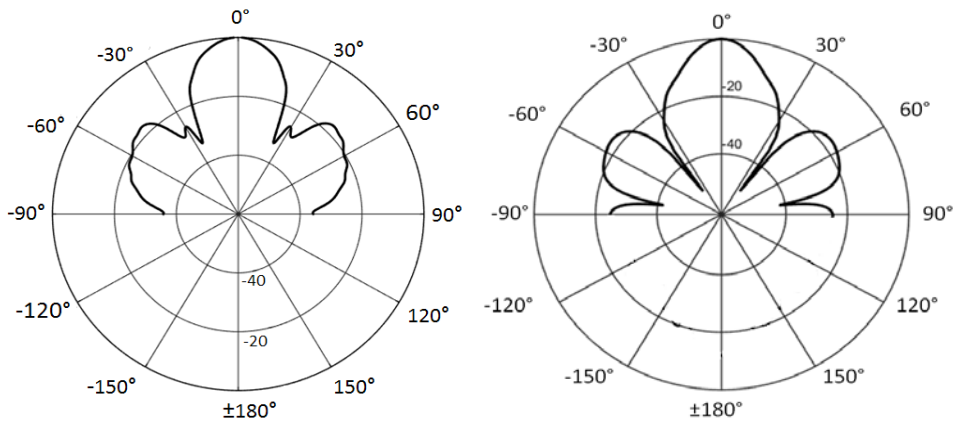


Figure 5.37. – Prototype 2: Directivity comparison between measurement and FEM simulation model respectively.

Like in prototype 1, simulation trend follows the experimental results although deviation reach 3% in the *TVR* results and 6% in *OCV* results.

The conclusions drawn from the results are that the simulation models performed are valid to be used as a design tool.

Although variables values under study are overestimated the behaviour trend is reliable and they contribute to give information of great interest.

5.6.2. DESIGN IMPROVEMENT

Two new design are presented in order to improve the parameters of interest. These alternative configurations involve matching and backing modification. In the former, is introduced Eccosorb MF114 as a matching layer (Aanes 2013). This material has an acoustic impedance closer to the ideal, for proper energy transfer, and bigger attenuation than the current material (EL217C).

On the other hand, the latter introduce a backing modification by changing Cork TD1049 for Insulcast 501 (Mansoura et al. 2012; Pedro Acevedo and Israel Sánchez Domínguez 2015). The main different characteristics are:

- Insulcast 501 is an elastic material instead of porous with an acoustic impedance higher than TD1049 and closer to the piezoelectric ceramic acoustic impedance.
- Material attenuation is almost three times lower than cork

Table 5.21 collect the materials acoustic properties.

Material	Insulcast 501	Eccosorb MF114
Densidad [kg/m ³]	3860	2850
v_L [m/s]	1975	2250
V_s [m/s]	1055	1000
Z[MRayls]	7.26	6.4
Q	127.3	20
α [dB/m]	0.0138	72.76

Table 5.21. Insulcast 501 and Eccosorb MF114 acoustic material properties

TVR and OCV results from simulation model are represented graphically in Figures 5.38 and 5.39. Frequency operation values are summarized in table 5.22 and 5.23

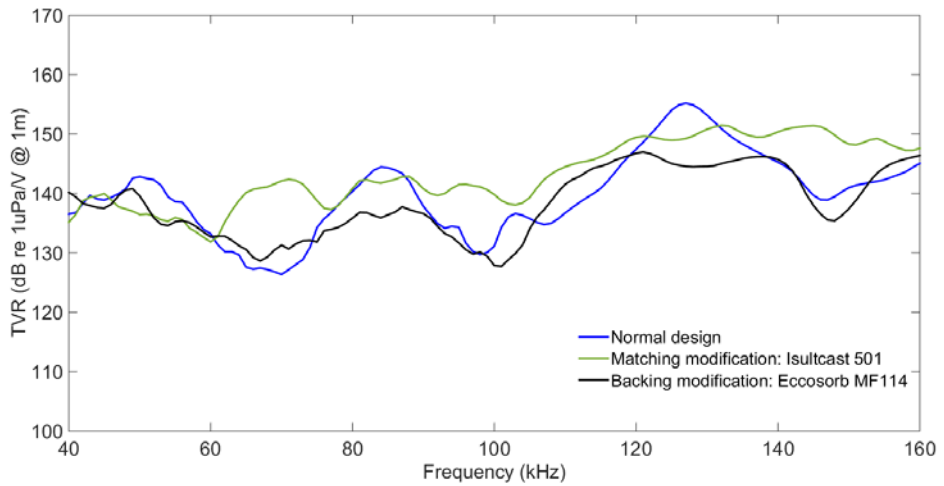


Figure 5.38. –Projector sensitivity comparison between three FEM simulation models with different design parameters modification

FREQ(kHz)	TVR (dB re 1uPa/V)		
	NORMAL	MACTHING	BACKING
120	147.4	149.4	146.8

Table 5.22. TVR values at 120 kHz for the four FEM simulation models.

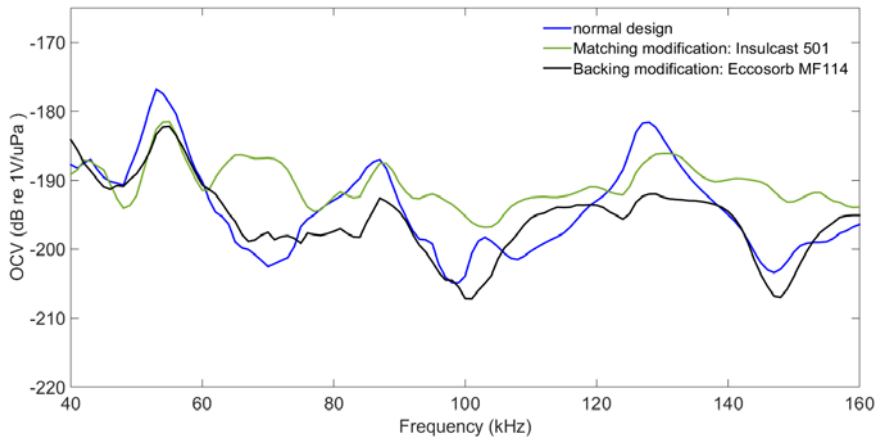


Figure 5.39. –Receiver sensitivity comparison between three FEM simulation models with different design parameters modification

FREQ(kHz)	OCV (dB re 1V/uPa)		
	NORMAL	MATCHING	BACKING
120	-193	-191	-193.7

Table 5.23. TVR values at 120 kHz for the four FEM simulation models.

From these it is observed that by modifying the matching layer, at the operation frequency, sensitivity increase in 2dB in both, emission and reception and presents a higher bandwidth, obtaining a stable value range from 120 kHz to 150 kHz.

On the other hand, when modifying the backing, it is observed that although a greater transfer of energy reflected in greater bandwidth is achieved, transmission and reception efficiency are lower

5.7. CONCLUSIONS

This chapter presents an ultrasonic transducer design for fisheries acoustics application, especially for fish biomass estimation and species characterization, with certain acoustic properties establish. These are: 120 kHz operation frequency, between 15° and 20° Beamwidth and a Projector sensitivity value, at operation frequency, not lower than 150 dB re 1uPa/V.

For its development, is proceeded to the acoustic characterization of all the materials involved in the design. Simultaneously, a finite element simulation model is created to serve as a future design tool, with which to estimate full transducer behaviour in water.

Once materials properties are extracted, two prototypes are built with the most optimal configuration for each element. Both prototypes have the same characteristics except for the active element. Piezoelectric ceramics, PIC255 and PZ37, are the active elements used. Prototypes characterization shows that prototype n°2, with PZ37 piezoelectric ceramic, meets the specified requirements in its entirety, while prototype n°1, with PIC255 ceramic, presents in terms of projector sensitivity -3dB less than the set value.

As far as the simulation model is concerned, it is validated with the comparison made with the experimental measurements. In the adjustment of both prototypes, it is observed that prototype n°1 has better agreement due to the lower dispersion of the piezoelectric coefficients (PIC255).

Therefore, this numerical model is chosen to introduce various improvement design options. From this study, it is observed that materials selection with acoustic properties more adequate to the general design rules, offers transducers with greater bandwidth and more stable sensibilities all over the frequency range

6

Parametric echosounding in shallow water

Throughout this thesis has been introduced different concepts necessary for ultrasonic transducer design and its use in underwater acoustics. In this chapter, will be studied the capability of the designed prototypes as part of a parametric scientific echosounder for shallow water measurements. In this section, a previous study, based in numerical simulation, is presented as a tool to establish some measurements parameters. In next point, materials and methods are described in detail. Finally, results and simulation comparison are presented and in finally, feasibility of their use in different applications (aquaculture, fisheries, etc.) is presented.

6.1. PARAMETRIC ARRAY: PRELIMINARY STUDY

Before proceeding with experimental measurements, a 2D simulation has been performed with K-Wave Toolbox, to observe in which range of input pressures starts the parametric generation. In addition, field obtained at different distances is also evaluated in order to effectively see that parametric effect is a power effect that occurs in the medium.

For this purpose, a 19 mm radius flat piston is simulated, same radius than designed prototypes. First a linear simulation, at 120kHz, is realized in order to compare with the prototypes characterization and validate the simulation. Figure 6.1 presents the directivity comparison between simulation and experimental measurements for both prototypes at 120kHz.

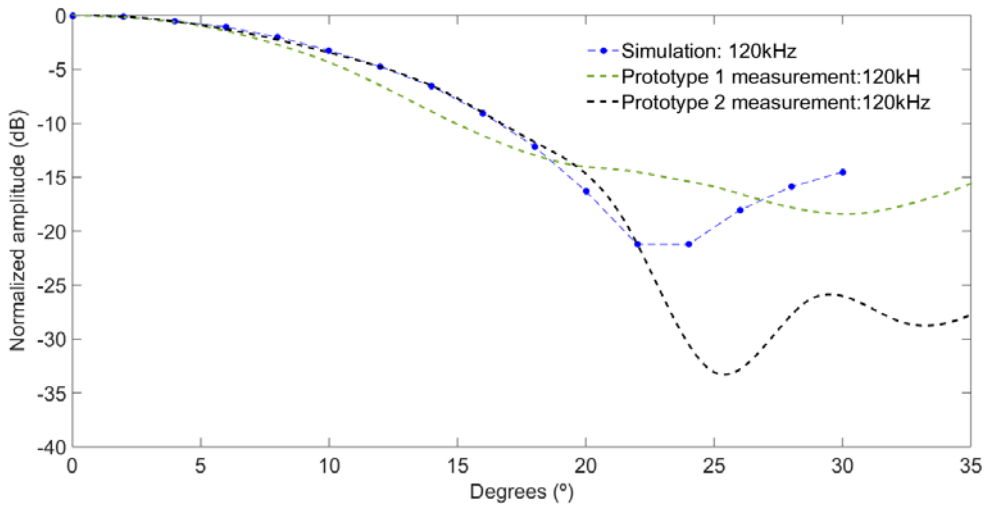


Figure 6.1. Directivity comparison between K-wave simulation and experimental measurements at 120 kHz

Through the results, it is observed that both, simulation and experimental measurements have good agreement. Slightly discrepancy is presented in prototype 1, while prototype 2 fits perfectly until 20°. Sidelobe level in simulation overestimate the real value.

Once model is validated, input signal is changed to generate parametric effect. A Byfrequency signal, of 90 and 150 kHz that will generate a difference harmonic of 60 kHz and 240kHz sum harmonic is chosen following the experimental setup. This signal is evaluated at different pressure ranges, from 50000 Pa to 1MPa, and power spectral density (PSD) is obtained for different distances (1cm, 40cm ... up to 1.61m).

In Figure 6.2, results are presented for each simulation. Through PSD, it is obtained the energy contained in each spectral component. In the graphics it is observed, that in all pressure levels there is parametric generation. On the other hand, higher harmonics are clearly observed in each level, however, difference harmonic for a pressure of 50000 Pa presents very little level being seen clearly around the 250000Pa.

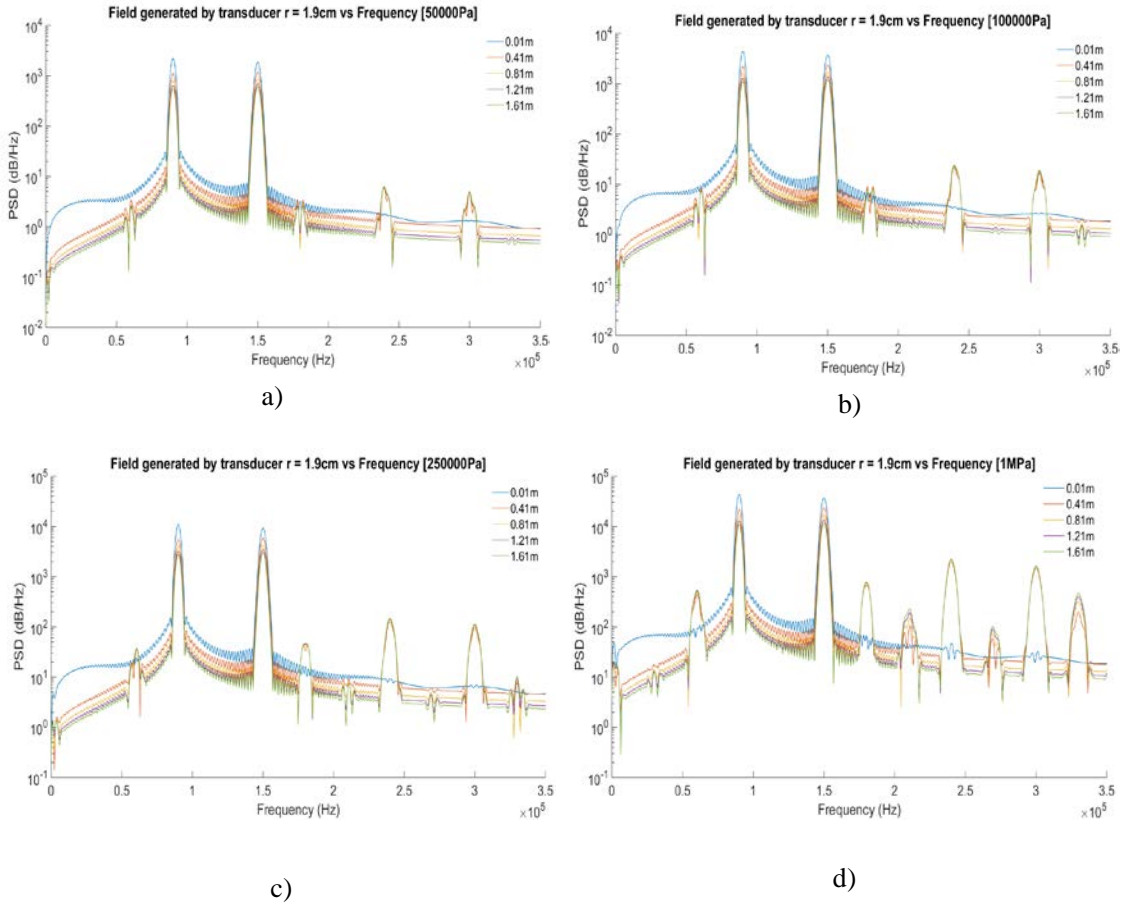


Figure 6.2. Byfrequency K-Wave simulation for 19mm radius transducer at different distances. a) Field generated with an input pressure of 50000 Pa. b) Field generated with an input pressure of 100000 Pa. c) Field generated with an input pressure of 250000 Pa. d) Field generated with an input pressure of 1MPa.

In figure 6.3 this harmonic generation is observed in detail at a certain distance (1.61m). As pressure amplitude increases, primary frequencies energy is transferred to the different harmonics. From 100,000 Pa, it is possible to discriminate difference and sum harmonic, that are those that interest in this study.

Finally, if return to Figure 6.2 , it can be seen that this phenomenon, is an effect that occurs in the medium since, at 1 cm from the source, for all cases there is no parametric generation and begins to observe from the 40 cm.

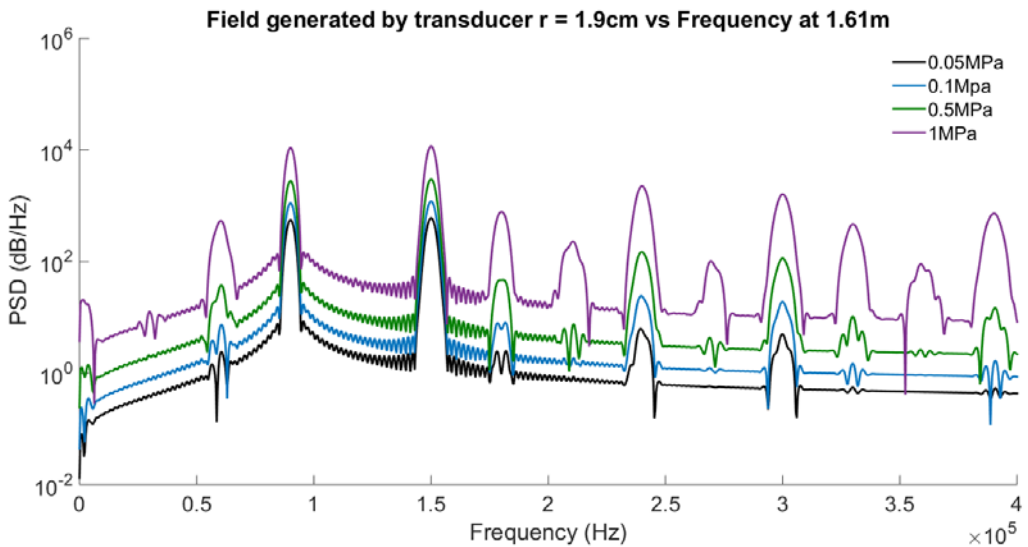


Figure 6.3. Byfrequency K-Wave simulation for a 19mm radius transducer with different input pressure level at distance of 1.61m.

6.2. MATERIALS AND METHODS

In this section, we explain the used materials and experimental measurements carried out to characterize the non-linear behaviour of the two designed prototypes. For the study of parametric efficiency generation, three different measurement procedures are proposed. In addition, one more commercial transducers is evaluated, in order to investigate the influence of higher central frequency and side lobe relevance.

6.2.1. TRANSDUCER UNDER STUDY

Transducers under study are the two designed prototypes in Chapter 5. Both prototypes, work at 120 kHz and the only difference between them is the active element material. Prototype 1 has a PIC255 ceramic (PI Ceramic GmbH n.d.) With dimensions of 38X15.02 mm, while prototype 2 has a PZ37 ceramic, dimensions 38X12.25mm (Ferroperm n.d.). From characterization obtained in section 5.5.2 , it is established that the beam aperture at -3dB is 17° and 19° respectively, with side lobes of -10dB respect to the main lobe for prototype 1 and -17dB for prototype 2. In addition to these transducers, in this chapter, as mentioned earlier, one more transducers from AIRMAR (AIRMAR technology) will be evaluated. This is:

- AIRMAR P19:



It works with an operation frequency greater than the prototypes, 200kHz. Beam aperture is similar, around 15°, and it presents a side level lobe of -12dB. With this transducer characterization, it is tried to evaluate if for a similar aperture, with primary frequencies greater, we improve parametric generation efficiency.

From transmitting voltage response graphic of each transducer (Figure 6.3) and table (6.1) different guidelines can be obtained to take into account when selecting parametric frequencies.

	PROTOTYPE 1	PROTOTYPE 2	AIRMAR P19
TVR (120kHz/200kHz)	146,2	152,1	156,9
TVR (50kHz)	142,1	136,6	119,3
120/200kHz vs 50kHz (dB)	4,1	15,5	37,6

Tabla 6.1. TVR values at thickness and radial frequency for each Transducer.

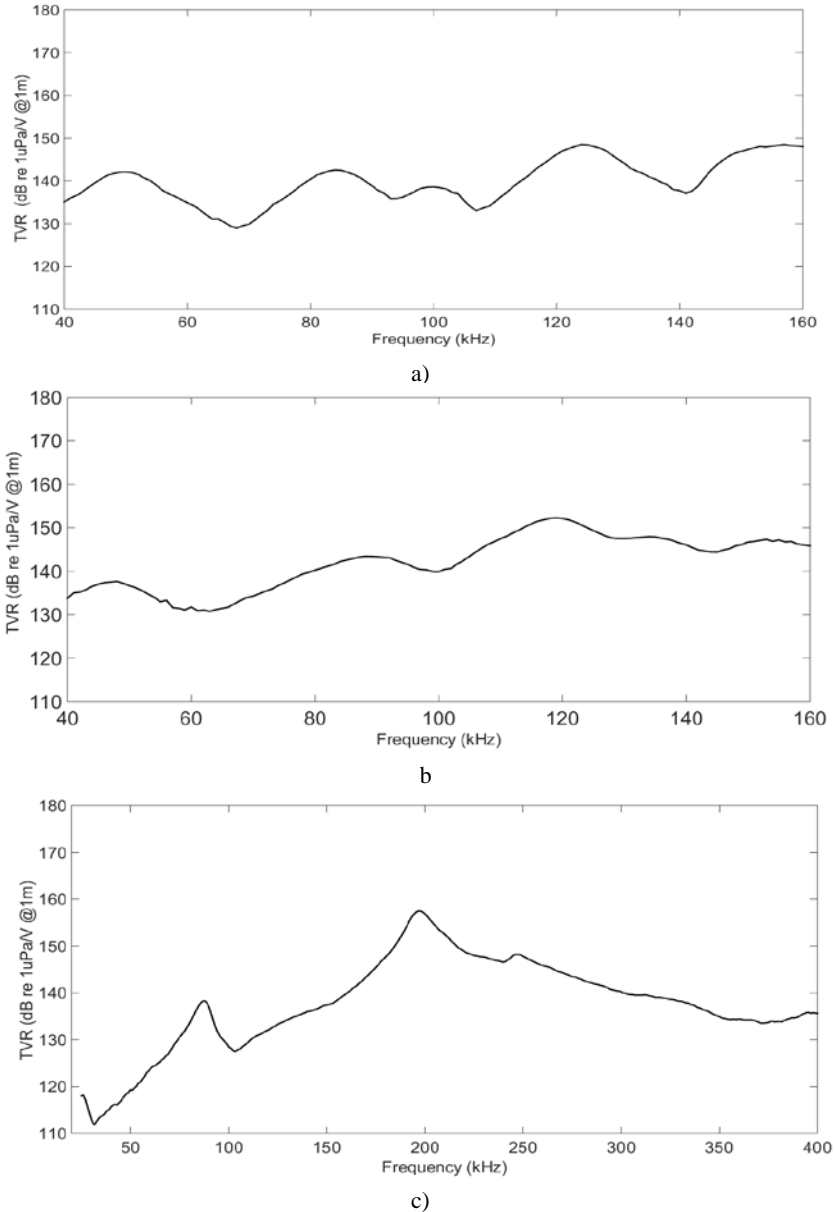


Figure 6.4. Transmitting Voltage Response as a function of frequency for each transducer. Prototype 1, prototype 2 and Airmar P19 respectively.

If vibrational modes are observed, two prototypes have their radial resonance frequency around 50 kHz. However, relationship between the resonance frequency in the thickness mode and the radial mode is quite different. The first prototype (PIC255) presents a difference level of only 4dB, while in the second, difference arose to 15dB. In both cases, the frequency in the thickness mode presents greater amplitude.

6.2.2. EXPERIMENTAL SET-UP

Experimental set-up is the same as that introduced in transducer characterization (Section 5.5) inside of sensibility and directivity measurements (5.5.1.2). Methodology employed is different and it will be explain following.

6.2.3. METHODOLOGY

Three measurement procedures are used to characterize parametric generation in each transducer. The explanation is below.

6.2.3.1. AMPLITUDE IN FUNCTION OF VOLTAGE MEASUREMENT

Parametric effect is a non-linear phenomenon that occurs in the medium. As it was shown in Section 5.3, with K-wave simulations, from certain input pressure level in the transmitter transducer is when the harmonic generation appear. To check measurements and theory agree, amplitude as function of voltage measurements are done.

On-axis transducer measurements are taken with distance between hydrophone and the device active face of 1.5m. A Byfrequency modulated signal is measured for 5 different voltage values and for each of them, pressure value for each spectral component is obtained. (Figure 6.5).

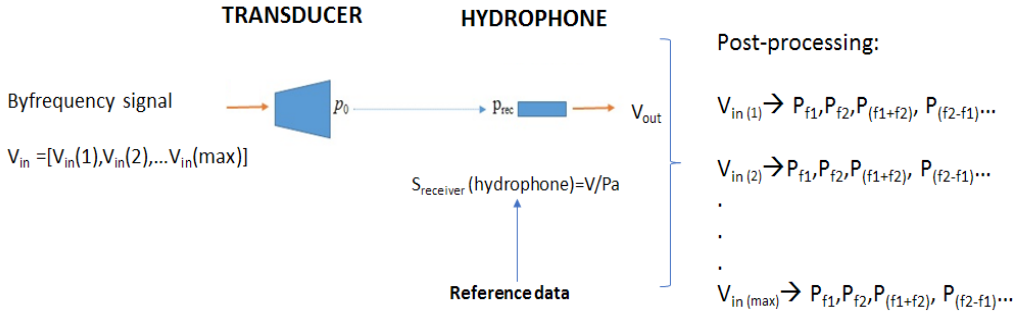


Figure 6.5. Amplitude as function of voltage measurement esqueme

It must be ensured that all transducers under study transmit the same pressure in the medium for each voltage. How impedance differences exists between them, voltage applied will be different, to make sure measurements are comparable, the next approach is made.

Measurements are first realized with Prototype 2. Arbitrary voltage is chosen. Once receive pressure is record by the hydrophone, pressure is linearly backward retro-propagated using Piston equation. A pressure approximation in the front face transducer (P0) is obtain and then, it is scaled for the rest of amplitude levels.

Transmitting voltage response, at the interest frequencies and the calculated pressure, will give the necessary voltage for the rest of transducers to obtain similar pressure in the medium, making measurements comparable.

Analysis methodology to obtain amplitude pressure for each spectral component in this measurement is applied to all procedures explain in this section. It is made with MATLAB software and steps in the post processing are the next:

1. Cut the signal (To avoid undesirable reflections)
2. Signal filtering in every interest frequency band. Filter used is an infinite impulse response (IIR), particularly, a Butterworth. These filters are made with the minimum order possible. Analysis have been done with three different band frequencies: 2kHz,4kHz and 10kHz,
3. Amplitude for each signal obtained from filtering is calculated. This amplitude is obtain through the mean value of the absolute Hilbert envelope.
4. Amplitude obtained and Hydrophone receiver sensitivity are used to give the pressure at each spectral component.

6.2.3.2. DIRECTIVITY MEASUREMENT

To verify that harmonics generated by the parametric array have a similar radiation pattern than primary frequencies, directivity measurements are realized. On-axis transducer measurements have been taken with distance between the hydrophone and the device active face of 1.5m. In this case, transducer is fix to a rotation motor. A Byfrequency signal is transmitted. Transducer move for -81° to 81° in steps of 1.8° . Signal is detected for the hydrophone and by the post-processing explain in the last point, signal amplitude

for each spectral component and degree is obtained. The result is a diagram plot for this frequency depending on the angle.

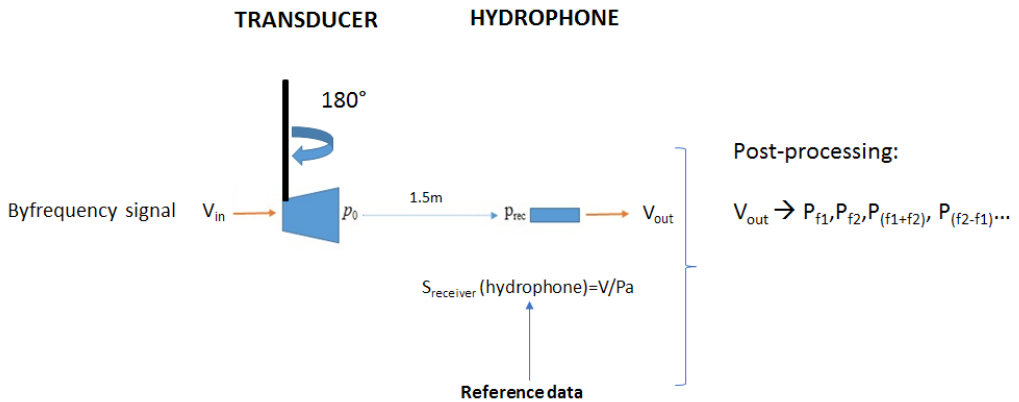


Figure 6.6. Directivity measurement esqueme.

6.2.3.3. AMPLITUDE IN FUNCTION OF DISTANCE MEASUREMENT

Finally, amplitude decay of the primary and secondary waves is measured. A Byfrequency signal is transmitted with a constant amplitude and signal is recorded by the hydrophone in different distances. (Figure 6.7)

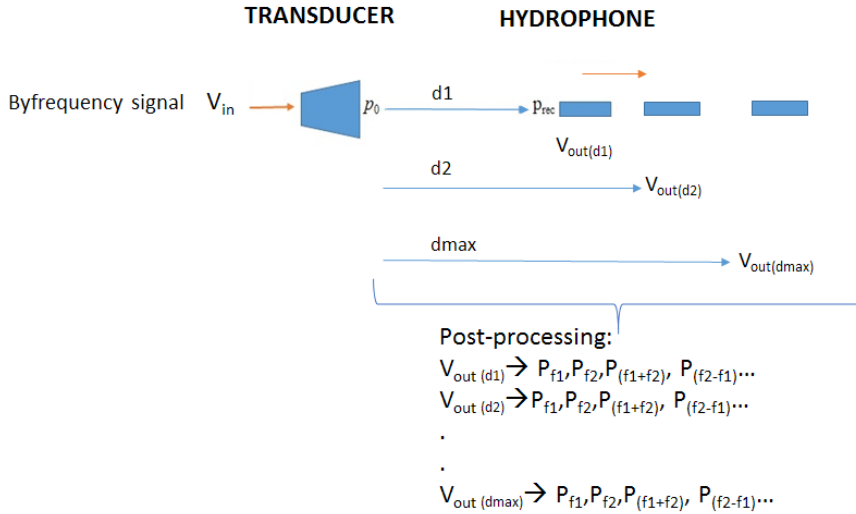


Figure 6.7. Amplitude as function of distance measurement escheme.

6.2.4. MEASUREMENT PARAMETERS

6.2.4.1. PARAMETRIC FREQUENCIES SELECTION

Parametric difference frequencies chosen are 50 and 60 kHz. The first of them has been chosen to place us in the radial mode present in both prototypes (Figure 6.4) and to observe the effects that causes.

The second one, 60 kHz, has been chosen to avoid the radial mode but remain in a frequency range separate from the resonance frequency in thickness mode.

Byfrequency signals are generated to obtain these frequencies. These signals have frequencies equidistant from transducer operation frequency. For the two prototypes signals will be composed by:

- 95 kHz and 145 kHz to 50 kHz
- 90 kHz and 150 kHz for 60 kHz

In the case of Airmar P19, with operation frequency of 200 kHz, to obtain the same parametric signals, combination of frequencies will be as follows:

- 175 kHz and 225 kHz for 50kHz
- 170 kHz and 230 kHz for 60 kHz.

In table (6.2) ratio between primary beam and 60 kHz frequency has been added in terms of sensitivity.

	PROTOTYPE 1	PROTOTYPE 2	AIRMAR
TVR (120kHz/200kHz)	146,2	152,1	156,9
TVR (50kHz)	142,1	136,6	119,3
TVR (60kHz)	134,9	131,7	123,8
120/200kHz vs 50kHz (dB)	4,1	15,5	37,6
120/200kHz vs 60kHz(dB)	11,3	20,4	33,1

Tabla 6.2.TVR values and difference levels relation for each transducer.

In both cases, sum frequency corresponds to 240 kHz. This frequency is going to be also evaluated in the results.

6.2.4.2. *AMPLITUDE SIGNAL*

All transducers have been measured emitting the same pressure in the medium. Pressures chosen are as follows:

	Medium Pressure (Pa)
P1	14960
P2	29920
P3	74800
P4	149600
P5	224400
P6	374000

Tabla 6.3. Medium pressure amplitude selected.

6.2.4.3. *SIGNAL LENGTH*

Before starting to measure, a linear study of the signal optimal length is performed.

Three measurements are made at different lengths until the transfer of energy to other vibrational modes than the transducer operation frequency is minimized.

Below is a graphic of power spectral density as a function of frequency for three signal lengths (20, 60 and 80 cycles).

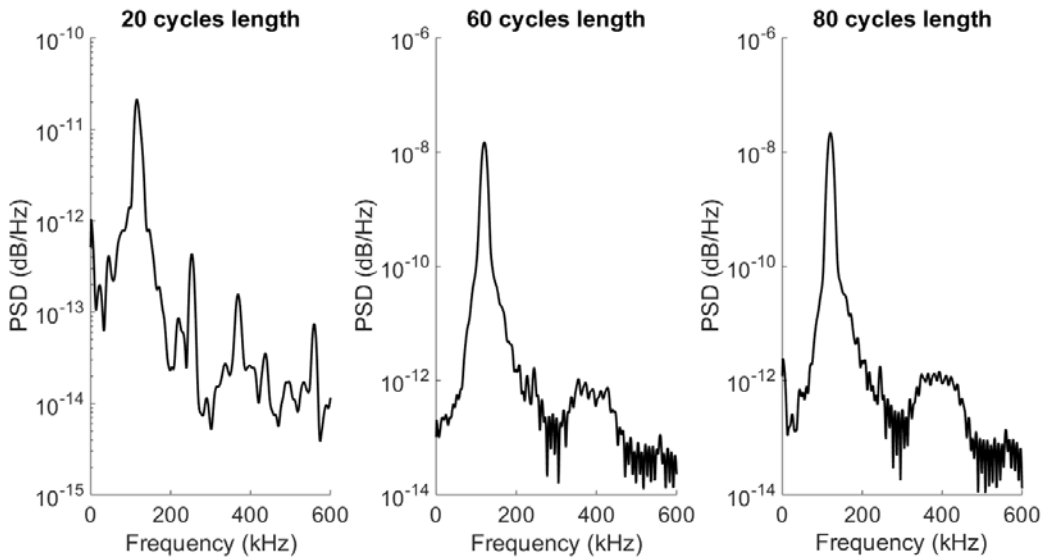


Figure 6.8. Power spectral density as function of frequency depending on signal length

From these results, an 80 cycle’s signal length is chosen to carry out the parametric measurements. 60 cycles is dismissed to show some noise around 400 kHz.

6.3. RESULTS

In this section is presented the most significant results obtained from experimental measurements. These are divided into three points that correspond to the different measurement methodologies carried out. In addition, an extra point is added to compare experimental measurements and results obtained in the numerical simulation model.

6.3.1. PARAMETRIC AMPLITUDE IN FUNCTION OF VOLTAGE

As mentioned in the amplitude signal section (6.2.4.2), all transducers are measured at the same pressure level. However, differences in sensitivity between them, make the voltage required for each pressure different on each transducer. Table 6.4 below presents the peak voltage values required to obtain the selected input pressures for each transducer.

Input Pressure (Pa)	PROTOTYPE 1 (V_{peak})	PROTOTYPE 2 (V_{peak})	AIRMAR P19 (V_{peak})
14960	21	24	11
29920	43	28	23
74800	107	70	57
149600	215	140	114
224400	322	210	171
374000	538	350	286

Table 6.4. Peak voltage transducer required as function of input pressure

Next figures show primary beam behaviour, which includes both primary frequencies, and the beams that correspond to difference and sum harmonics as a function of the voltage for each transducers.

Byfrequency signal of 95 and 145 kHz is represented for both prototypes and 175 and 225 kHz signal for Airmar P19. Results are the following:

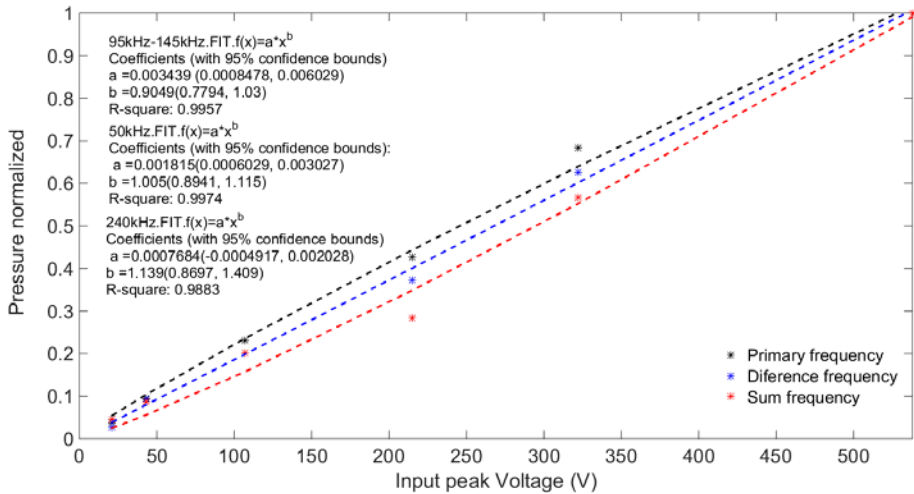


Figure 6.9. Normalized pressure of primary and parametric beam as function of voltage in prototype 1

Prototype 1 presents a linear behaviour in all frequencies in the studied voltage range as it can be observed in the realized fits. Sum frequency at 240 kHz shows the same tendency.

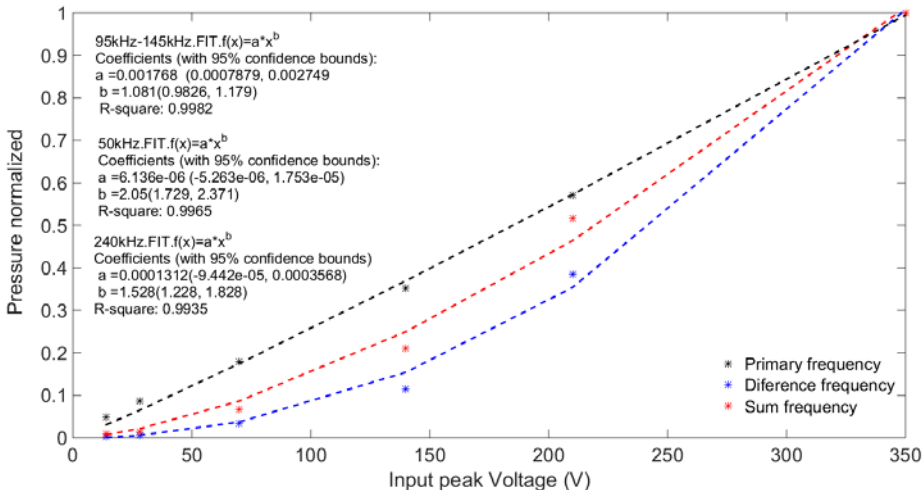


Figure 6.10. Normalized pressure of primary and parametric beam as function of voltage in prototype 2

Prototype 2 is closer to theory(Hamilton et al. 2008) obtaining a nonlinear adjustment for both parametric harmonics, presenting a linear behaviour in the primary frequency.

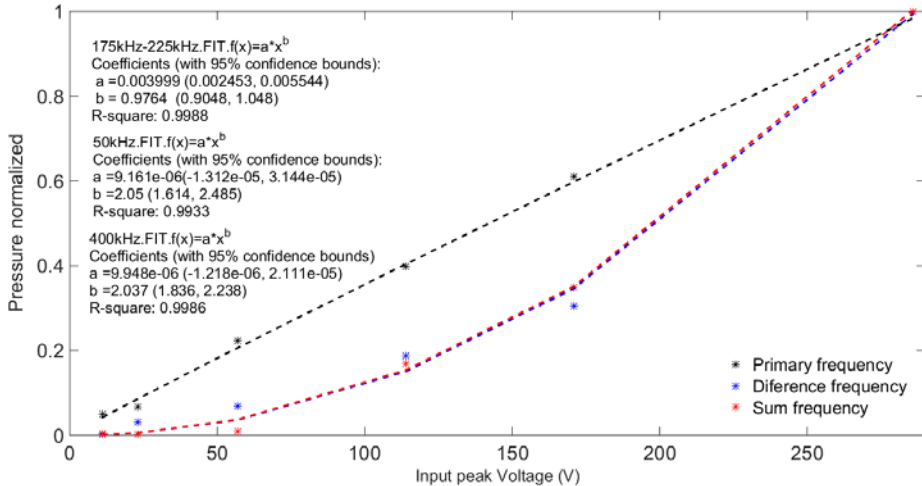


Figure 6.11. Normalized pressure of primary and parametric beam as function of voltage in transducer Airmar P19 and Airmar n°X respectively

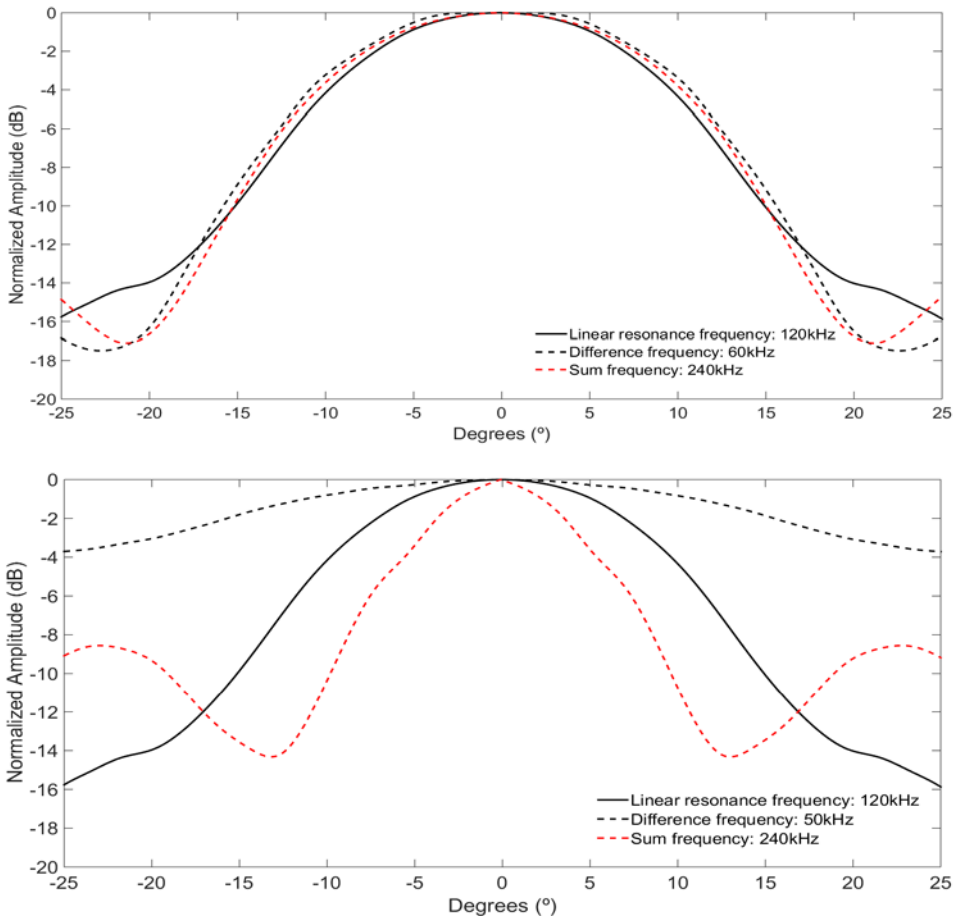
It can be pointed out that for Airmar P19, with a primary frequency greater than prototypes, harmonic beams fit perfectly to the behaviour predicted by theory(Hamilton et al. 2008).

6.3.2. DIRECTIVITY MEASUREMENTS RESULTS

In this section each transducer is evaluated for the two byfrequency signals measured. Figure 6.11 shows results for prototype 1. It can be observed that for signal (90-150 kHz) directivity results for difference harmonic (60 kHz) and sum harmonic (240 kHz), both spectral components, are very close compared with the transducer operation frequency (120 kHz). However, as is suspected in the amplitude study, for 95 145 kHz byfrequency signal, which has as difference frequency of 50 kHz and 240 kHz of sum harmonic,

parametric generation is not achieved. If we look the admittance for prototype 1 (Figure 5.20) Radial mode is stronger than thickness mode, this causes the parametric generation to be masked by the linear behaviour of transducer.

Figure 6.12. Directivity beam pattern for 90-150 kHz Byfrequency signal and 95-145 kHz Byfrequency



signal respectively for prototype 1. Linear resonance frequency, difference frequency and sum frequency are represented

As for prototype 2 in both cases, parametric generation is observed although harmonics tend to widen, not observing a reduction of the side lobes in relation to the main lobe. This can be due to the transducer aperture and the piezoelectric ceramic efficiency mentioned in Chapter 5. These ceramics presents a dependency between the vibrational modes. Although result is optimal for main lobe you have to take this into account.

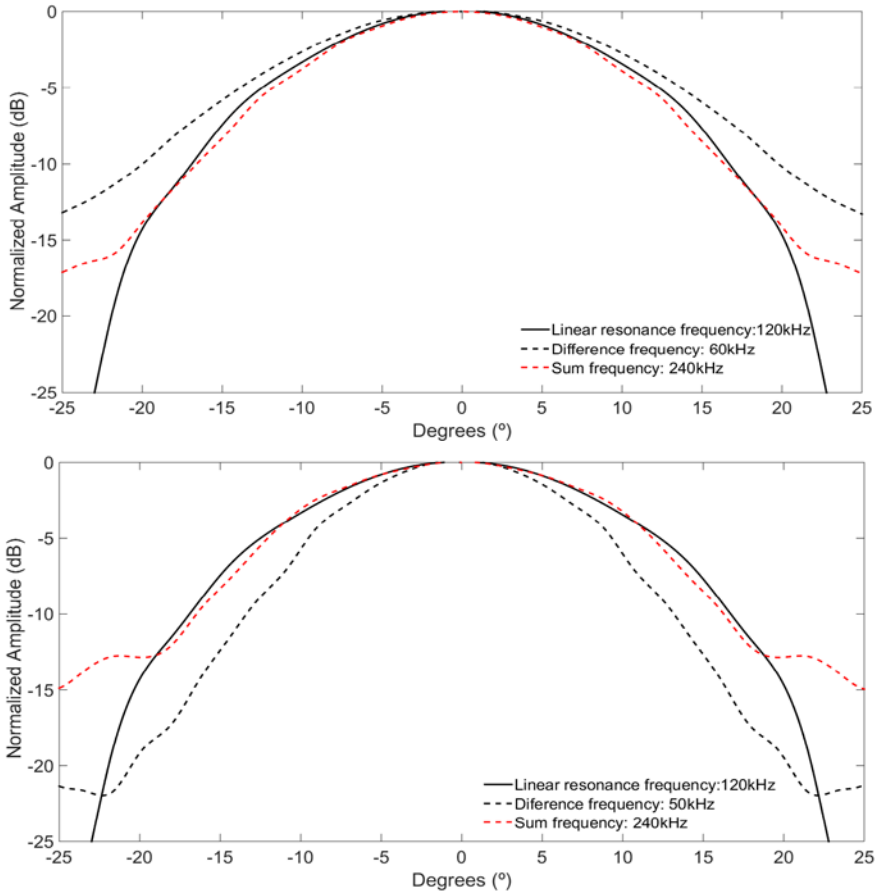


Figure 6.13. Directivity beam pattern for 90-150 kHz Byfrequency signal and 95-145 kHz Byfrequency signal respectively for prototype 2. Linear resonance frequency, difference frequency and sum frequency are represented.

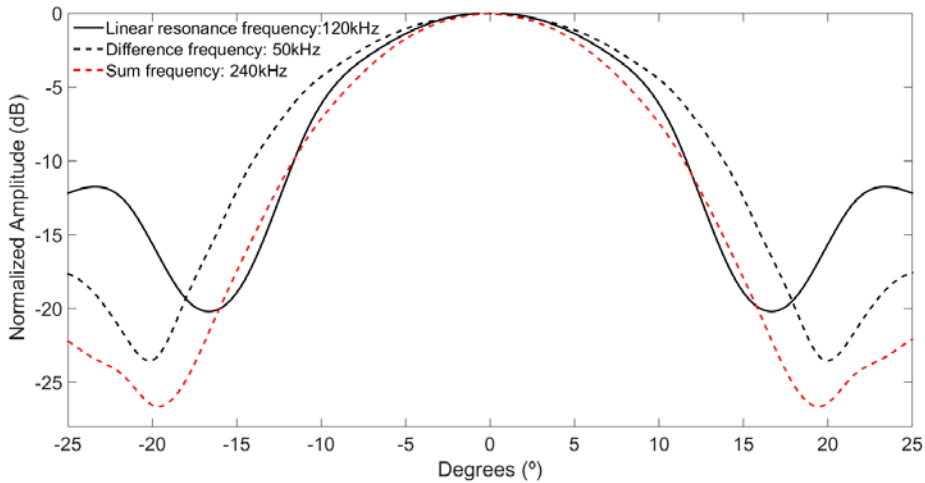


Figure 6.14. Directivity beam pattern for 175-225 kHz Byfrequency signal for Airmar P19. Linear resonance frequency, difference frequency and sum frequency are represented.

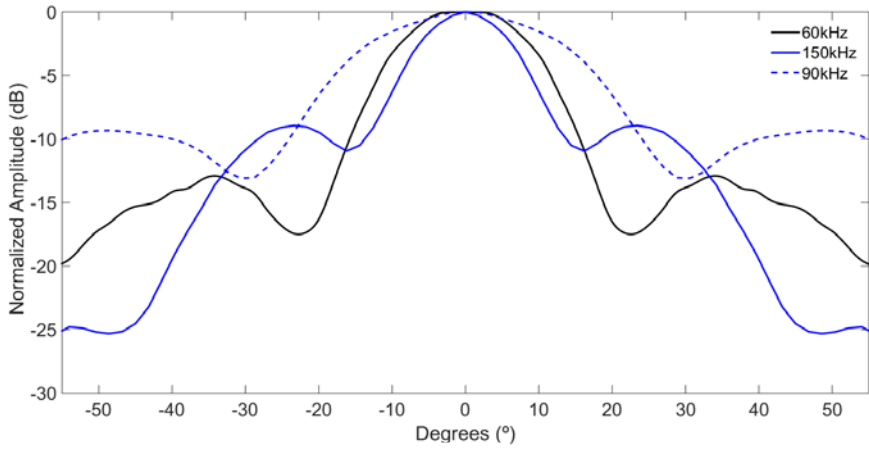
Figure 6.14 shows results for Airmar P19. Radiation pattern for the sum and difference harmonic present a reduction of side lobe level with respect to the main lobe, widening a little more in the difference harmonic.

The second one, difference frequency obtained (50 KHz) improves behaviour regarding prototype 1 and 2. Table 6.5 collects the -3dB beam width comparison between frequencies for each transducer

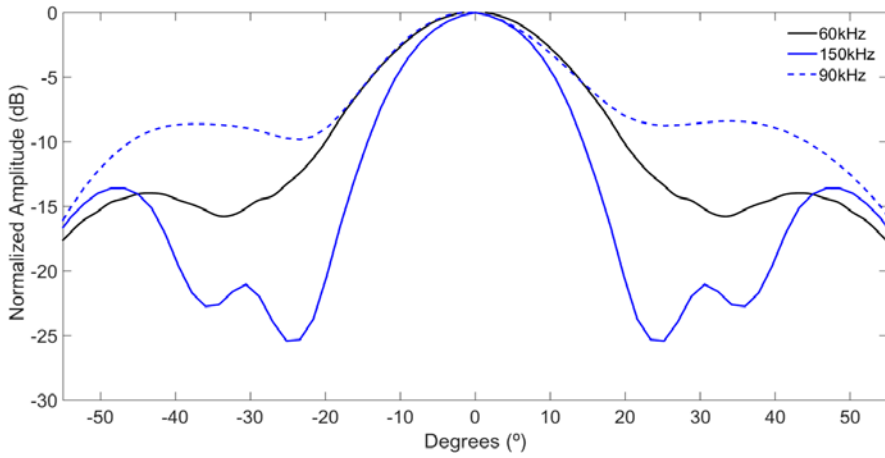
-3dB Beamwidth (°)	PROTOTYPE 1	PROTOTYPE 2	ARMAR P19
$f_{120\text{kHz}/200\text{kHz}}$	17	19	15
$f_{60\text{kHz}}$	19	18	17
$f_{240\text{kHz}/400\text{kHz}}$	18	21	13

Table 6.5. -3dB beamwidth at each interesting frequency for each transducer

Finally, Figure 6.15 shows an example, for all transducers, the representation for primary frequencies and difference frequency in the case of 90-150 kHz byfrequency signal (prototypes) or 175-225 kHz byfrequency signal (Airmar P19). In the two first cases difference beam is formed between the regions of the two primary beam, otherwise, in Airmar P19, the difference beam is narrower than both primary beams



a)



b)

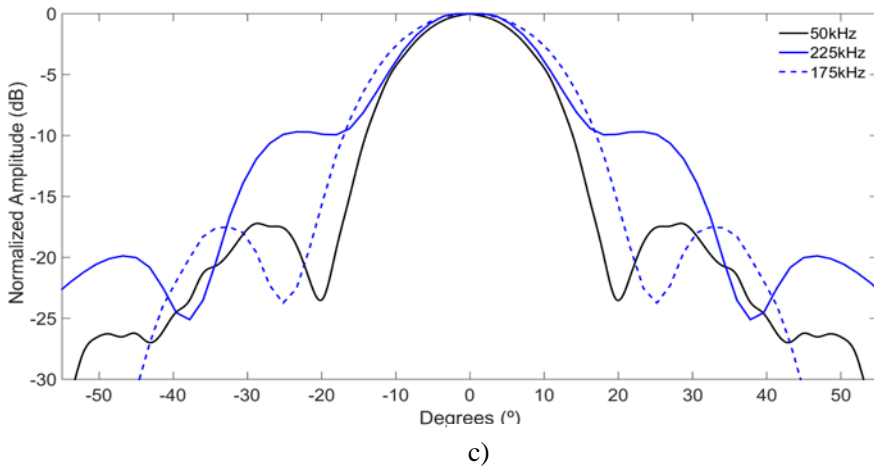


Figure 6.15. Directivity beam pattern for 90-150 kHz Byfrequency signal for all transducers. Primaries and difference frequency are represented. a) Prototype1: Pic255; b) Prototype 2:Pz37; c) Airmar P19.

If we look at the beamwidth of the parametric signals, we observe that for 60 kHz signals, in both prototypes, parametric beam tends to resemble more to the lower primary frequency. However, for AIRMAR P19, this tends to be reduced even more than the higher range frequency. In order to analyse if the weight of each frequency influences the parametric directivity, a simulation with different weights in the amplitude of modulation and the effect that they produce in the directivities is introduced in section 6.3.4.

6.3.3. AMPLITUDE AS FUNCTION OF DISTANCE RESULTS

In this section, beam propagation as function of distance is shown. Normalized pressure as function of distance is represented for Primary and difference beam. Prototype 2 and Airmar P19 have been selected to represent the results (Figure 6.16 and 6.17). It is observed that, in both cases, difference parametric beam is taking longer to be attenuated compared to primary beam. This is due to the fact that this frequency is generated in the medium and moreover it has a lower frequency than the primary beam being the

absorption also lower. Comparing both transducer, Airmar P19 has a stronger parametric component than prototype 2 for the same parametric difference frequency. This difference can be for the primary frequency range, due to Airmar P19 works at higher frequencies or just to the mechanical active element efficiency.

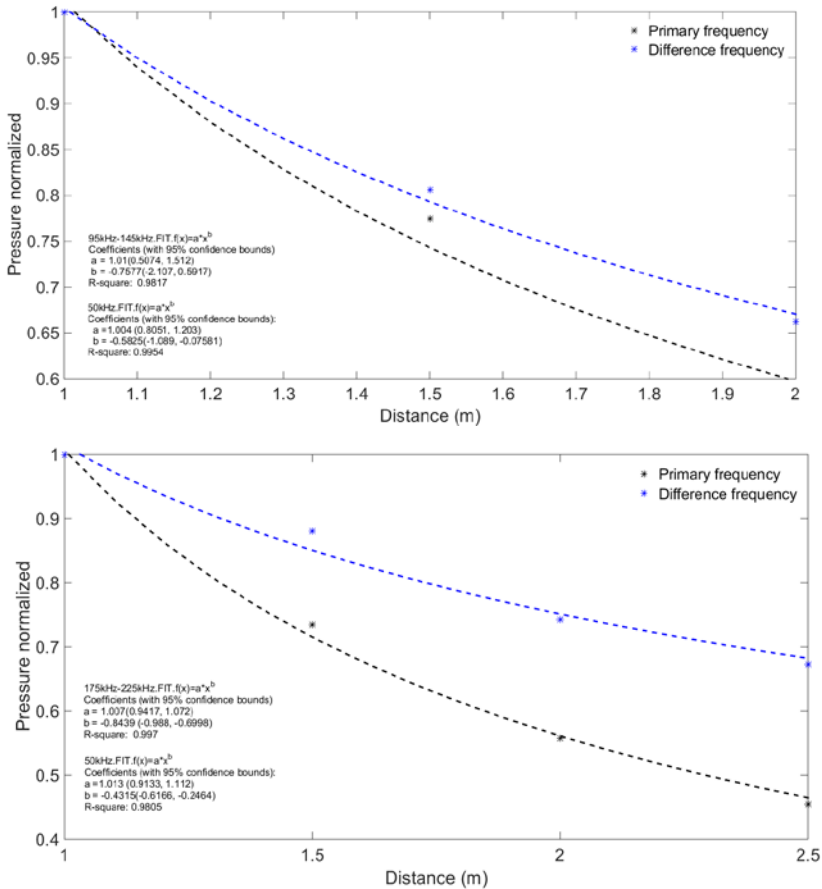


Figure 6.16. Prototype 2: Normalized pressure as function of distance for a Byfrequency signal of 95-145 kHz, having a parametric difference frequency of 50 kHz
 Figure 6.17. Airmar P19: Normalized pressure as function of distance for a Byfrequency signal of 175-225 kHz, having a parametric difference frequency of 50 kHz

6.3.4. EXPERIMENTAL MEASUREMENTS VS NUMERICAL SIMULATION

In order to perform the comparison between experimental measurements and simulation, as well as, to study the feasibility of the transducers, explained in the following section, pressure levels of primary frequencies, and both harmonics, sum and difference, are obtained until reaching the maximum voltage allowed by the measuring system. This maximum voltage equals a maximum pressure on the transducer face of approximately 1 MPa. Table 6.6 collects the sound pressure level obtained at 1.5m from the source at maximum pressure.

LP_{received} (dB)	PROTOTYPE	PROTOTYPE 2	AIRMAR P19
$F_{90-150\text{kHz}/170-230\text{kHz}}$	173.3	173,8	178.8
$f_{60\text{kHz}}$	141.4	141	152
$f_{240\text{kHz}/400\text{kHz}}$	143.3	137.4	151.7

Table 6.6. Sound Pressure Level at each interesting frequency for each transducer.

With this data we proceed to simulate 60 kHz parametric beam, for 1.9cm transducer radius, obtaining the results shown in Figure 6.18 and 6.19. Figure 6.18 shows the difference-beam and the primary frequencies directivity. As shown in Figure 6.15, in the prototypes measurements, the 60 kHz parametric beam fits between the two primary beams.

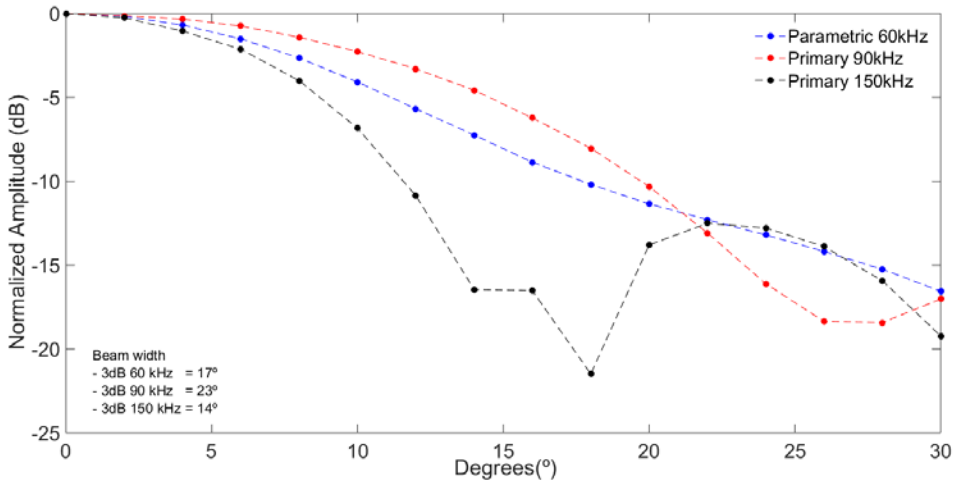


Figure 6.18.K-wave: Directivity for primary and difference frequency at 1MPa as input pressure.

Figure 6.19 shows the difference frequency beam comparison between simulation and prototype measurements.

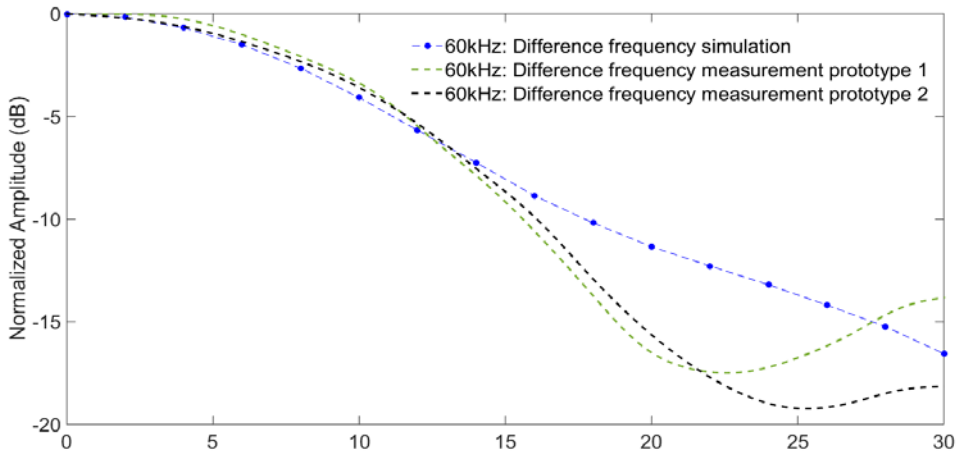


Figure 6.19. Difference frequency directivity comparison. Prototypes experimental measurement Vs K-wave simulation

With the same input pressure (1MPa), a pressure level study, of difference frequency, has been performed for different transducer apertures. Figure 6.20 shows the pressure levels obtained for the harmonic difference as a function of the radius. At higher apertures, more directional beams, pressure level increases considerably. This is due to the energy is more concentrated along the axis of the transducer and there is less beam divergence.

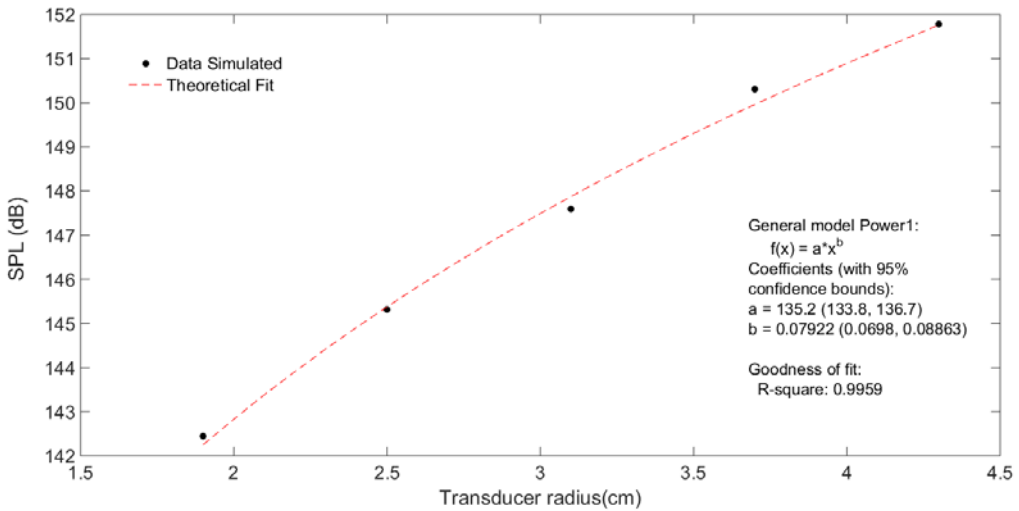


Figure 6.20. Source pressure level at 1.5m for different transducer radius with 1MPa as input pressure

Table 6.7 shows the experimental values of each prototype and simulation. It is observed that the simulation tends to overestimate experimental results, more especially in the primary beam.

LP_{received} (dB)	PROTOTYPE	PROTOTYPE 2	SIMULATION
F _{90-150kHz/170-230kHz}	173.3	173,8	179.5
f _{60kHz}	141.4	141	142.4
f _{240kHz/400kHz}	143.3	137.4	----

Table 6.7. Sound Pressure Level at each interesting frequency for each prototype VS simulation.

Finally, a directivity study has been performed, depending on the weight of each primary frequency in the parametric generation (Figure 6.21). It is observed that a change in the amplitudes in the modulation can affect the beam width. When working at frequencies too far apart from the resonant frequency of the transducer, each can have different efficiencies that can modify the final parametric beam obtained. In this case, comparing experimental and simulated results, it can be observed that the parametric frequencies, in the case of prototypes, tend to be more influenced by the lower frequency corresponding to 90 kHz.

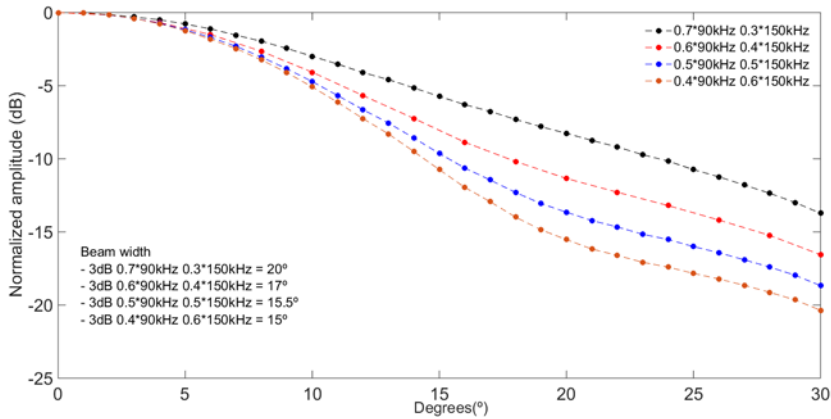


Figure 6.21. Difference frequency beam aperture in function of weighing primaries frequencies

6.4. TRANSDUCER VIABILITY

After carrying out the entire measurement campaign and analysing the results obtained, it is necessary to define a range of applicability for the transducers and, therefore, for the parametric echo sounder of which they would be part.

During the development of this thesis, has been defined fisheries acoustics as the main application. However, within it, different characteristics must be established to contextualize the specific work to be devoted. These characteristics are for example the definition of marine species under study, measurement medium conditions, distance to the target, and so on.

As mentioned in the introduction, aquaculture industry has increased its production in recent years due to the need to provide sustainable fisheries cages. The use of several frequencies, giving information of TS frequency dependence different (2.1.1), for the same species, which allows the classification of these, being one more tool for a sustainable fishing development.

Multifrequency transducers can be control tools within fish farms where more than one species can be present in the same cage to investigate beam extinction due to high densities, or research tools to extrapolate methods in the open sea.

In the Mediterranean Sea, three species are the main protagonists within the marine farms. These are: sea bream (*Sparatus aurata*), seabrass (*Dicentrarchus labrax*) and more recently Bluefin tuna (*Thunnus Thynnus*).

Several studies have been carried out to define Target Strength (TS) of these species (Puig et al. 2012; Soliveres 2009). In them, operation frequencies oscillate between 120 kHz and 200 kHz, at distances no higher than 30 meters in depth, which would be called shallow water. This section presents a practical case, defining the minimum detection threshold (DT) that can discern our device electronically. In this case, it should be at least 12 dB over the noise level. Using sonar equation (3.6) the process is as follows: From a determined Source Level (SL), in this case, pressure level of the chosen parametric frequency, is calculated, for different TS (different species) and for different distances, the minimum echo level that would arrive at the echo sounder with a given noise level (NL).

This process is carried out with the two prototypes designed taking into account that the environmental conditions are those of the Mediterranean Sea and are as follows:

	Mediterranean Sea
S(ppt)	35
T _a (°)	18
ph	8
NL(dB)	40

Table 6.8. Mediterranean Sea environmental conditions.

In addition to these conditions, we must also know the receiver sensitivities (OCV) for the selected frequencies ($f_2 - f_1$ and $f_1 + f_2$) and the medium absorption for each one of them (table 6.9)

	PROTOTYPE 1		PROTOTYPE 2	
	60 kHz	240kHz	60kHz	240kHz
α (Np/m)	0.0016	0.0092	0.0016	0.0092
OCV (dB re 1V/uP)	-188.5	-195	-195.5	-195

Table 6.9. Medium absorption and receiver sensitivity for each prototype at different frequencies

On the other hand, according to the literature, sea bream (Soliveres 2015) usually has a *TS* value that varies between -50 to -40 dB according to weight and size. In the case of sea bass, the values are slightly higher, remaining between -40 and -30 dB. For Bluefin tuna can rise to -28, in large targets (Puig et al. 2012).

To cover the full range of values explained above, *TS* has been defined, from -50 to -25 dB in steps of 5 dB. All of them, are analysed in 5 different distances (1.5, 5, 10, 15 and 30 meters). Source Level values are split in two for each transducer: 141 dB for 60 kHz

and 137.8dB for 240 kHz dB in prototype 1 and 141.4dB for 60 kHz and 143.2dB for 240 kHz dB in prototype 2. Tables 6.10 and 6.11 shown the results. The boxes marked with an X, are those that comply, that for these conditions, transducers would give a minimum reception voltage.

Prototype													
1		60kHz						240kHz					
Distance (m)													
TS (dB)		1.5	5	10	15	20	30	1.5	5	10	15	20	30
-50		X	X					X	X				
-45		X	X	X				X	X	X			
-40		X	X	X	X			X	X	X			
-35		X	X	X	X	X		X	X	X	X		
-30		X	X	X	X	X	X	X	X	X	X	X	
-25		X	X	X	X	X	X	X	X	X	X	X	X

Table 6.10. Prototype 1: Application range viability table as function of TS and distance

Prototype		60kHz						240kHz					
2													
Distance (m)													
TS (dB)		1.5	5	10	15	20	30	1.5	5	10	15	20	30
-50		X	X	X				X	X	X			
-45		X	X	X				X	X	X	X		
-40		X	X	X	X			X	X	X	X	X	
-35		X	X	X	X	X		X	X	X	X	X	
-30		X	X	X	X	X	X	X	X	X	X	X	
-25		X	X	X	X	X	X	X	X	X	X	X	X

Table 6.11. Prototype 2: Application range viability table as function of TS and distance

It can be observed that for both prototypes at 60 kHz for TS, between -30 and -25dB, range is up to 30 meters. For lowest TS values range is reduce to 10 meters in prototype 2 and 5 meters in prototype 1. In the case of 240 kHz, prototype 1 presents the same

behaviour than in 60 kHz. However, prototype 2 improves for TS values from -45 to -35dB being able to measure up to 20 meters.

It is an optimal result to estimate biomass at distances between 10 and 30 meters. These transducers can be used in fish farms of seabream and seabass, or to discriminate among species, in the first 30 meters, in the open sea. In the fish farms, the seabreams and sea bass, tend to form quite dense volumes at depths from 7m to 20m. To obtain reliable data of biomass it is necessary to know, between other parameters, the *TS* value from only one individual. It can be found in the first 7 meters where fish swim more disperse and traces can be analysed separately. On the other hand, in the open sea, for example through the use of satellite buoys, it is necessary to classify different species existing to fish only those that are under interest. A study in the first few meters (always taking into account the transducer's near field) would lead to a more sustainable fishing and a costs reduction.

This study is limited to power transmission used, which corresponds to the parametric generation tests. To increase the applicability range of the transducers, two studies are carried out using the K-wave simulation program. In them, attention is focused on the difference frequency of 60 kHz, and it is intended is to increase the level obtained with the current measurements (Table 6.7).

The first one, is based on maintaining the prototypes' aperture radius, but increase the input pressure in order to observe at what level should be excited to get to reach greater distances. Figure 6.22 shows the pressure level of the parametric frequency as a function

of the input pressure. For lower values, experimental values have been superimposed to validate that both results follow the same trend.

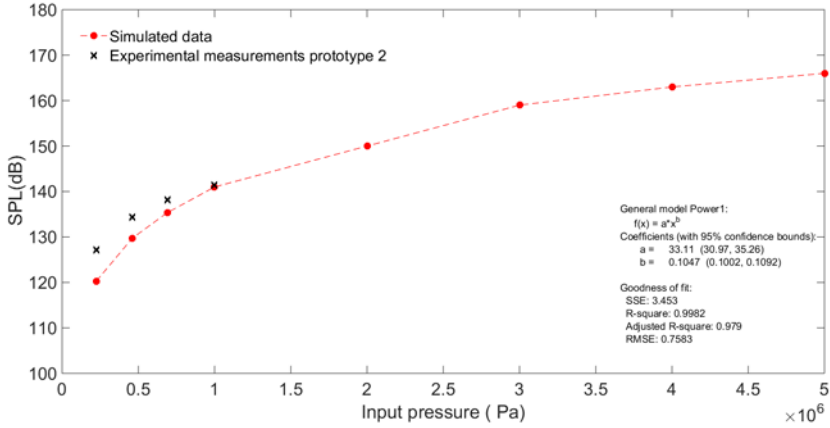


Figure 6.22. SPL in function of input pressure. Simulation data compare with experimental results

If, for example, 3MPa was chosen as input pressure, a parametric level of 160dB would be obtained. The modified applicability range for prototype 2 is shown in Table 6.12

Prototype		60kHz						240kHz					
2													
Distance (m)													
TS (dB)		1.5	5	10	15	20	30	1.5	5	10	15	20	30
-50		X	X	X	X	X		X	X	X	X	X	
-45		X	X	X	X	X	X	X	X	X	X	X	X
-40		X	X	X	X	X	X	X	X	X	X	X	X
-35		X	X	X	X	X	X	X	X	X	X	X	X
-30		X	X	X	X	X	X	X	X	X	X	X	X
-25		X	X	X	X	X	X	X	X	X	X	X	X

Table 6.12. Prototype 2: Application range viability table as function of TS and distance. Table in the left hand side corresponds to values with 1MPa as an input pressure. Table in the right hand side, corresponds to values for 3MPa as an input pressure.

This solution will always be linked to the electronics of the entire system. Considering the ability to supply high voltages without distorting the signal or provoking another class of

nonlinearities. To avoid or to complement use of such high voltages, the second studio is introduced. It works at primary frequencies greater, 170 kHz and 230 kHz, to obtain the same difference frequency: 60 kHz. From there, pressure level of this parametric is simulated as a function of the transducer aperture. The increase of the primary frequencies aims to increase the efficiency of the parametric generation. Also at higher frequency, beams are more directional and a higher concentration of energy is achieved along the axis causing a conversion of parametric generation, as in the AIRMAR P19 transducer. Figure 6.23 shows that for the same radius as the prototypes there is an increase of about 10dB with respect to the values obtained in Figure 6.20.

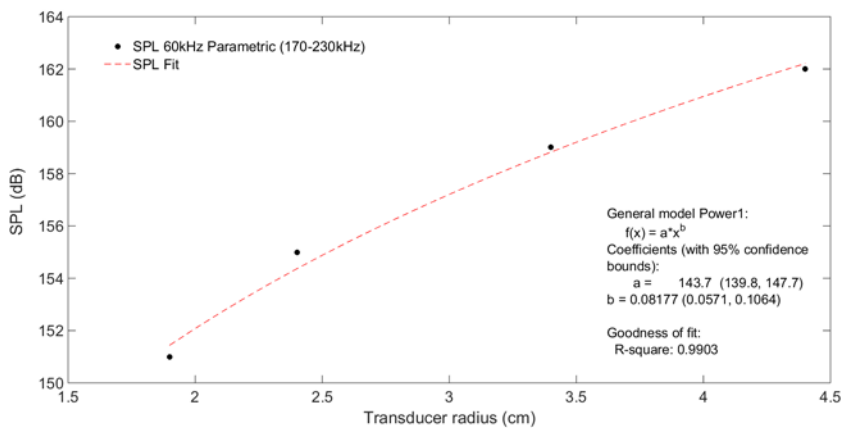


Figure 6.23. SPL of difference parametric beam as function of transducer radius for a Byfrequency signal of 170-230 kHz, having a parametric difference frequency of 60 kHz

Finally, it should be noted that other types of applications outside of fisheries acoustics have been considered, such as sub-bottom profile. Sub-bottom profilers based on parametric acoustics offer many advantages. Usually high resolution is needed, therefore narrow beams are selected with parametric frequencies around 4-15 kHz. For this reason,

due to prototypes have wide aperture and its frequencies are not in this range, they are not considered the best suitable for this kind of application, not being of interest to this thesis.

6.5. CONCLUSIONS

This chapter has covered in one hand the study of a nonlinear phenomenon, such as parametric generation and on the other hand the ability presented by the designed prototypes in the previous chapter, to operate optimally in a nonlinear regime so that they can be used as multi-frequency transducers within a parametric echo sounder.

An experimental campaign has been carried out in which through measures of amplitude as function of voltage or distance, and directivity measurements, it is shown that prototypes are able to obtain parametric spectral components. The study has focused on the difference and sum beam harmonic for all the signal considered. Results show that radiation pattern of the parametric frequencies approaches the primary mean frequency directivity (around 120 kHz).

Amplitude as a function of voltage increases exponentially and not linearly as the primary mean frequency. In terms of distance, it is verified that experiment coincides with theory, confirming that is an effect that occurs in the medium. Frequencies generated through it, are attenuated less than the primary frequencies due to the transfer of energy from these to the parametric spectral components.

It has also been found that operate at parametric difference frequencies close to the radial mode influence negatively by imposing the linear behaviour to the nonlinear regime, not achieving the desired result. This can be minimized reducing the bandwidth of the excitation signal.

Increase of primary frequencies, as well as, reduction of transducer aperture generates a parametric acoustic array more efficient, in both, obtained pressure levels and radiation pattern due to side lobe level reduction.

On the other hand, a simulation tool have been developed that is in agreement with experimental measurements and with which it is possible to establish operating ranges as minimum and maximum pressures for the parametric generation, distances in which the phenomenon begins to be observed, and their directivity characteristics.

Finally through the pressure level obtained and TS data of different species found in the literature, it is demonstrated that both prototypes can be multifrequency transducers (from 2 to 3 frequencies) being able to realize measurements in sea cages at distances between 1meters and 30 meters, of the main aquaculture of species in Spain. Parametric efficiency shows a dependence with transducer aperture and primary frequencies. This dependency allows to improve the design characteristics and bring more capabilities to the transducers performance.

Conclusions

In this thesis it has been possible to design and to implement two piezoelectric transducers for their subsequent application in biomass estimation. Both have achieved the established design premises obtaining two prototypes with an operating frequency of 120 kHz, beam aperture between 17° and 19° and a projector sensitivity around 150 dB re 1uPa / V at the resonance frequency.

In order to characterize all the transducer's constituent elements, experimental measurements and numerical simulation models based on finite elements have been used. The validity of these models, for parameters and coefficients adjustment, both in the active and passive elements characterization have been demonstrated.

In addition, a numerical model has been developed that collects both, piezoelectric behaviour and the acoustic interaction with the medium. Turning numerical simulation into a powerful design tool with which to introduce improvements, for example in sensitivity and bandwidth, without developing new prototypes.

On the other hand, this thesis presents the capacity of the prototypes to operate in nonlinear regime. A campaign of measurements is carried out that demonstrates the parametric harmonic generation produced in the medium. The study focuses on three frequencies of interest: 50 kHz and 60 kHz, corresponding to the difference frequency, and 240 kHz corresponding to the sum frequency. Results show that, for prototype 2, the three frequencies acquire similar characteristics in radiation as 120 kHz in linear emission, while for prototype 1 only 60 kHz and 240 kHz are valid.

From the study it is also extracted that for a transducer with a strong radial mode, if the parametric frequency is located in that vibrational mode, the parametric generation is not efficient, predominating linear behaviour.

Moreover, due to the control measurements performed by another transducer, with a similar beam aperture but with a higher operation frequency (200 kHz), it is concluded that working at higher primary frequencies favours parametric generation, obtaining narrower beams than the primary beams and with greater reduction of side lobes.

At a practical level, point out that for parametric generation a byfrequency emission is performed in all measurements, in which parametric beam, sum or difference, is defined between the low frequency beam and the high beam, not forming in another region

Finally, a feasibility study is presented for the highest pressure measured during campaign, in which all factors involved in the sonar equation show that both prototypes

can perform multifrequency measurements in sea cages at distances between 1 and 30 meters. Simulation studies show that this range can improve by three changes: increasing transducer radius, with higher input pressures or increasing the range of primary frequencies.

Acknowledgements

Institutional acknowledgements:

I would like to thank the Programa de Ayudas de Investigación y Desarrollo (PAID) de la Universitat Politècnica de València The granting of financial support through the scholarship programme FPI subprograma 2 (2012-S2-002-650).

To the financial support received from Ministerio de Medio Ambiente y Medio Rural y Marino to the project “Diseño de tecnología para el cálculo de la biomasa total de peces en instalaciones offshore” (ARM/1790/010), as well as the direct participation of Ctaqua y Apromar in the project.

To Instituto Español de Oceanografía to promote and support the project: “Caracterización del comportamiento del atún rojo (*Thunnus thynnus*) ante estímulos externos y mediante sistema acústico-óptico en granjas de engorde de atún rojo (As part of the project AZIMUT)”.

Likewise, also to appreciate to UE Comisión to support the project “Sistema de medida de biomasa en transferencias atún rojo por técnicas acústicas (BIACOP (ES/13/41 mediante la decisión ejecutiva de la Comisión de la UE de 10 de julio de 2013 (2013/410/UE)).

Special thanks to Zunibal S.L. to promote the project “Adaptación y desarrollo de sistemas acústicos en boyas satelitarias para la caracterización de biomasa (TUNASPOT)” and collaborating actively throughout the thesis development, offering materials, support and knowledge.

Personal acknowledgements:

For me, obtaining my Phd qualification meant no only the beginning of a new phase for me professionally speaking but also a new phase at a personal level, when, after two years I returned home when the possibilities were very slight. For this I would thank my Tutor Mr. Victor Espinosa for that phone call and the opportunity he offered me.

During these last years many great people have appeared in my life to guide and help me. In the first place may I offer my thanks to Ester and Vicent. To Ester for accepting me into the Pescanova clan even though I like pink, and to Vicent for being a great battle companion and best friend, who has put up with me more than I could explain THANKS!!.

A thousand thanks to my girls, Maria and Nuria, who are more than friends, they are sisters. To Maria for being my battle companion, for loving me unconditionally, for understanding me, for being the shoulder to cry on when I was feeling low and for being there on almost every happy moment of my life. To Nuria for being there after all these years, both having gone through so much supporting each other, for loving, taking care of and protecting me, actually for being me, my family. Thanks again!

To my friend Alvarico, travelling and life companion who never failed me no matter what. To Ana and Susana. To Ana for being my happiness and to Susana for being something great found on the way passing on her happiness wherever she went.

A special thanks to Manu. Without you I wouldn't be writing this letter of thanks. There are not enough pages to thank you for your work, effort, generosity and friendship. No one can separate the union made by a bridge.

Thanks also to Miguel Jover and Isabel Perez for supervising my work and for helping me during this time.

I would also like to thank the technicians of the Polytechnic University of Valencia for their patience and support. To Fernando and Carlos, thanks for responding to all my queries with a smile and above all for their professionalism. At the same time may I thank all my colleagues at office E201, both new and old for their jokes, support and quirks. A special thanks to Jandri and Noe who even although were far away always took the time to clarify my doubts.

I cannot finish this missive of thanks without mentioning my family. To my parents who offered me all their support without asking anything in return, frankly I owe them everything. I love you! To my sister, my brother-in-law and to my nieces for being so great and for taking care of me more than I deserve, and finally to those people who

suddenly appear in your life to make you even happier. To all of you, THANK YOU FROM THE BOTTOM OF MY HEART.

Referencias

- Aanes, Magne. 2013. "Interaction of Piezoelectric Transducer Excited Ultrasonic Pulsed Beams with a Fluid-Embedded Viscoelastic Plate. Finite Element Modeling, Angular Spectrum Modeling and Measurements." University of Bergen.
- Abboud, Najib N. 1998. "Finite Element Modeling for Ultrasonic Transducers." *Proceedings of SPIE* 3341(212): 19–42. <http://link.aip.org/link/?PSI/3341/19/1&Agg=doi>.
- Acosta Aparicio, V.M., G. Rodriguez Corral, E. Riera Franco de Sarabia, and J.A. Gallego-Juarez A. Pinto del Corral, I. Martinez Gonzalez. 2010. "Aplicación del metodo de elementos finitos al estudio y diseño de transductores ultrasonicos de placa vibrante." In *41º CONGRESO NACIONAL DE ACÚSTICA 6º*.
- Ainslie, Michael A, and James G McColm. 1998. "A Simplified Formula for Viscous and

- Chemical Absorption in Sea Water.” *Journal of the Acoustical Society of America* 103(3): 1671.
- Al-Budairi, H. 2012. “Design and Analysis of Ultrasonic Horns Operating in Longitudinal and Torsional Vibration.” University of Glasgow.
- “AMORIM Cork Composites.” <http://www.amorimcorkcomposites.com>.
- Andersen, B et al. 2000. “Performance of Piezoelectric Ceramic Multilayer Components Based on Hard and Soft PZT.” *Acuator 2000: Seventh International Conference on New Actuators* (August): 419–22.
- APROMAR. 2009. “La Acuicultura Marina de Peces En España.” : 1–68.
- Arnau, Antonio. 2008. *Piezoelectric Transducer and Applications*. Second edi. Springer.
- Balk, Helger, and T Linderm. 2008. “Sonar 4 and Sonar 5-Pro Post Processing Systems”. Operator Manual Version 5.9.9.”
- Barnet, D.M and Lothe, J. “Dislocations and Line Charges in Anisotropic Piezoelectric Insulators.” *Physica Status Solidi*.
- Berktaý, H O. 1965. “Possible Exploitation of Non-Linear Acoustics in Underwater Transmitting Applications.” *Journal of Sound and Vibration* 2(4): 435–61. <http://www.sciencedirect.com/science/article/pii/0022460X65901227>.
- Bjørnø, Leif. 2017. *Applied Underwater Acoustics*. eds. Thomas Neighbors and Thomas Bradley. Elsevier.
- Boucher, Stephen. “AIRMAR Technology Corporation.” <http://www.airmar.com/>.
- Brissaud, Michel. 1991. “Characterization of Piezoceramics.” *IEEE Transactions on*

-
- Ultrasonics, Ferroelectrics, and Frequency Control* 38(6): 603–17.
- Cheeke, J. David N. 2002. *Fundamentals and Applications of Ultrasonic Waves*.
<https://books.google.com/books?id=Lnb4PeTbeYC&pgis=1>.
- Clough, R. W. 1960. “The Finite Element Method in Plane Stress Analysis.” *Proceedings, American Society of Civil Engineers*: 345–378.
- Comsol, AB. 2010. *Building Comsol Multiphysics User’s Guide*.
- Coppens, Alan B. 1981. “Simple Equations for the Speed of Sound in Neptunian Waters.” *The Journal of the Acoustical Society of America* 69(3): 862.
- Craig, R. E., and S. T. Forbes. 1969. “Design of a Sonar for Fish Counting.” *Fiskeridir. Skr. Ser. Havunders* 15: 210–19.
- Currie, Jacques, and Pierre Currie. 1880. “Développement, Par Pression, de L’électricité Polaire Dans Les Cristaux Hémiedres À Faces Inclinées.” *Comptes rendus de l’Académie des sciences* 91: 294–95.
- Eckert, Michael. 2007. *The Dawn of Fluid Dynamics: A Discipline between Science and Technology* *The Dawn of Fluid Dynamics: A Discipline between Science and Technology*.
- Fardal, R. 2002. “Endelig Element Analyse Av Elektriske Egenskaper Til Piezoelektriske Skiver.” University of Bergen.
- “FEMP Version 3.5 - Documentation.” file:///D:/SIMULACION_FEMP/FEMP_5.1/Documentation/Documentation_FEMP3.0/doc.html.
- Ferroperm. “Ferroperm Piezoceramics.”

- Feuillade, Chris, and María P Raveau. "Sound Extinction by Fish Schools: Forward Scattering Theory and Data Analysis." *Acoustical Society of America* 134(5):399.
- Fonteneau, Alain, Emmanuel Chassot, and Nathalie Bodin. 2013. "Global Spatio-Temporal Patterns in Tropical Tuna Purse Seine Fisheries on Drifting Fish Aggregating Devices (DFADs): Taking a Historical Perspective to Inform Current Challenges." *Aquatic Living Resources* 26(1): 37–48.
http://www.alrjournal.org/action/article_S0990744013000466
<http://journals.cambridge.org/action/displayAbstract?fromPage=online&aid=8897405&fileId=S0990744013000466>
<http://journals.cambridge.org/action/displayFulltext?type=1&fid=8897410&jid=ALR&volumeI>.
- Foote, Kenneth G. 1989. "If1."
- Foote, Kenneth G. 1990. "Correcting Acoustic Measurements of Scatterer Density for Extinction." *The Journal of the Acoustical Society of America* 88(3): 1543–46.
- Foote, Kenneth G., Egil Ona, and Reidar Toresen. 1992. "Determining the Extinction Cross Section of Aggregating Fish." *The Journal of the Acoustical Society of America* 91(4): 1983.
- Francois, R. E., and G. R. Garrison. 1982. "Sound Absorption Based on Ocean Measurements. Part I: Pure Water and Magnesium Sulfate Contributions." *The Journal of the Acoustical Society of America* 72(3): 896–907.
- Godø, Olav Rune, and Kenneth G Foote. 2010. "Detecting Atlantic Herring by Parametric Sonar." (March): 153–59.
- González, Ester Soliveres. 2015. "Granjas Marinas Mediante Ultrasonidos." Universitat Politècnica de Valencia.

-
- Hamilton, Mark F et al. 2008. "Nonlinear Acoustics." *Acoustical Society of America, Austin, Texas*.
- Hellier, Charles J. 2012. 69 *Procedia Engineering Handbook of Nondestructive Evaluation*.
<http://linkinghub.elsevier.com/retrieve/pii/S1877705814003580>.
- Hobaek, H, and M Vestrheim. 1977. "Parametric Acoustic Arrays Formed by Diverging Sound Beams." *Acustica* 37: 74–81.
- Hossack, John A., and Gordon Hayward. 1991. "Finite-Element Analysis of 1-3 Composite Transducers." *IEEE Transactions on Ultrasonics, Ferroelectrics, and Frequency Control* 38(6): 618–29.
- Hrennikoff, A. 1941. "Solution of Problems of Elasticity by the Frame-Work Method." *Applied Scientific Research* A8: 169–75.
- Jordan, T L, and Nasa Langley. 2001. *Contract Piezoelectric Ceramics Characterization*. Virginia.
- Kino GS. 1987. *Acoustic Waves*. Third edit. ed. NJ Englewood Cliffs. Prentice Hall.
- Kinsler, Lawrence E. 2000. "Fundamentals of Acoustics." : 548.
- Knudsen, F., Fosseidengen, J., Oppedal, F., Karlsen, Ø, Ona, E. 2004. "Hydroacoustic Monitoring of Fish in Sea Cages: Target Strength (TS) Measurements on Atlantic Salmon." *Fisheries Research* 69(2): 205–9.
- Kocbach, J. 2000a. "Finite Element Modeling of Ultrasonic Piezoelectric Transducers." University of Bergen.
- . 2000b. "Finite Element Modeling of Ultrasonic Piezoelectric Transducers."

(September): 214.

Kocbach, J, P Lunde, and M Vestrheim. 2001. "Resonance Frequency Spectra with Convergence Tests of Piezoceramic Disks Using the Finite Element Method." *Acustica* 87(2): 271–85.

<http://www.ingentaconnect.com/content/dav/aaau/2001/00000087/00000002/art00014>.

Kopp, Laurent et al. 2000. "Potential Performance of Parametric Communications." 25(3): 282–95.

Krimholtz, R., D. A. Leedom, and G. L. Matthaei. 1970. "New Equivalent Circuits for Elementary Piezoelectric Transducers." *Electronic Letters* 6(13): 398–99.
<http://ieeexplore.ieee.org/stamp/stamp.jsp?arnumber=04234776>.

Landajuela, Mikel. 2011. "Burgers Equation." *BCAM Internship-summer*: 1–20.

Leissa, A. W. 2005. "The Historical Bases of the Rayleigh and Ritz Methods." *Journal of Sound and Vibration* 287(4–5): 961–78.

Levy, S. "Structural Analysis and Influence Coefficients for Delta Wings." *Journal of Aeronautical Sciences* 20: 449–454,.

Lopez, J, G Moreno, I Sancristobal, and J Murua. 2014. "Evolution and Current State of the Technology of Echosounder Buoys Used by Spanish Tropical Tuna Purse Seiners in the Atlantic, Indian and Pacific Oceans." *Fisheries Research*.

López, Víctor Jaime. 2014. "Software de Control Para Un Sistema Tridimensional de Medición de Intensidad Acústica." Universidad Nacional Autónoma de Mexico.

Mackenzie, Kenneth V. 1981. "Nine-Term Equation for Sound Speed in the Oceans." *The Journal of the Acoustical Society of America* 70(3): 807.

- Mansoura, S A et al. 2012. "Characterization and Fatigue of the Converse Piezoelectric Effect in PZT Films for MEMS Applications." *IEEE Transactions on Ultrasonics, Ferroelectrics, and Frequency Control* 59(6): 1–8.
- <http://www.springerlink.com/index/10.1134/S1064226907090136>
<http://www.m-hikari.com>
<http://dx.doi.org/10.1016/j.sna.2011.10.004>
<http://dx.doi.org/10.1121/1.4904498>
<http://scholar.google.com/scholar?hl=en&btnG=Search&q=intitle:Etude+mat+h?matique+et+num?rique+>.
- Marek, Moszynski, and Gdansk Poland Tel. "Time-Variied-Gain Correction for Digital Echosounders." 2(1).
- Mason, W.P. 1948. "Electromechanical Transducers and Wave Filters." *Van Nostrand, New York*.
- Massa, Donald P. "An Overview of Electroacoustic Transducers."
- Medina, L., E. Moreno, G. González, and L. Leija. 2003. "Circular Ultrasonic Transducer Characterization: Theoretical and Experimental Results." *Revista Mexicana de Fisica* 49(6): 511–18.
- Moffet, Mark.B. "Large-Amplitude Pulse Propagation--A Transient Effect." : 1–2.
- Moszynski, Marek. 2002. "Indirect Methods of Fish Target Strength Estimation in Absolute and Logarithmic Domain." *Acta Acustica united with Acustica* 88: 726–729(4).
- Moten, S. 2010. "Modeling of an Ultrasonic Transducer for Cardiac Imaging."
- . 2011. "Finite Element Modeling of an Ultrasonic Transducer." *131.155.54.17*: 33.
<http://131.155.54.17/mate/pdfs/12848.pdf>.

- Neil, W. 1992. "AN INVESTIGATION OF A LARGE STEP-DOWN RATIO PARAMETRIC SONAR AND ITS USE IN SUB- BOTTOM PROFILING." (August).
- Nikishkov, GP. 2004. "Introduction to the Finite Element Method." *University of Aizu*: 1–70.
<http://nliebeaux.free.fr/ressources/introfem.pdf>.
- Oleg.A, Godin, and David. Palmer.R. 2008. *History of Russian Underwater Acoustics*, ., World Scientific Pblshng Co. Pte. Ltd. Singapore.
- Pedro Acevedo, and Israel Sánchez Domínguez. 2015. "Simulation of an Ultrasonic Transducer for Medical Applications Using the Finite Element Method."
Journal of Materials Science and Engineering B 5(8): 293–97.
<http://www.davidpublisher.org/index.php/Home/Article/index?id=21809.html>.
- Peña, Rocio. 2014. "“ Diseño , Construcción Y Caracterización de Un Transductor Ultrasónico Focalizado .”" EPSG (UPV).
- PI Ceramic GmbH. "https://www.piceramic.com/en/piezo-Technology/piezoelectric-Materials/."
- Puig, V et al. 2012. "Biomass Estimation of Bluefin Tuna in Sea Cages By the Combined Use of Acoustic and Optical Techniques." *Collect. Vol. Sci. Pap. ICCAT* 68(1): 284–90.
- Qi, H. J. 2006. "Finite Element Analysis." *Unpublished lecture notes*.
- Radulescu, E. G., J. Wójcik, P. A. Lewin, and A. Nowicki. 2003. "Nonlinear Propagation Model for Ultrasound Hydrophones Calibration in the Frequency Range up to 100 MHz." *Ultrasonics* 41(4): 239–45.
- Ramadas, S N, R L O Leary, and A Gachagan. 2009. "Ultrasonic Sensor Design for NDE

- Application: Design Challenges & Considerations.” *Proceedings of the National Seminar and Exhibition on Non-Destructive Evaluation*: 88–91.
- “Redpitaya.” <https://redpitaya.com/>.
- Redwood, M. 1961. “Transient Performance of a Piezoelectric Transducer.” *Acoustical Society of America* 33(4): 527–36.
- Relaño Iborra, Helia. 2014. “Characterization of Ultrasound Transducers.” Universidad Autónoma de Madrid.
- “Robnor ResinLab Ltd.” <http://www.robnor-resinlab.com/>.
- Rozanova-Pierrat, Anna. 2006. “Mathematical Analysis of Khokhlov-Zabolotskaya-Kuznetsov (KZK) Equation.” *Analysis* 19(September): 99–103.
- Rubio, C, and O Marrero. “Fabricación de Transductores Ultrasónicos Para Equipos Automatizados de Inspección de Líneas de Tuberías.” *The open Access DNT Database*.
- Rudstam, G, S Hansson, T Lindem, and D.H Einhouse. 1999. “Comparison of Target-Strength Distributions and Fish Densities Obtained with Split- and Single-Beam Echosounders.” *Fisheries Research* 42: 207–14.
- Sanchez Carnero, Noela. 2012. “Técnicas Acústica Y Software libre:Aplicaciones En La Gestión Costera.”
- Schleicher, Jörg, Martin Tygel, Bjorn Ursin, and Norman Bleistein. 2001. “The Kirchhoff-Helmholtz Integral for Anisotropic Elastic Media.” *Wave Motion* 34(4): 353–64.
- Silva, Leonardo B M, and Edval J P Santos. 2006. “Quartz Transducer Modeling for Development of BAW Resonators.” 61(4): 69107.

Simmonds, John ; MacLennan David. 2005. *Acoustics, Fisheries*. Second. Blackwell Publishing company.

Simmonds John, Machennan David. 2007. *Fisheries Acoustics, Theory and Practice*. Second Edi. Blackwell Science.

Soliveres, E. 2009. ““ Estudio de La Relación de Las Propiedades Biométricas Y Acústicas de La Dorada .””

Standard, National. 1988. “IEEE Standard on Piezoelectricity.” *East*: 74.
<http://scholar.google.com/scholar?hl=en&btnG=Search&q=intitle:IEEE+Standard+on+Piezoelectricity#0>.

Treeby, Bradley, Ben Cox, and Jiri Jaros. 2016. “K-Wave,Manual Version 1.1.” 1.

Tura, Armando, and Zuomin Dong. 2012. “A Review of Finite Element Analysis Method.”

A Review of Finite Element Analysis Method: 49.

http://www.engr.uvic.ca/~mech410/nhttp://www.engr.uvic.ca/~mech410/lectures/FEA_Theory.pdf.

Urick, Rj. 1985. “Fundamentals of Underwater Sound.” (406): 24.
<http://scholar.google.com/scholar?hl=en&btnG=Search&q=intitle:Fundamentals+of+u+nderwater+sound#8>.

Valencia Iarregui, Jorge. 2009. “Caracterización Mediante Técnicas de Ultrasonido de Un Laminado de Fibra de Vidrio.” Iniversidad Carlos III de Madird. <http://e-archivo.uc3m.es/handle/10016/7533>.

Westervelt, Peter J. 1963. “Parametric Acoustic Array.” *The Journal of the Acoustical Society of America* 35(1960): 535–37.

Woodward, B, J C Cook, A D Goodson, and P A Lepper. 1994. "A Phase Steered Parametric Array for Sub-Bottom Profiling." *IEE Electronic Engineering in Oceanography* (394): 77–82.

Wunderlich, Jens. 2003. "High-Resolution Sub-Bottom Profiling Using Parametric Acoustics." 7(4).

"www.ndt.net." <http://www.ndt.net/links/proper.htm>.

Yoneyama, Masahide. 1983. "The Audio Spotlight: An Application of Nonlinear Interaction of Sound Waves to a New Type of Loudspeaker Design." *The Journal of the Acoustical Society of America* 73(5): 1532.

Zienkiewicz, O.C., M. Watson, and I.P. King. 1968. "A Numerical Method of Visco-Elastic Stress Analysis." *International Journal of Mechanical Sciences* 10(10): 807–27. <http://www.sciencedirect.com/science/article/pii/0020740368900222>.

Table Index

Table 5.1. Material properties under characterization for a piezoelectric ceramic with polarization along Z axis	106
Table 5.2. Piezoelectric ceramic general description.....	107
Table 5.3. Manufacturer piezoelectric ceramic properties for Pz37 and PIC255 respectively.....	109
Table 5.4. Thickness ceramics values.....	118
Table 5.5. Convergence study results.....	123

Table 5.6. Mesh element size for each piezoelectric ceramic depending on simulations parameters.....	125
Table 5.7. Propagation velocities experimental results and associated error.....	128
Table 5.8. Acoustic Impedance Theoretical values & Experimental results	129
Table 5.9. Manufacturer piezoelectric ceramic properties for Pz37	132
Table 5.10. Manufacturer piezoelectric ceramic properties for PIC255	133
Table 5.11. Matching and Backing materials investigated.	138
Table 5.12. Materials samples dimensions for electrical admittance measurement ...	143
Table 5.13. Mesh element size for each material under test.....	144
Table 5.14. Materials acoustic properties measurements	145
Table 5.15. Materials acoustic properties measurements	145
Table 5.16. Materials acoustic properties Theoretical estimation	147
Table 5.17. Acoustic material properties adjusted.....	147
Table 5.18. ABS acoustic properties	150
Table 5.19. Water acoustic properties	150
Table 5.20. TVR and OCV values at 120 kHz for both prototypes.....	163
Table 5.21. Insulcast 501 and Eccosorb MF114 acoustic material properties.....	171

Table 5.22. TVR values at 120 kHz for the four FEM simulation models..... 172

Table 5.23. TVR values at 120 kHz for the four FEM simulation models..... 173

Table 6.1. TVR values at thickness and radial frequency for each Transducer..... 181

Table 6.2. TVR values and difference levels relation for each transducer. 188

Table 6.3. Medium pressure amplitude selected..... 189

Table 6.4. Peak voltage transducer required as function of input pressure..... 191

Table 6.5. -3dB beamwidth at each interesting frequency for each transducer 197

Table 6.6. Sound Pressure Level at each interesting frequency for each transducer. . 201

Table 6.7. Sound Pressure Level at each interesting frequency for each prototype VS simulation. 204

Table 6.8. Mediterranean Sea environmental conditions..... 207

Table 6.9. Medium absorption and receiver sensitivity for each prototype at different frequencies..... 207

Table 6.10. Prototype 1: Application range viability table as function of TS and distance 208

Table 6.11. Prototype 2: Application range viability table as function of TS and distance 209

Table 6.12. Prototype 2: Application range viability table as function of TS and distance.
 Table in the left hand side corresponds to values with 1MPa as an input pressure.

Table in the right hand side, corresponds to values for 3MPa as an input pressure.

..... 212

Figure index

Figure 2.1. Waveform parameters	26
Figure 2.2. Transversal and longitudinal wave propagation.....	30
Figure 2.3. Harmonic frequency generation in a non-linear acoustic system.....	35
Figure 2.4. Sine wave transformation in saw-tooth wave.....	36
Figure 2.5. Source virtual representation depending on interaction distance	37
Figure 2.6. Validity model regions for parametric arrays. ((Kopp et al. 2000)).....	38

Figure 2.7. Frequency dependent attenuation, for the relaxation processes of oxygen and nitrogen in air, and magnesium sulphate and boric acid in seawater..... 43

Figure 3.1. Piezoelectric effect in a piezoelectric ceramic. Honda Electronics CO.LTD source..... 50

Figure 3.2.-Polarization process. (a)Random dipoles orientation. Prior polarization. (b) Polarization in DC electric field. (c) Remanent polarization after electric field... 52

Figure 3.3.-Simmetria axis in piezoelectric ceramic 55

Figure 3.4. Ultrasonic sound beam propagation 57

Figure 3.5. On-axis SPL from a circular piston 58

Figure 3.6. Coordinate system used for describing the propagation of an acoustic wave, where the source is a disc centred at the origin of coordinates..... 60

Figure 3.7. Source point propagation with spherical divergence..... 63

Figure 3.8. Circular piston pattern with 4 cm radius, mounted in an infinite screen, at 200 kHz ($kr = 33.5$). 70

Figure 3.9. KLM equivalent circuit of a thickness extensional piezoelectric transducer(Arnau 2008) 78

Figure 4.1.-Substructural division by Finite element method..... 88

Figure 4.2.-Model convergence tendency..... 92

Figure 4.3.-Model geometry with axial symmetry 93

Figure 4.4.-Example of model geometry from COMSOL and FEMP respectively. 96

Figure 4.5. Schematic showing the computational steps in the solution of the coupled first-order equations using a staggered spatial and temporal grid in 2D. Here $\hat{\partial}p/\hat{\partial}x$ and u_x are evaluated at grid points staggered in the x-direction (crosses), while $\hat{\partial}p/\hat{\partial}y$ and u_y evaluated at grid points staggered in the y-direction (triangles)(Treeby, Cox, and Jaros 2016)..... 98

Figure 5.1. - Piezoelectric ceramic scheme 110

Figure 5.2.-Longitudinal sound speed measurement. Experimental set-up (left side) and blocks diagram (right side) 111

Figure 5.3.-Oscilloscope signal detail. Receive transducer signal from piezoelectric ceramic eco-impulse test..... 112

Figure 5.4.-Electrical admittance measurement set up. 115

Figure 5.5. - Piezoelectric ceramic FE modelling detail..... 116

Figure 5.6. – Boundary conditions scheme for a piezoelectric ceramic disc 119

Figure 5.7. – Convergence graphic results for PIC255 and PZ37 ceramic respectively124

Figure 5.8. –Detail geometry PIC255 ceramic, in FEMP model, with 16 elements wavelength..... 125

Figure 5.9. – Electrical admittance for Pic255 Piezoelectric ceramic: FE modelling & Experimental measurement 130

Figure 5.10. - Electrical admittance for Pz37 Piezoelectric ceramic: FE modelling & Experimental measurement 131

Figure 5.11. – PZ37 Resonant Frequencies depending on the ratio between its diameter and thickness..... 134

Figure 5.12. – PIC255 Resonant Frequencies depending on the ratio between its diameter and thickness..... 135

Figure 5.13. – Contact method experimental set-up..... 140

Figure 5.14. – Contact method diagram block..... 141

Figure 5.15. – Conductance comparison between simulation and measurement. PIC255 piezoelectric ceramic + 6.5 mm of TD1049 backing material..... 146

Figure 5.16. – Conductance comparison between simulation and measurement. PIC255 piezoelectric ceramic + 3mm of EL217C front layer material 146

Figure 5.17. – FEMP simulation model: Full transducer in water..... 151

Figure 5.18. – Geometry dimension 151

Figure 5.19. – Transducer construction steps. (a) Backing adhesion, (b) Piezoelectric ceramic wired (c) Housing introduction, (d) Matching filling, (e) Elements encapsulation and (f) Transducer finalized..... 152

Figure 5.20. – Transducer prototypes placement for electrical admittance measurements. Air and water measurements respectively. 155

Figure 5.21. – 3D AutoCAD diagram for UPV positioning system. 156

Figure 5.22. – Transducer and hydrophone measurement disposition. 3D AutoCAD representation and real image respectively..... 157

Figure 5.23. – Procedure for the Projector Sensitivity measurement	159
Figure 5.24. – Procedure for the Receiving Sensitivity measurement.....	159
Figure 5.25. – Procedure for the Directivity measurements	160
Figure 5.26. – Admittance measurement comparison between prototype 1 and prototype 2.....	161
Figure 5.27. – TVR measurement comparison between prototype 1 and prototype 2.	162
Figure 5.28. – OCV measurement comparison between prototype 1 and prototype 2	162
Figure 5.29. –Directivity measurement comparison between prototype 1 and prototype 2 at resonance frequency.	163
Figure 5.30. –Prototype 1: Electrical admittance comparison between FEM simulation model and measurement	165
Figure 5.31. – Prototype 1: Projector sensitivity comparison between FEM simulation model and measurement	165
Figure 5.32. – Prototype 1: Receiver sensitivity comparison between FEM simulation model and measurement.	166
Figure 5.33. – Prototype 1: Directivity comparison between measurement and FEM simulation model respectively.	166
Figure 5.34. – Prototype 2: Electrical admittance comparison between FEM simulation model and measurement.	168

Figure 5.35. – Prototype 2: Projector sensitivity comparison between FEM simulation model and measurement 168

Figure 5.36. – Prototype 2: Receiver sensitivity comparison between FEM simulation model and measurement 169

Figure 5.37. – Prototype 2: Directivity comparison between measurement and FEM simulation model respectively. 169

Figure 5.38. –Projector sensitivity comparison between three FEM simulation models with different design parameters modification 171

Figure 5.39. –Receiver sensitivity comparison between three FEM simulation models with different design parameters modification 172

Figure 6.1. Directivity comparison between K-wave simulation and experimental measurements at 120 kHz..... 176

Figure 6.2. Byfrequency K-Wave simulation for 19mm radius transducer at different distances. a) Field generated with an input pressure of 50000 Pa. b) Field generated with an input pressure of 100000 Pa. c) Field generated with an input pressure of 250000 Pa. d) Field generated with an input pressure of 1MPa. 178

Figure 6.3. Byfrequency K-Wave simulation for a 19mm radius transducer with different input pressure level at distance of 1.61m..... 179

Figure 6.4. Transmitting Voltage Response as function of frequency for each transducer. Prototype 1, prototype 2 and Airmar P19 respectively..... 182

Figure 6.5. Amplitude as function of voltage measurement esqume 184

Figure 6.6. Directivity measurement esqueme.	186
Figure 6.7. Amplitude as function of distance measurement esqueme.....	187
Figure 6.8. Power spectral density as function of frequency depending on signal length	190
Figure 6.9. Normalized pressure of primary and parametric beam as function of voltage in prototype 1	192
Figure 6.9. .Normalized pressure of primary and parametric beam as function of voltage in prototype2.....	192
Figure 6.10. .Normalized pressure of primary and parametric beam as function of voltage in transducer Airmar P19 and Airmar n°X respectively	193
Figure 6.12. Directivity beam pattern for 90-150 kHz Byfrequency signal and 95-145 kHz Byfrequency signal respectively for prototype 1. Linear resonance frequency, difference frequency and sum frequency are represented.....	194
Figure 6.13. Directivity beam pattern for 90-150 kHz Byfrequency signal and 95-145 kHz Byfrequency signal respectively for prototype 2. Linear resonance frequency, difference frequency and sum frequency are represented.....	195
Figure 6.14. Directivity beam pattern for 175-225 kHz Byfrequency signal for Airmar P19. Linear resonance frequency, difference frequency and sum frequency are represented.....	196
Figure 6.15. Directivity beam pattern for 90-150 kHz Byfrequency signal for all transducers. Primaries and difference frequency are represented. a) Prototype1: Pic255; b) Prototype 2:Pz37; c) Airmar P19.	199

Figure 6.16. Prototype 2: Normalized pressure as function of distance for a Byfrequency signal of 95-145 kHz, having a parametric difference frequency of 50 kHz..... 200

Figure 6.17. Airmar P19: Normalized pressure as function of distance for a Byfrequency signal of 175-225 kHz, having a parametric difference frequency of 50 kHz.... 200

Figure 6.18.K-wave: Directivity for primary and difference frequency at 1MPa as input pressure..... 202

Figure 6.19. Difference frequency directivity comparison. Prototypes experimental measurement Vs K-wave simulation 202

Figure 6.20. Source pressure level at 1.5m for different transducer radius with 1MPa as input pressure..... 203

Figure 6.21. Difference frequency beam aperture in function of weighing primaries frequencies..... 205

Figure 6.22. SPL in function of input pressure. Simulation data compare with experimental results..... 211

Figure 6.23.SPL of difference parametric beam as function of transducer radius for a Byfrequency signal of 170-230 kHz, having a parametric difference frequency of 60 kHz 213

